

Micro-and Nano Engineering for Polymerase Chain Reaction

Dissertation

zur Erlangung des Grades

der Doktorin der Ingenieurwissenschaften

der Naturwissenschaftlichen-Technischen Fakultät

der Universität des Saarlandes

von

Xiangping Li

Saarbrücken

2018

Tag des Kolloquiums:	20.08.2018
Dekan:	Prof. Dr. Guido Kickelbick
Berichterstatter:	Prof. Dr. Andreas Manz Prof. Dr. Uwe Hartmann
Vorsitz:	Prof. Dr. Joachim Rudolph
Akad. Mitarbeiter:	Dr. Andreas Tschöpe

Eidesstattliche Versicherung

Hiermit versichere ich an Eides statt, dass ich die vorliegende Arbeit selbstständig und ohne Benutzung anderer als der angegebenen Hilfsmittel angefertigt habe. Die aus anderen Quellen oder indirekt übernommenen Daten und Konzepte sind unter Angabe der Quelle gekennzeichnet. Die Arbeit wurde bisher weder im In- noch im Ausland in gleicher oder ähnlicher Form in einem Verfahren zur Erlangung eines akademischen Grades vorgelegt.

Ort, Datum

Unterschrift

Contents

Abstract.....	I
Zusammenfassung.....	III
摘要	V
Acknowledgement.....	VI
Road map/preface.....	VII
Chapter 1.....	1
Deoxyribonucleic acid.....	1
1.1 The discovery of deoxyribonucleic acid.....	1
1.2 Uses in technology.....	4
1.3 Methods.....	8
1.3.1 DNA biosensors.....	8
1.3.2 DNA sequencing.....	11
1.3.3 PCR.....	13
References.....	14
Chapter 2.....	19
Micro-Nano fabrication	19
2.1 Miniaturization.....	19
2.2 Scaling laws.....	23
2.3 Diffusion	25
2.3.1 Scaling and diffusion	26
2.3.2 Scaling in fluid mechanics / microfluidics	27
2.4 Micro-Nano fabrication	28
2.4.1 Microfabrication techniques	28

2.4.2 Nanofabrication techniques	34
2.4.3 Materials for Desktop MNF and applications	41
References.....	46
Chapter 3.....	51
Microfluidic systems and “lab-on-a-chip”	51
3.1 Microfluidic Sanger sequencing.....	52
3.2 Polymerase chain reaction.....	53
3.2.1 Quantification of DNA.....	55
3.2.2 Real-time PCR.....	57
3.2.3 Optimization.....	61
3.3 Digital PCR.....	64
3.3.1 Droplet microfluidics	66
3.3.2 Recombinase Polymerase Amplification.....	68
3.4 Biomimetics	71
Nature as a guide	71
References.....	76
Chapter 4.....	87
Thermal gradient for fluorometric optimization of droplet PCR in virtual reaction chambers.....	87
Abstract.....	88
4.1 Introduction	88
4.2. Materials and methods	91
4.2.1. Surface preparation.....	91
4.2.2. Temperature calibration	92
4.2.3. Reagents.....	93

4.2.4. On-chip PCR thermocycling.....	93
4.2.5. Image acquisition and processing.....	96
4.2.6. Melting analysis	96
4.2.7. Commercial instrument.....	97
4.3. Results.....	97
4.3.1. Temperature gradient.....	97
4.3.2. Gradient PCR.....	100
4.4. Discussion.....	104
4.5. Conclusion	105
Acknowledgements	106
Electronic Supporting Information.....	107
Surface preparation.....	107
Temperature calibration	107
Template and primer information.....	109
References.....	110
Chapter 5.....	113
Precise definition of starting time by capillary-based chemical initiation of digital isothermal DNA amplification	113
Manuscript in submission	113
Abstract.....	114
5.1 Introduction.....	115
5.2 Experimental	118
5.2.1 Materials	118
5.2.2 PCR reagents	120
5.3 Results and discussion.....	122

5.4 Conclusion	128
Reference.....	129
Chapter 6.....	133
Duplex-imprinted Nano well arrays for promising nanoparticles assembly	133
Abstract.....	134
6.1. Introduction.....	134
6.2. Experimental.....	137
6.2.1 Materials.....	137
6.2.2 Duplex imprint.....	137
6.3. Results and discussion.....	140
6.4. Conclusions	145
Conflicts of interest	146
Acknowledgements	146
Supporting Information.....	147
Experimental Methods.....	147
References.....	151
Chapter 7.....	155
Conclusion and outlook.....	155
Outlook.....	156
Appendix	159
List of abbreviations	159

Abstract

In the frame of this thesis, polymerase chain reaction (PCR) is analyzed from analogue to digital, from thermal cycling to a single temperature. An "analogue" measurement infers certain measurements based on the measured pattern, whereas a "digital" measurement method measures a variable quantitatively and discretely.

First, an open system with a thermal gradient feature to optimize PCR is described. The gradient is measured through encapsulated aqueous beads of a temperature-dependent dye with volumes in the low microlitre range within slightly larger oil droplets, forming virtual reaction chambers (VRCs). VRCs exploit the advantages of microfluidics and droplets in a simple way while circumventing many practical problems. As the gradient feature allows for testing a range of annealing temperatures simultaneously, the optimal annealing temperature can be determined easily in a single run.

Second, a microfluidics platform using capillaries was built to generate nanoscale droplets. Those monodisperse, isolated compartments are used as nano-reactors for isothermal PCR – recombinase polymerase amplification (RPA). By precise definition of the starting time of RPA, the method detects nucleic acid at the single molecule level by counting the presence or absence of the amplification of individual molecules confined to isolated compartments.

Third, a biomimetic chip with a nanowell structure was duplex-imprinted from a natural insect, Cicada, to run digital PCR. The glassy wings of Cicada, which are abundant in nature, exhibit a strikingly highly organized nanopillar structure over its membrane on both sides. A duplex nanoimprint technique was proposed to fabricate the chip out of the cleanroom, which combines the top-down and bottom-up nanofabrication technique to speed up the fabrication process and achieve higher throughput. Further experiments for digital PCR using the Cicada chip are

II

still ongoing. Additionally the Cicada nanowell chips has a potential to be employed in other applications, such as nanoparticles self-assembly, Matrix assisted laser desorption ionization (MALDI) etc.

Zusammenfassung

Im Rahmen dieser Arbeit wurde die Polymerase-Kettenreaktion (Polymerase chain reaction; PCR) untersucht, von Analog bis Digital als auch bei zyklisch wechselnden Temperaturen und festen Temperaturwerten. Eine „digitale“ Messung misst hierbei quantitativ und eigenständig eine bestimmte Variable, wohingegen „analoge“ Messungen bestimmte Messwerte extrapolieren, basierend auf einem gemessenen Muster.

Zuerst wird ein offenes System mit einem Temperatur-Gradienten zur Optimierung der PCR beschrieben. Der Gradient wurde vermessen mittels verkapselter, wässriger Mikrobeads mit einem temperaturabhängigen Farbstoff mit Volumina im niedrigen Mikroliter-Bereich innerhalb leicht größerer Öltröpfen, die hierbei eine Virtuelle Reaktionskammer (VRC) bilden. VRCs stellen einen simplen Weg zur Untersuchung der Vorteile der Mikrofluidik und Droplettechnologie dar, wobei viele praktische Probleme verhindert werden können. Durch die Eigenschaften des Gradienten war es möglich, eine große Breite von Temperaturen zu testen, um die optimale Annealing-Temperatur in einem einzelnen Experiment zu ermitteln.

Zweitens wurde eine mikrofluidische Plattform hergestellt, um Tropfen in Nano-Größe zu generieren. Diese monodispersen, isolierten Kompartimente wurden als Nanoreaktoren für isothermale PCR-Rekombinase Polymerase Amplifikation (RPA) verwendet. Durch genaue Definition der Startzeit der RPA konnte die Methode verwendet werden, um Einzelmoleküle von Nucleinsäuren nachzuweisen über Präsenz oder Absenz einer Amplifikation des jeweiligen Moleküls in den isolierten Kompartimenten.

Drittens wurde ein bio-mimetischer Chip mit Nanowell-Strukturen für PCR als Duplex-Abdruck eines Insektes, Cicada, geformt. Die Glasflügel von Cicada, welche in großer Fülle in der Natur vorliegen, besitzen eine hoch-organisierte Nanopillar-

Struktur, verteilt über die Membranen auf beiden Seiten. Eine Duplex-Nanoabdruck Technik wurde verwendet, um die Chips außerhalb eines Reinraums herstellen zu können, was sowohl die Top-Down- als auch die Bottom-Up-Nanoherstellungstechniken kombiniert, um somit den Fabrikationsprozess beschleunigen und einen höheren Durchsatz generieren zu können. Weitere Experimente mit dem Digital-PCD Cicada Chip sind in Vorbereitung. Des Weiteren hat der Cicada Nanowell-Chip großes Potential in unterschiedlichen Anwendungen weiter genutzt zu werden, wie beispielsweise selbstorganisierende Nanopartikel, Matrix-assisted laser desorption ionization MALDI etc.

摘要

本论文从模拟到数字，从热循环到单一温度对聚合酶链式反应(PCR)进行了分析。“数字”测量方法定量且离散地测量某个变量，而“模拟”测量则是基于测量的模式推断某些测量结果。

首先，本文描述了一个开放的，用于优化 PCR 的温度梯度系统。温度梯度通过温度依赖性荧光染料的胶囊化水珠测量。水珠的体积在低微升范围内，外面被体积稍大的油滴包裹起来，形成虚拟反应室(VRC)。由于梯度特征允许同时测试一系列退火温度，所以可以在单个实验中很容易地确定最佳退火温度，从而达到优化 PCR 的目的。

其次，本文介绍了一个基于毛细管的微流体平台，用来产生纳米级的液滴用于运行数字液滴 PCR。这些单分散的液滴隔离室被用作等温 PCR - 重组酶聚合酶扩增 (RPA) 的纳米反应容器。通过精确定义 RPA 的起始时间，该方法计数被限制在隔离液滴中的单个分子的扩增结果的存在与否达到检测单分子水平核酸的目的。

最后，本文介绍了具有纳米孔结构的仿生芯片，用以运行数字 PCR。该创意是从天然昆虫 - 蝉(Cicada)得到灵感。蝉在自然界储藏丰富，它的透明翅膀在膜的正反面上呈现出惊人的高度有序的纳米柱状结构。本文的第六章提出了一种双面纳米压印技术，无需无尘室制造芯片，将自上而下和自下而上的纳米加工技术结合起来，以加快制造过程并实现更高的生产量。由于检测仪器的限制，使用 Cicada 芯片的数字 PCR 实验仍在进行中。此外，蝉纳米芯片将用于其他应用，如纳米粒子自组装，基质辅助激光解吸电离(MALDI)等。

Acknowledgement

For support and scientific discussions during my time working on this thesis, I would like to thank my supervisor – Prof. Andreas Manz. Also I would like to thank Dr. Wenming Wu, Dr. Christian Daniel Ahrberg, Thomas Janson and Dr. Tijmen Hageman for the help with the first paper. I would like to thank Associate Prof. Zhenjun Chang for the revising advice to the first and second publication. Also I would like to thank Prof. Leon Abelmann and Dr. Matthias Altmeyer for their kind help during the research work.

Furthermore I am grateful to Agu Vahtrik (Master student, Saarland University), helped taking Scanning electron microscope (SEM) images. Carsten Brill (KIST Europe) and Dr. Markus Koch (INM institute, Saarbrücken) also helped with SEM imaging, for which I want to thank them.

I gratefully acknowledge the Chinese Scholarship Council for supporting my PhD study in Germany.

Lastly I would like to thank all members of KIST Europe and the Universität des Saarlandes for their valuable inputs to this work through discussions.

Road map/preface

In this section, the logic behind the organization of this thesis into 7 chapters is presented.

The first chapter gives a brief introduction about DNA, aimed at engineers who have little knowledge about it, what DNA is and its structure, why it is important, the applications of DNA and how the understanding of copy mechanism of DNA helps in the medical field.

The second chapter introduces the micro-nanofabrication methods while keeping in mind the scaling laws, and is aimed at biologists who know little about fabrication techniques. It explains how miniaturization helps to advance the technology and its applications. Principal fabrications, namely photolithography, soft lithography and nanoimprint technology, are discussed in detail.

The third chapter is an introduction to the essence of this thesis. All techniques and concepts intimated in the thesis are included. It is the most informative chapter with regard to quick understanding the contribution of the thesis.

The fourth chapter is the first publication, aiming to optimize PCR in a single experiment with a gradient of annealing temperatures. For detailed information, the reader should refer to the graphical abstract and subsequent main text.

The fifth chapter is a manuscript in submission, adopting a single temperature PCR – RPA – in a capillary-based setup, to achieve nucleic acid amplification at the single molecule level.

The sixth chapter is the second publication utilizing nature as a guide to fabricate nanowell array chips for digital PCR. This is a novel nanoimprint technique capable of duplex imprinting at ambient conditions within a short time. For detailed information, the reader should refer to highlights and subsequent main text.

VIII

The final chapter is the conclusion, summarizing what has been achieved in this PhD study. An insight into future work is also provided.

The appendix gives abbreviations and their descriptions.

The publications are attached at the end.

Chapter 1

Deoxyribonucleic acid

1.1 The discovery of deoxyribonucleic acid

Deoxyribonucleic acid (DNA) was first shown to be capable of transforming the properties of cells in 1944 [1], many decades after its discovery and isolation in 1869 by the young Swiss physician Friedrich Miescher [2]. The reason for DNA not being studied in depth at that time was that proteins were thought to hold the genetic blueprint to life, rather than DNA.

DNA has a structure that is sufficiently complex and yet simple enough, with a double helix as the only structural component and four nitrogen-containing complementary nucleotides (cytosine [C], guanine [G], adenine [A] and thymine [T]) repeated throughout the whole structure. The right-twisted, double helix structure of DNA was proposed in 1953 based on X-ray crystallography structures [3,4]. The two polynucleotide strands are oriented in opposite directions, coiled around each other and linked by weak hydrogen bonds in a spiral configuration. The hydrophilic backbones, which are composed of the sugar groups (called deoxyribose) and phosphate groups that support the subunits of the polymer, are on the outside of the helix. The hydrophobic bases are on the inside, as shown in Figure 1.1. The sequence of bases forms a code to store and transmit genetic information.

The pairing rule of the bases (A=T, G=C) allows each strand to be used to reconstruct the other; these strands carry genetic instructions and facilitate the passing on of hereditary information [3,4]. When the two chains separate, each

Chapter 1 Deoxyribonucleic acid

serves as a template for a complementary new chain, suggesting a copy mechanism for DNA.

The discovery of the double helix marked a major milestone; significant advances in science all have their origins in the inspired work of the double helix discovery. The double helix not only reshapes biology, but also becomes a cultural icon, represented in sculpture and visual arts. It has given rise to modern molecular biology, and yielded ground breaking insights into the genetic code and protein synthesis. Moreover, the unique material properties of DNA have attracted material scientists and engineers who are interested in micro-nanofabrication, using it as structural material rather than a genetic embody [5,6].

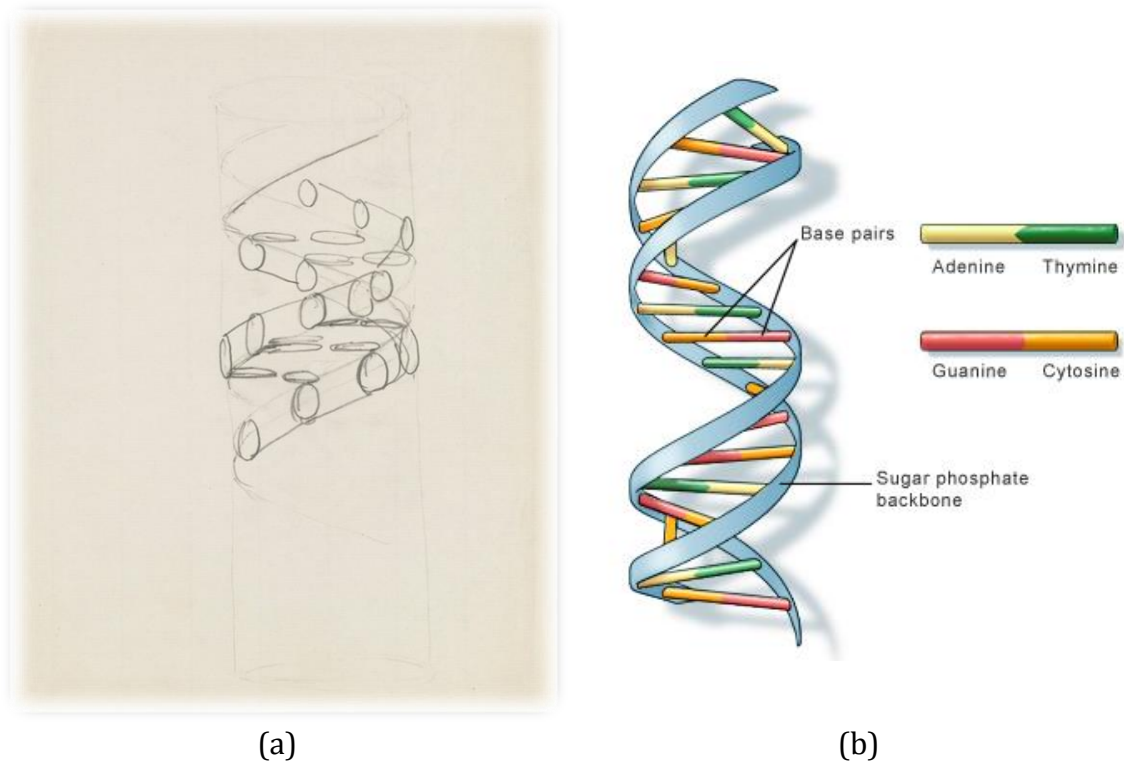


Figure 1.1 DNA right-twisted, double helix structure representations in sketch and recent form. The diameter of a DNA molecule is about 2 nm. (a) Pencil sketch of the DNA double helix in Crick's notebook, 1953. Credit: Wellcome Library, file PP/CRI/H/1/16. (b) A more recent representation showing how the nucleotides are arranged. Credit: U.S. National Library of Medicine.

Chapter 1 Deoxyribonucleic acid

There are two types of nucleic acids – DNA and ribonucleic acid (RNA). There is a transition process between DNA, RNA and proteins. Transcription creates RNA strands using DNA strands as a template, while translation process translates those RNA strands, from the genetic code, into a specific sequence of amino acids within a protein. The arrangement of nucleotides in DNA determines the amino acid sequence in proteins, which in turn helps determine the function of a protein [7]. A diagram showing the relationship between DNA and messenger RNA (mRNA) in protein analysis is shown in Figure 1.2.

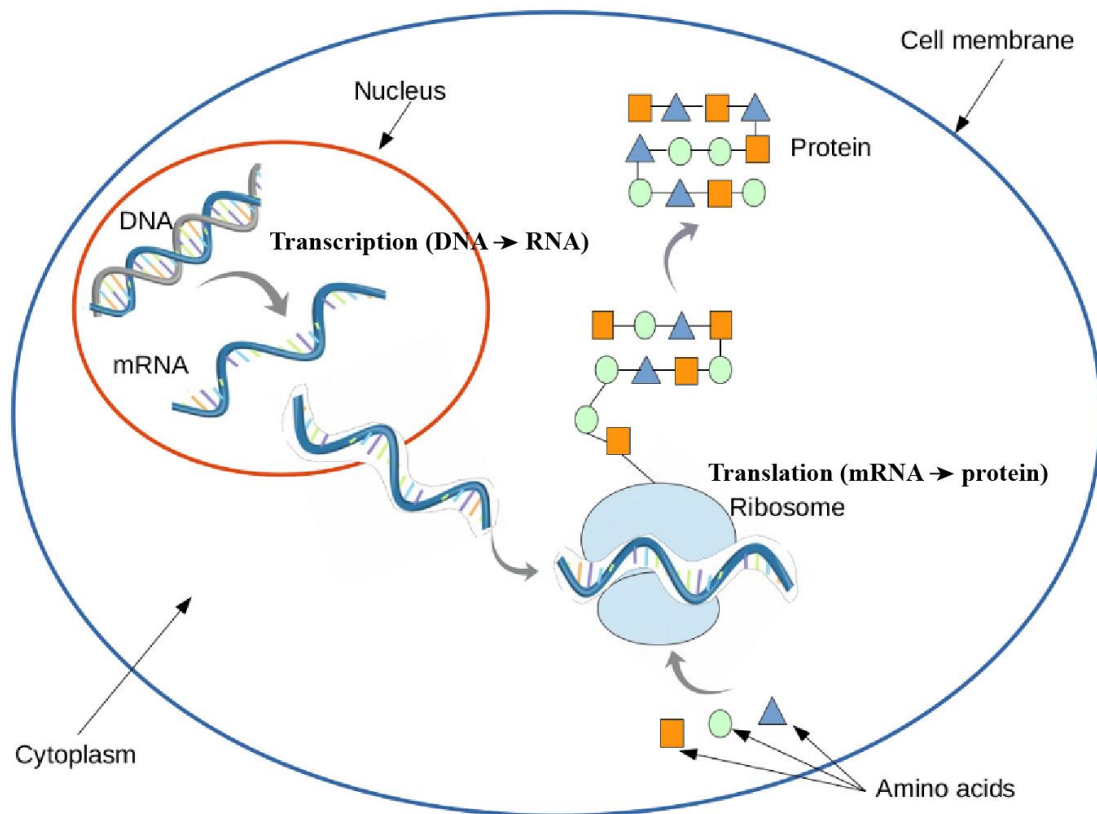


Figure 1.2 The relationship between DNA and mRNA in protein synthesis. Adapted from [8] with modification, p.65. Credit: U.S. National Library of Medicine.

1.2 Uses in technology

Genetic engineering

Genetic engineering, also referred to as genetic modification, first coined by Jack Williamson [9], directly manipulates DNA to alter the genetic makeup of an organism's genome, thus changes its phenotype. The alterations generated by nuclear transplantation, gene targeting, viral insertion, or transfection of synthetic chromosomes, etc., are used to enhance or modify the characteristics of an individual organism.

The artificial manipulation and modification of DNA can produce genetically modified organisms from a recombinant DNA or other nucleic molecules [10–12]. For instance, genetically modified crops with improved resilience, nutritional value, and growth rate have provided benefits in many countries. Figure 1.3 shows how to produce insulin, a protein that helps to regulate sugar levels in human body, in bacteria using genetic modification.

Chapter 1 Deoxyribonucleic acid

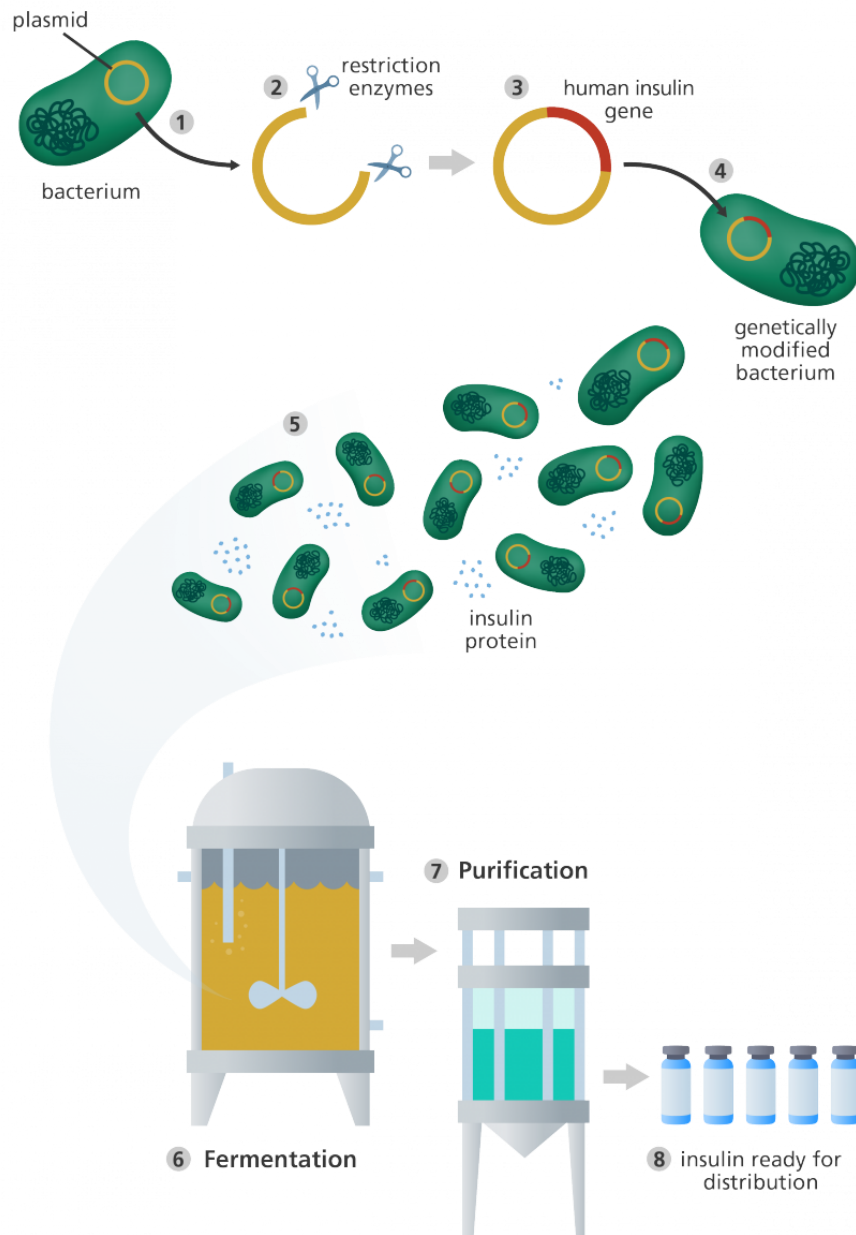


Figure 1.3 An illustration showing how genetic modification is used to produce insulin in bacteria. Credit: Genome Research Limited.

DNA profiling or genetic fingerprinting

DNA profiling is an extremely reliable technique for identifying a matching DNA by comparing the lengths of variable section of short tandem repeats (STRs) or mini-satellites [13]. The DNA samples include skin cells, hair, blood, semen, saliva, etc. Figure 1.4 shows DNA profiling examining sites on chromosomes.

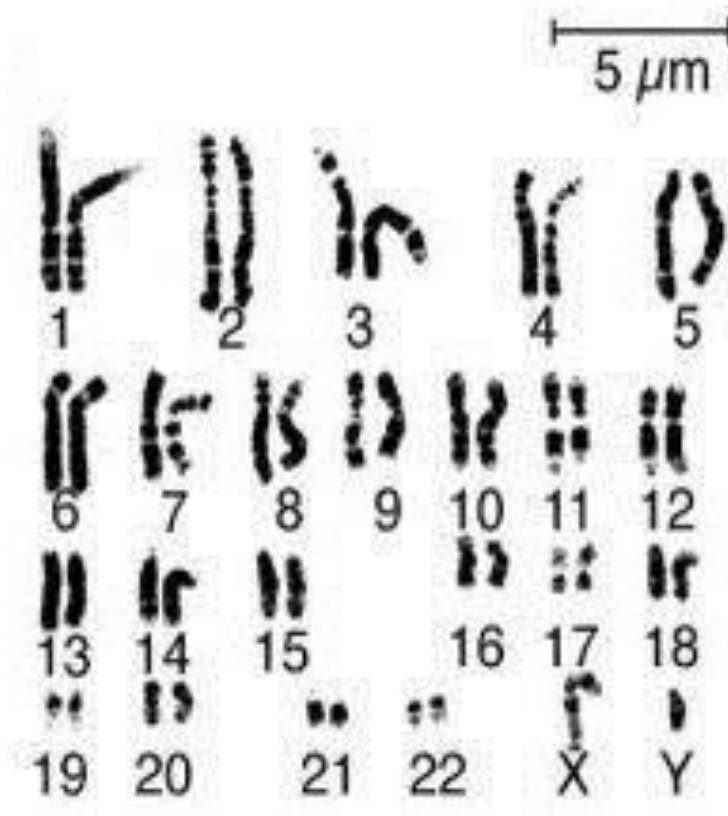


Figure 1.4 DNA profiling examines sites on several chromosomes. Copyright: © 2007 ESR Limited.

DNA profiling has found great importance in forensic analysis and paternity disputes. The procedures are: 1, DNA sample collection and amplification; 2, cut the satellite DNA with specific restriction enzymes into fragments, the length of fragments differ due to the variable length of STRs; 3, fragments separation and resulting profile comparison.

DNA enzymes

Deoxyribozymes, first discovered in 1994, are mostly single stranded DNA (ssDNA) sequences isolated from a large pool of random DNA sequences [14]. Deoxyribozymes catalyze variety of chemical reactions, and greatly enhance catalytic rate of chemical reactions up to 10^{11} fold over un-catalyzed reaction [15]. Those chemical reactions include RNA-DNA cleavage and ligation, carbon-carbon bond formation, etc. The most extensively studied class of deoxyribozymes is RNA-cleaving types [14].

Bioinformatics

Bioinformatics use various techniques to store, search, and manipulate biological data and data mine. Information storage is a mechanism taking advantage of DNA's ability to code information and store digital data. DNA, as a witness or proof of life, accumulates mutations over time. That historical information, including mutations, is then passed to next generation.

Bioinformatics shed light on the evolutionary history of particular organism, their phylogeny [16]. It has been used in studies ranging from ecological genetics to anthropology, permitting the examination of complex evolutionary events and search for specific sequences of nucleotides and mutations [17]. It can predict the presence of particular gene products and their possible functions [18], as well as study phylogenetic relationships and protein function [19].

DNA nanotechnology

DNA nanotechnology self-assembles useful branched DNA complexes by virtue of the unique molecular recognition properties of DNA and other nucleic acids [20], using them as structural materials [21]. An example is shown in Figure 1.5.

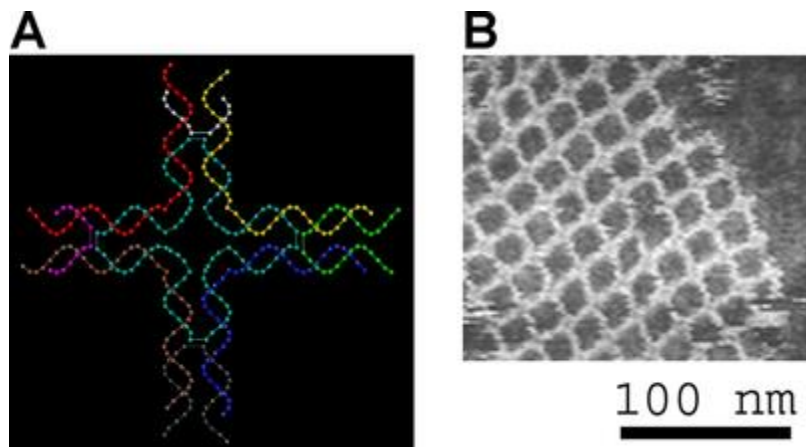


Figure 1.5 The schematic DNA structure shown on the left will self-assemble into the two-dimensional periodic lattices visualized by atomic force microscopy on the right. Adapted from [22]. Copyright: © 2004 Michael Strong.

1.3 Methods

1.3.1 DNA biosensors

In biosensors, the biochemical reaction of the assay and the measurement system are intimately combined onto a single chip to directly measure the target analyte without any additional reagents [23].

Biosensor = molecular recognition + signal transduction

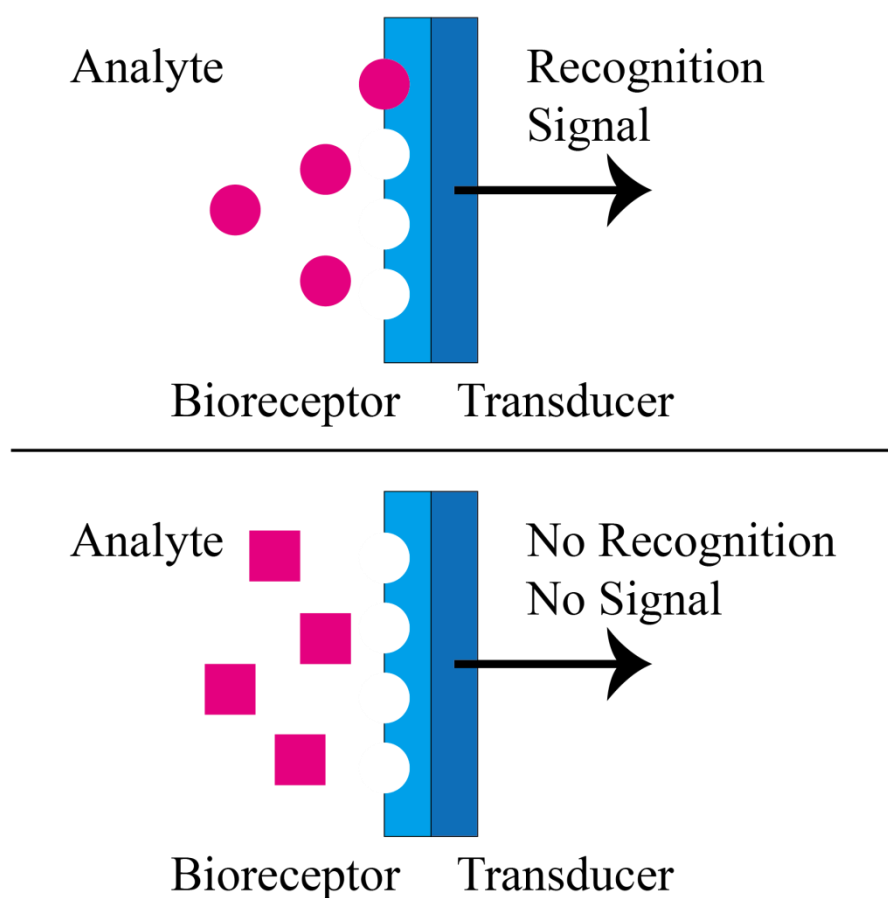


Figure 1.6 How a biosensor with a specific surface and transducer works.

The bioreceptor which specifically recognizes the target analyte [24] is integrated with a physical transducer into a single sensor. When a recognition event occurs, the physical transducer will translate the immediate bioreceptor changes into measurable signals. A simple sketch is shown in Figure 1.6. The main advantages of biosensors are their simplicity, cost-effectiveness and the fast speed of measurements. Applications of biosensors are summarize in Table 1.1.

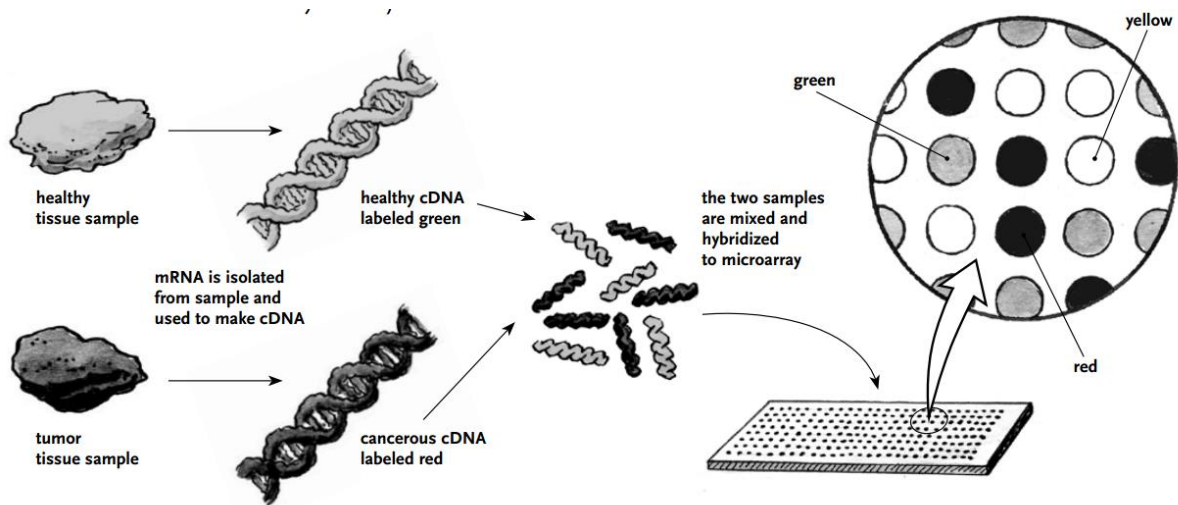
Chapter 1 Deoxyribonucleic acid

Table 1.1 applications for biosensors, reproduced from [23]. Copyright © 2015 Imperial College Press

Field	Applications
Health care	Markers of diseases like myocardial infarction or cancer monitoring of administered drugs diagnosis of infectious diseases, analysis of glucose and hormone levels
Environmental	Water and soil analysis pesticides and other toxic substances, industrial effluent control
Agriculture	Pesticide, crop diseases Food refreshness determination of fruit ripeness by glucose
Food control	content quantification of cholesterol in butter pathogenic organisms like E.coli
Process control	Fermentation monitoring
Microbiology	Bacterial and viral analysis

DNA biosensors are based on the recognition of complementary nucleic acid sequences (analyte or target). They can measure changes in mass, and optical, electronic, and electrochemical properties. Applications include the rapid diagnosis of genetic and infectious diseases [25,26], and the detection of DNA damage and interactions [27], with the advantage of readily synthesized and regenerated nucleic acid recognition layers for multiple uses [28].

A DNA microarray, also called a DNA chip or biochip, is a collection of DNA spots attached to a solid surface. Each chip has multiple probes for the same gene or fragment. The array fabrication is often performed using photolithographic technique, which will be discussed further in **Chapter 2**. Figure 1.7 shows how a DNA microarray works.



A microarray is an orderly arrangement of rows and columns on a surface like a glass slide. Each of the spots on an array contains single-stranded DNA molecules that correspond to a single gene. An array can contain a few, or thousands, of genes.

© 2007 WGBH Educational Foundation

Figure 1.7 How DNA microarrays work [29]. Copyright © 2007 WGBH Educational Foundation.

1.3.2 DNA sequencing

DNA sequencing is the most accurate method to determine the precise order of nucleotides within a DNA molecule and the exact nature of a mutation or variable position. There are many methods and technologies used to determine the order of the four bases in a strand of DNA. Sanger sequencing is the classical form of sequencing, prior to which either cloning procedures or PCR are required. It was proposed by Frederick Sanger, the pioneer of DNA and protein sequencing [30,31]. Figure 1.8 shows the main steps in Sanger DNA sequencing, which is also referred to as the dideoxy chain-termination method. Four dideoxynucleotides (ddNTPs) labelled with fluorophores are randomly inserted to terminate the synthesis of the

chain, because DNA polymerase cannot react with the missing hydroxyl, producing all possible lengths of chains.

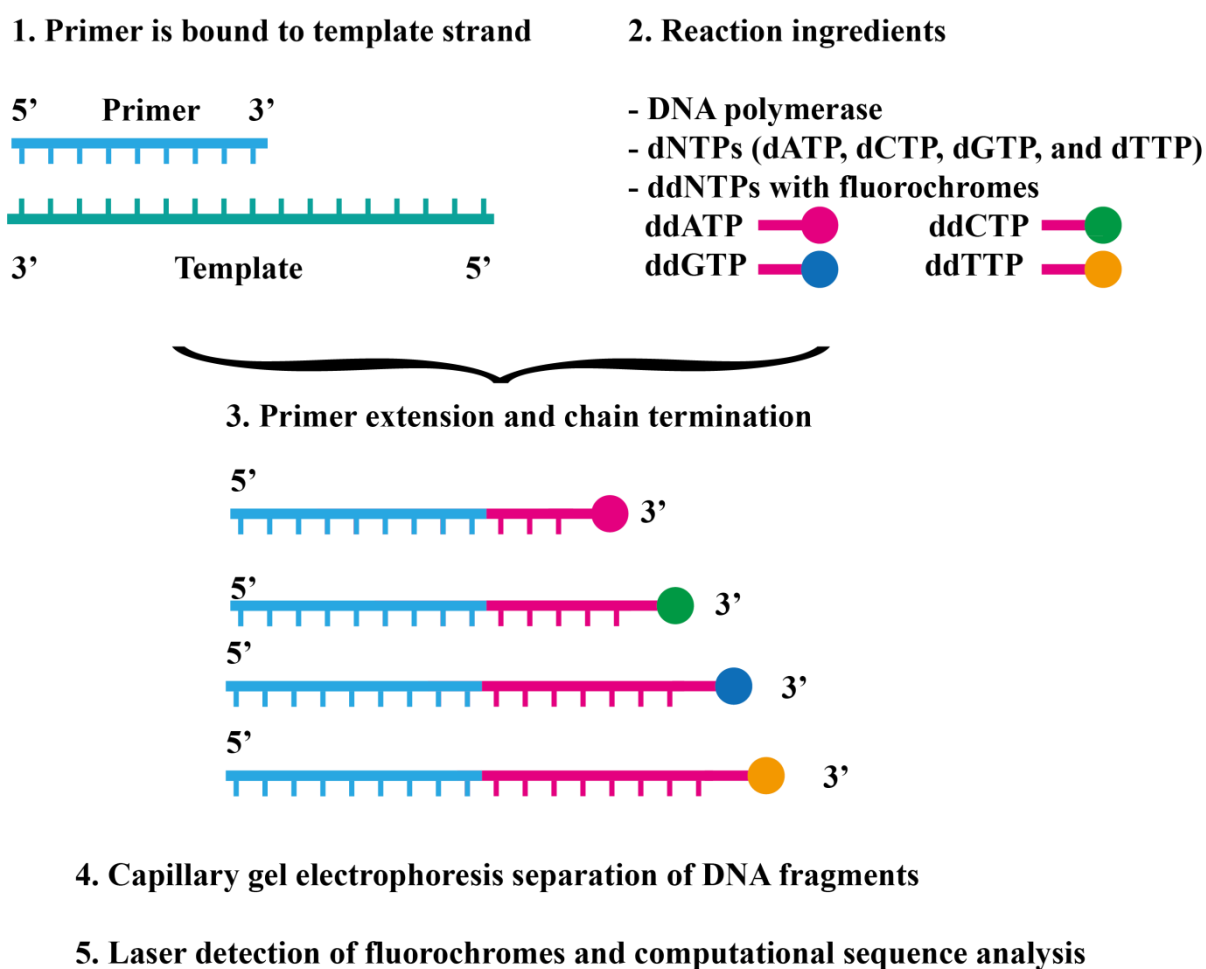


Figure 1.8 The key steps of Sanger (dideoxy chain-termination) DNA sequencing. (1) A primer is annealed to the target template DNA. (2) Reagent mixture is added. Note: each experiment with only one type of ddNTP is added. (3) Primer extension.

Applications

Biological and medical research and discovery [32] has been greatly accelerated through rapid DNA sequencing methods. It can be used in metagenomics, molecular biology, evolutionary biology, medicine, forensics, or anthropology, to determine the sequences of

- individual genes
- larger genetic regions
- full chromosomes
- operons or entire genomes of any organism.
- RNA or protein sequences

1.3.3 PCR

PCR is an *in vitro* molecular biology technique used for DNA amplification. As the amplification process is exponential, target molecules can be amplified from a few copies to millions within a short number of cycles. The exponential process allows for the rapid determination of information about the target DNA fragments, both qualitatively and quantitatively. Substantial improvements and modifications have been reported since its advent, including multiplex PCR [33], hot-start PCR [34], asymmetric PCR [35], nested PCR [36], touchdown PCR [37], etc. In Bridge PCR, fragments are amplified upon the attachment of primers to a solid surface [38–40] and form "DNA colonies" or "DNA clusters". This method is used by the Illumina Genome Analyzer sequencers.

A simple drawing of PCR is shown in Figure 1.9. More information about PCR will be detailed in in ***Chapter 3, subsection 3.2 Polymerase chain reaction***, in which the invention, quantification and optimization of PCR, etc., are discussed.

Polymerase chain reaction - PCR

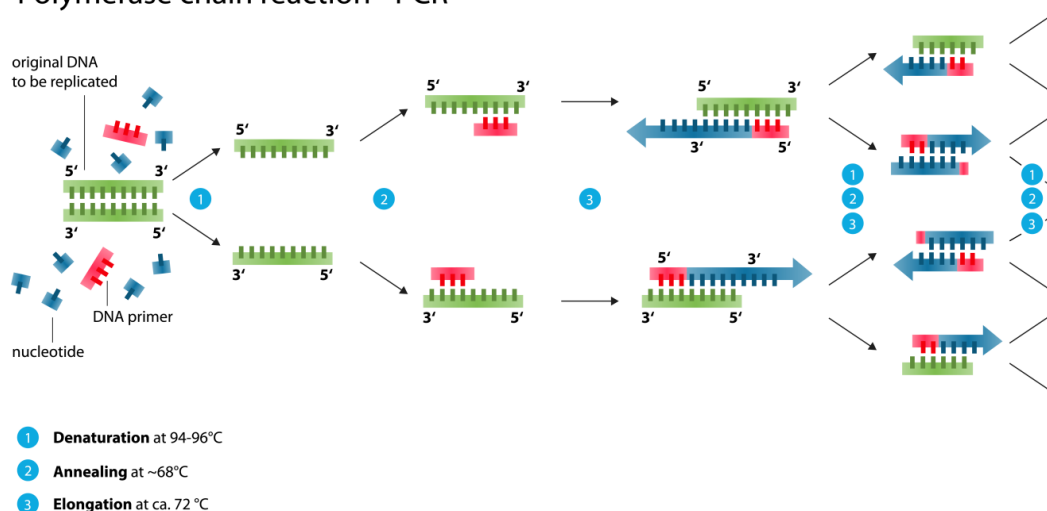


Figure 1.9 Schematic drawing of PCR. Adapted from [41].

References

- [1] Oswald T. Avery, Colin M. MacLeod and M M 1944 studies on the chemical nature of the substance inducing transformation of pneumococcal types: induction of transformation by a deoxyribonucleic acid fraction isolated from pneumococcus type iii *J. Exp. Med.* **79** 137–58
- [2] Dahm R 2005 Friedrich Miescher and the discovery of DNA *Dev. Biol.* **278** 274–88
- [3] Watson J and Crick F C 1953 MOLECULAR STRUCTURE OF NUCLEIC ACIDS: A Structure for Deoxyribose Nucleic Acid
- [4] WATSON J D and CRICK F H 1953 The structure of DNA. *Cold Spring Harb. Symp. Quant. Biol.* **18** 123–31
- [5] Mashaghi A and Katan A 2013 A physicist’s view of DNA
- [6] Aldaye F A, Palmer A L and Sleiman H F 2008 Assembling materials with DNA as the guide. *Science* **321** 1795–9
- [7] The path to sequencing nucleic acids,
<http://www.whatisbiotechnology.org/exhibitions/sanger/path>. Accessed

Chapter 1 Deoxyribonucleic acid

May 5, 2018.

- [8] Hesketh R 2012 *Betrayed by nature : the war on cancer* (Palgrave Macmillan)
- [9] Stableford B M 2004 *Historical Dictionary of Science Fiction* (Scarecrow Press)
- [10] Houdebine L-M 2007 *Transgenic Animal Models in Biomedical Research Target Discovery and Validation Reviews and Protocols* (New Jersey: Humana Press) pp 163–202
- [11] Daniell H and Dhingra A 2002 Multigene engineering: dawn of an exciting new era in biotechnology *Curr. Opin. Biotechnol.* **13** 136–41
- [12] Job D 2002 Plant biotechnology in agriculture *Biochimie* **84** 1105–10
- [13] Collins A and Morton N E 1994 Likelihood ratios for DNA identification. *Proc. Natl. Acad. Sci. U. S. A.* **91** 6007–11
- [14] Breaker R R and Joyce G F 1994 A DNA enzyme that cleaves RNA. *Chem. Biol.* **1** 223–9
- [15] Ritchie J 2015 Probabilistic DNA evidence: the layperson's interpretation *Aust. J. Forensic Sci.* **47** 440–9
- [16] Finnerty J R and Martindale M Q 1999 Ancient origins of axial patterning genes: Hox genes and ParaHox genes in the Cnidaria *Evol. Dev.* **1** 16–23
- [17] Gusfield D and Dan 1997 *Algorithms on strings, trees, and sequences: computer science and computational biology* (Cambridge University Press)
- [18] Mount D W 2004 *Bioinformatics : sequence and genome analysis* (Cold Spring Harbor Laboratory Press)
- [19] Sjolander K 2004 Phylogenomic inference of protein molecular function: advances and challenges *Bioinformatics* **20** 170–9
- [20] Rothmund P W K 2006 Folding DNA to create nanoscale shapes and patterns *Nature* **440** 297–302
- [21] Andersen E S, Dong M, Nielsen M M, Jahn K, Subramani R, Mamdouh W, Golas M M, Sander B, Stark H, Oliveira C L P, Pedersen J S, Birkedal V, Besenbacher F, Gothelf K V. and Kjems J 2009 Self-assembly of a nanoscale DNA box with a controllable lid *Nature* **459** 73–6
- [22] Strong M 2004 Protein Nanomachines *PLoS Biol.* **2** e73
- [23] Manz A (Andreas), Dittrich P S, Pamme N and Iossifidis D *Bioanalytical chemistry.*

Chapter 1 Deoxyribonucleic acid

- [24] Taylor R F and Schultz J S (Jerome S 1996 *Handbook of chemical and biological sensors* (Institute of Physics Pub)
- [25] Christopoulos T K 1999 Nucleic Acid Analysis *Anal. Chem.* **71** 425–38
- [26] Zhai J, Cui H and Yang R 1997 DNA based biosensors *Biotechnol. Adv.* **15** 43–58
- [27] Palecek E, Fojta M, Tomschik M and Wang J 1998 Electrochemical biosensors for DNA hybridization and DNA damage. *Biosens. Bioelectron.* **13** 621–8
- [28] Wang J 2000 From DNA biosensors to gene chips. *Nucleic Acids Res.* **28** 3011–6
- [29] How DNA Microarrays Work 2007,
<https://1.cdn.edl.io/mdhSXohfWUhpWAmRw6Fbn317Tnk1mZ8BaVSKDVUIFw85QtgH.pdf>. Accessed May 7, 2018.
- [30] Sanger F, Nicklen S and Coulson A R 1977 DNA sequencing with chain-terminating inhibitors. *Proc. Natl. Acad. Sci. U. S. A.* **74** 5463–7
- [31] Sanger F 1988 Sequences, Sequences, and Sequences *Annu. Rev. Biochem.* **57** 1–29
- [32] Introducing “dark DNA” – the phenomenon that could change how we think about evolution, <https://theconversation.com/introducing-dark-dna-the-phenomenon-that-could-change-how-we-think-about-evolution-82867>. Published 2017.
- [33] Chamberlain J S, Gibbs R A, Rainer J E, Nguyen P N and Thomas C 1988 Deletion screening of the Duchenne muscular dystrophy locus via multiplex DNA amplification *Nucleic Acids Res.* **16** 11141–56
- [34] Chou Q, Russell M, Birch D E, Raymond J and Bloch W 1992 Prevention of pre-PCR mis-priming and primer dimerization improves low-copy-number amplifications. *Nucleic Acids Res.* **20** 1717–23
- [35] Shyamala V and Ames G F 1989 Amplification of bacterial genomic DNA by the polymerase chain reaction and direct sequencing after asymmetric amplification: application to the study of periplasmic permeases. *J. Bacteriol.* **171** 1602–8
- [36] Haqqi T M, Sarkar G, David C S and Sommer S S 1988 Specific amplification with PCR of a refractory segment of genomic DNA. *Nucleic Acids Res.* **16** 11844
- [37] Don R H, Cox P T, Wainwright B J, Baker K and Mattick J S 1991 “Touchdown”

Chapter 1 Deoxyribonucleic acid

- PCR to circumvent spurious priming during gene amplification. *Nucleic Acids Res.* **19** 4008
- [38] Kawashima E H . L F P M WO 1998/044151 A1 - Method Of Nucleic Acid Amplification
- [39] Staden R 1979 A strategy of DNA sequencing employing computer programs *Nucleic Acids Res.* **6** 2601-10
- [40] Kron C P A J 1994 Method for performing amplification of nucleic acid with two primers bound to a single solid support
- [41] Enzoklop File:Polymerase chain reaction.svg - Wikimedia Commons, https://commons.wikimedia.org/wiki/File:Polymerase_chain_reaction.svg. Accessed May 28, 2018.

Chapter 2

Micro-Nano fabrication

2.1 Miniaturization

Miniaturization is one of the fastest changing megatrends to manufacture ever smaller products and devices for noteworthy applications in the medical, communication and automotive industries. Miniaturization is a powerful innovation tool for the ongoing technological revolution, as it has transformed microelectronics [1]. The science of Miniaturization comprises an intimate understanding of the specific application, in-depth knowledge of the available manufacturing options, familiarity with material selections, and an understanding of scaling laws [2], which describe the laws that express how structures scale when their dimensions are reduced.

In electronics, transistors haven been shrunk with technologies so fast that every year twice as many can fit onto a single chip, known as Moore's Law [3,4].

Miniaturization exhibits a lot of potential to make systems more intelligent and autonomous. Achieving a higher degree of intelligence demands that the sensory data are drastically increased by many orders of magnitude. It is fascinating and amazing to think about how much can be accommodated in small areas, or can fit into the palm of the hand. As versatile as miniaturization is, it is critical to consider that neither the cost nor energy consumption should exceed acceptable limitations after evaluation. Miniaturization allows for the production of hand-held, portable, implantable, or even injectable devices.

Miniaturization allows for high parallelization, which is of great importance when it comes to distributed systems, instead of confined to a few number of locations.

Chapter 2 Micro-Nano fabrication

Miniaturization and massive parallelism are very crucial for sensing and actuation for all living objects. Figure 2.1 shows the trend of miniaturization. This also influences the micro-nano fabrication (MNF) techniques. Miniaturization is a dominant force in product development today, and the process is more challenging than simply reducing the dimensions of a product. An easy assumption is that miniaturization merely involves scaling a component's dimension down. However, this scalar shrinking can work up to a point, where the approach breaks down, due to the fabrication process and/or materials being incompatible with the miniaturized component.

While the concept of reducing the size of individual components to make more intelligent and autonomous systems and devices is straightforward, their implementation is often more complex. In general, scaling different subsystems of a large system with a same factor might lead to different scaling performances. Every single component could have an extensive influence on the overall system; adapting the miniaturized component to incorporate the remaining components requires time and effort. Miniaturization of a product is only possible with the knowledge and intuition acquired through experiences in the macroscopic world while keeping in mind the scaling laws.

The phenomena and principle of life science will play an important role in futuristic engineering. Some characteristics are achieved through micro-, nano- and molecular level material manipulation. When the scalar shrinking technique breaks down, the phenomenon of "self-assembly" is utilized to make such manufacturing technologically feasible and economically viable. For instance, a branch of engineering – "synthetic biology" – where devices are artificially created following the emerging micro-, nano- and molecular techniques, but function mimicking the phenomena and principles of life science.

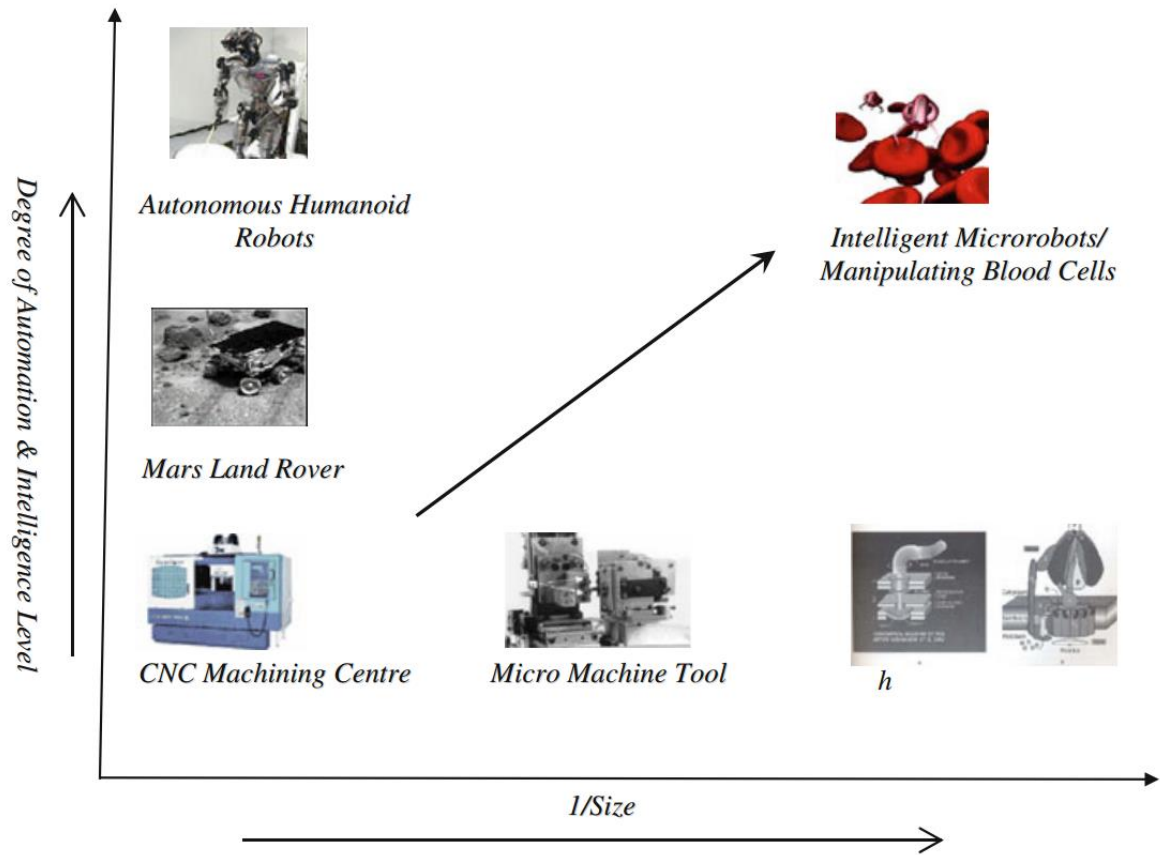


Figure 2.1 Trend of miniaturization, adapted from [5], Copyright © 2011 Springer Science+Business Media, LLC.

Miniaturization has had a far-reaching influence on many different industries, as shown in Table 2.1. A notable example of these microdevices with significant advantages is in medical care, which has reaped the benefits of miniaturization. Manufacturing portable, implantable or even injectable devices has been made possible through miniaturization. These devices save a lot of money and effort due to their minute size, less sample and lower reagent consumption. In addition, rapid analysis or operations is achieved by reducing lengthy diffusion times and increasing heat transfer. Improvements in portability have allowed for more treatments to be administered outside of traditional clinical settings. By reducing

Chapter 2 Micro-Nano fabrication

the time to diagnosis, these microdevices help physicians to make better patient management decisions, improve treatment outcomes and reduce overall costs. Advancements in microelectronics and biosensor tools fabricated using MNF techniques have been instrumental in facilitating the development of these point-of-care diagnostic devices.

Table 2.1 Reasons to miniaturize systems, actuators, power sources, sensors, and components.

Adapted from [2], p. 535. Copyright © CRC Press LLC 2002.

Miniaturization attributes	Reasons
Low energy and little material consumed	There are limited sources on planet earth
Arrays of sensors	Redundancy, wider dynamic range, and increased selectivity through pattern recognition
Small	Smaller is lower in cost, minimally invasive
Favorable scaling laws (in some cases)	Forces that scale with a low power become more prominent in the micro domain; if these are positive attributes, then miniaturization is favorable, e.g., surface tension becomes more important than gravity in a narrower capillary
Batch and beyond batch techniques	This lowers cost
Disposable	This helps avoid contamination
Breakdown of macro laws in physics and chemistry	New physics and chemistry might be developed
Increased sensitivity (in some cases)	Nonlinear effects can increase a sensor's sensitivity, e.g., amperometric sensors
Smaller building blocks	The smaller the building blocks, the more sophisticated the system that can be built

2.2 Scaling laws

As described in a previous section, scaling down the dimensions of an object might breakdown at a certain point. The counterintuitive features arise due to changes in the order of predominance of physical phenomena caused by scaling effects.

Scaling laws are laws in mathematical language to express proportionality functions of physical principles. They are used to predict the value of a system variable as a function of other significant variables [6]. With scaling laws, it is possible to determine which effects get stronger and which become weaker; that is, which physical phenomena become predominant due to scaling effects from an engineering point of view. It provides quantitative numbers and some kind of intuitive feel of how the world down there behaves.

Because of their importance scaling laws are presented at the beginning of the book *Nanosystems* [7]. Understanding the interplay between geometric characteristics and various physical phenomena provides clues to some fundamental aspects of a system.

As Newtonian mechanics (the basis of first principles) fails when size diminishes to extremely small levels, quantum mechanics is used to study such physical systems. Since the breakdown of Newtonian mechanics can readily occur before reaching such small dimensions, structural and functional consequences of shrinks in size or scale have to be taken care of for the successful design and analysis of microsystems.

Normal engineering intuition fails when dealing with microsystems, and is replaced by special microintuition. Table 2.2 shows the scaling of various physical phenomena.

The section will present the rudiments of scaling laws and their importance. To begin with, scaling laws involving surface and volume are briefly introduced.

Chapter 2 Micro-Nano fabrication

As evident as it is, surface area is $\propto l^2$ with volume $\propto l^3$. When the surface area divides by 4 and volume by 8, the surface to volume ratio doubles. The inverse volume to surface ratio shrinks linearly with size, which gives rise to instant heat transfer.

*Table 2.2 Scaling of various physical phenomena, reproduced from [2]. Copyright © 2002
CRC Press LLC.*

Physical quantity	Scaling exponent of l	Units
Area	2	m^2
Bending stiffness	1	Nm^{-1}
Buoyant force	3	
Capacitance	1	F
Capacitor electric field	-1	Vm^{-1}
Deformation	1	m
Drag and lift forces	$2+2\nu^*$	
Electrostatic energy	3	J
Electrostatic force	2	N
Frictional force		
Heat capacity	3	JK^{-1}
Inductance	1	L
Magnetic force	4	N
Mass (m)	3	kg
Mass moment of inertia	5	
Ohmic current	2	A
Resistance	-1	Ω
Resistive power loss	1	
Shear stiffness	1	Nm^{-1}
Strength	2	Nm^{-1}
Strength-to-weight ratio	-1	

Surface tension force	1	
Thermal conductance	1	WK^{-1}
Thermal time constant	2	s
Viscous forces	$1+\nu^*$	
Voltage	1	V
Volume (V)	3	L

* ν = fluid relative velocity

2.3 Diffusion

Diffusion is a physics process, driven by a gradient in chemical potential, as a result of the random walk of the diffusing species (molecules or atoms). A gradient is the change in the value of a quantity over a distance, e.g., concentration gradient. Figure 2.2 shows diffusion from microscopic to macroscopic scales.

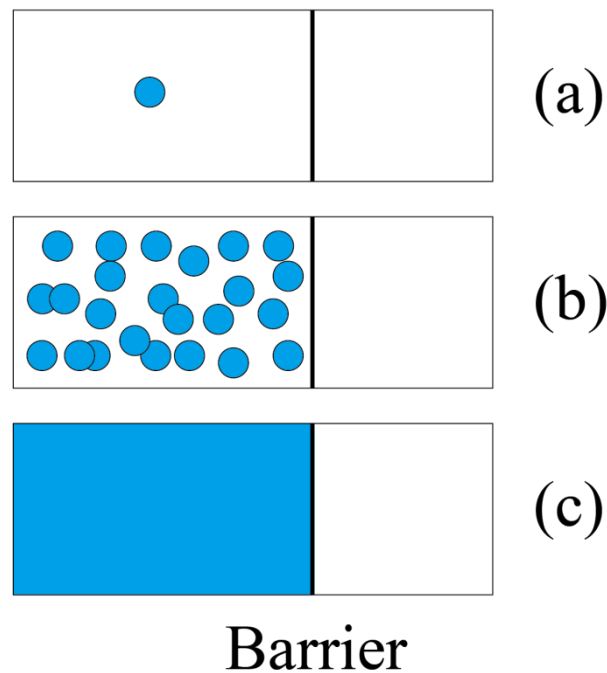


Figure 2.2 Diffusion at different concentrations of solutes. Initially, the solute molecules are on the left side. The barrier (black line) is then removed, and diffusion begins. (a) A single molecule moves around randomly. (b) At slightly higher concentrations, there is a statistical trend that the molecules will eventually become distributed randomly and uniformly. (c) At high concentrations, all randomness disappears. The molecules appear to move smoothly and are deterministically driven by concentration gradient.

2.3.1 Scaling and diffusion

Diffusional effects come into play yet a smaller scale than surface tension. The diffusion coefficient D for a spherical molecule is given by equation 2.1:

$$D = \frac{kT}{6\pi r\eta} \text{ (m}^2\text{/s)}$$

Where k = the Boltzmann constant ($1.38 \times 10^{-23} \text{ J K}^{-1}$)

T = absolute temperature (K)

η = absolute viscosity ($kg/m \cdot s$)

r = hydrodynamic radius

According to the random walk equation, the time τ required for a molecule to diffuse over distance x of a molecule in solution is given by equation 2.2

$$x = \sqrt{2D\tau}$$

From equation 2.2, a molecule diffuses a million times faster over a length of 10 μm than over 1 cm in the bulk of a liquid. Therefore, mixing is very fast at the micro level, although only mediated by diffusion [8]. Following this line, a large set of micro-chemical reactors arrays can be envisioned. Mixing small amounts of fluid in these parallel micro-reactors will lead to much greater mixing and reaction efficiency.

2.3.2 Scaling in fluid mechanics / microfluidics

Matters related to fluid flow are severely affected by scaling effects, with surface tension becoming predominant.

The flow pattern in different fluid flow situations can be predicted using the Reynolds number (Re) [9,10]. This is a dimensionless quantity of great importance in fluid mechanics. At low Re, the flow is extremely laminar, where mixing fluids in micro-channels is very difficult due to the dominance of viscous forces. Turbulent flow occurs at high Re due to the dominance of inertial forces. The Reynolds number is defined as [11]

$$Re \propto vd\rho/\eta$$

where d is the diameter of the channel, v , ρ and η are the velocity, density and viscosity of the fluid, respectively.

2.4 Micro-Nano fabrication

The fundamentals of MNF explore the science of miniaturization. Modern manufacturing has experienced a significant revolution in miniaturization and integration, evolving at a remarkable pace, as predicted by Moore's law [12], which was pioneered by integrated circuits in the semiconductor industry [13,14], and are, consequently, extended to other applications.

MNF techniques have the ability to control features to the nanometer scale for the highly reproducible mass-fabrication of systems with complex geometries and functionalities; the ability to miniaturize already-existing systems and the capacity to including electronics within structural devices.

Different MNF techniques have emerged to meet ever increasing industrial demands [15]; functional devices with 3D micro/nano-structures exhibit excellent performance over their macroscale counterparts.

The principal MNF techniques are described in this chapter. The applications of MNF techniques in the construction of devices for the study of electronical, chemical, biological, and physical processes are also briefly introduced. For example, the development of microelectromechanical systems (MEMS), ultra-large scale integrated circuits (ULSI), miniaturized total analysis system (m-TAS), and precision optics [13,16,17] etc.

2.4.1 Microfabrication techniques

The microfabrication process utilizes techniques adopted from the well-established field of semiconductors, or techniques that are specifically designed for microfabrication to produce the desired pattern. Photolithography selectively exposes a light sensitive polymer to transfer a customized shape onto the surface

of a material. Soft lithography generates and utilizes the mold of a patterned structure out of an elastic polymer. Film deposition consists of the formation of a micron-thick layer of materials (plastics, silicon-containing compounds, metals, and biomolecules) [18] on the surface of a substrate, playing a structural or functional role. Etching creates topographical features through either chemical or physical processes to selectively removes undesirable materials from the surface of the substrate. Bonding utilizes reversible or irreversible bonding formed between microstructures, with or without the intermediary layers to generate tight seals or to obtain the desired microstructures.

The following section will discuss photolithography and soft lithography in more detail.

Photolithography

Photolithography, also called optical lithography or ultraviolet (UV) lithography, is a simple, cost-effective and readily employed patterning method. It transfers a geometric pattern from a photomask to a light-sensitive photoresist on the substrate by exposing to UV light, which changes the solubility of the exposed resist. The photolithographic technique has been thoroughly reviewed previously [18,19]. Figure 2.3 summarizes the main steps in photolithography.

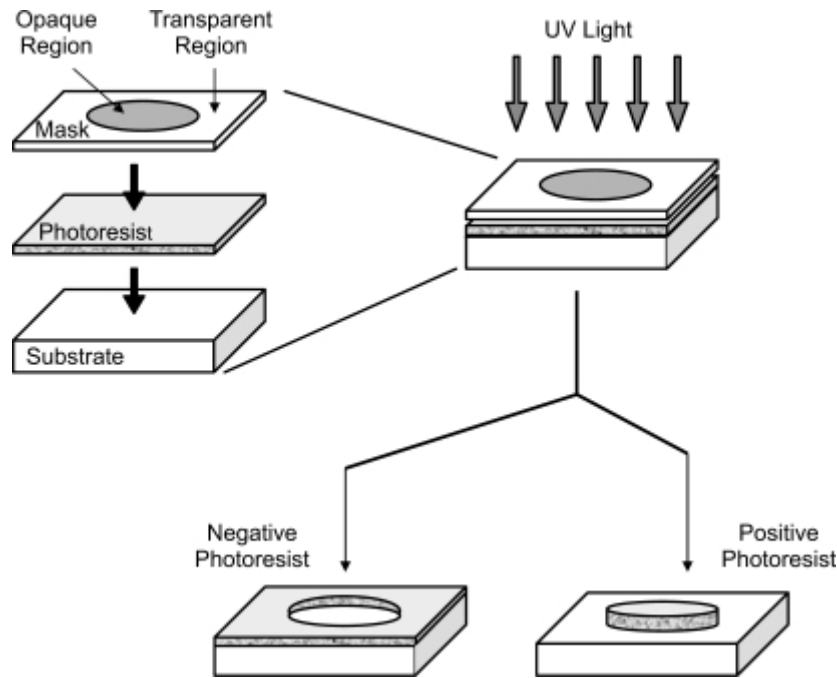


Figure 2.3 Process of photolithography. Adapted from [20], Copyright © 2006 Dove Medical Press Limited.

In the first step, a light-sensitive photoresist is spin-coated onto a substrate material (silicone or glass). A photomask with opaque regions in the desired pattern is placed on top of the substrate and photoresist. In the second step, the assembly is irradiated with UV light, selectively illuminating regions of the photoresist, generating the appropriate pattern. Depending on the purpose of lithography, two kinds of photoresists can be chosen: positive photoresists and negative photoresists. The fundamental difference between these two photoresists is the change in solubility when exposed to light. Upon exposure, a positive photoresist will become more soluble, such as SU-8 [21], while a negative photoresist will become crosslinked.

Photolithography has reached wide acceptance because of the high resolution, stringent requirements regarding alignment and a variety of pattern attributes.

Nonetheless, this technique has the limitation of requiring an electronics-qualified cleanroom facility. Photolithography is not capable of fabricating complicate 3D micro- and nanostructures due to rectilinear light propagation. Little or no control over surface chemistry is provided, thus it is not applicable to curved or non-planar substrates. The feature sizes are also limited by the wavelength of the light source, which ultimately restricts sub-100 nm scale patterning [22,23].

Soft lithography

Soft lithography [19] relies on photolithography to generate the reusable mold. Once the mold is ready, the subsequent fabrication tasks require no clean-room manipulation, only a printing, molding or embossing procedure with an elastomeric stamp is needed.

It provides access to 3D curved and complicated structures, and generates well-defined and controllable surface chemistries [24,25] at a low cost with wide choices of materials.

A large number of patterning techniques, using organic and polymeric materials referred to as soft matter by physicists, form the basis of soft lithography. The elastomeric stamp will generate patterns as relief structures on its surface, the mechanical properties of which are critical to transfer a pattern with high fidelity. Most of work has focused on silicone-based rubber or cross-linked PDMS due to their high stability and easy availability. As examples, the commonly used techniques, microcontact printing (μ CP), replica molding (REM) and solvent assisted micromolding (SAMIM) are described briefly and outlined in Figure 2.4.

μ CP, also known as microstamping, utilizes a PDMS mold to transfer molecules onto the surface of the stamp and are “printed” on a receiving surface upon stamping [18,26,27]. Both REM and SAMIM are based on molding or embossing with an elastomeric stamp. REM [28] transfers the PDMS pattern by solidifying a liquid polymer against the PDMS mold, embossing a structure in the polymer.

SAMIM [29,30] forms patterned structures using soft molds in a polymer under ambient conditions.

Photolithography versus soft lithography

Compared to photolithography, soft lithography has more material choices, as well as experimental simplicity and flexibility. It provides access to 3D structures on nonplanar, curved and soft substrates, and generates well-defined and controllable surface chemistry at a low cost. Nevertheless, it still relies on the use of photolithography to generate the master.

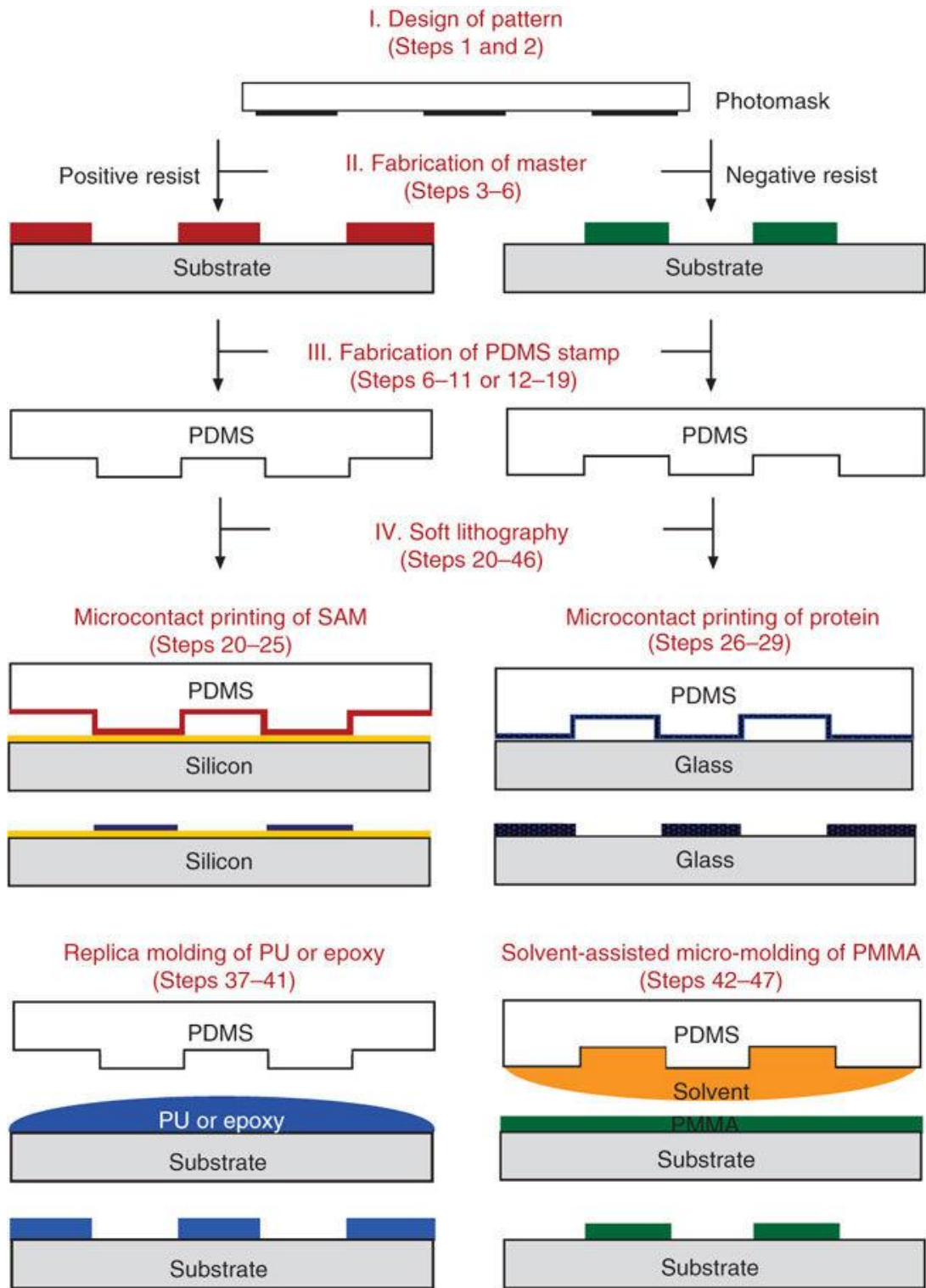


Figure 2.4 Schematic illustration of the four major steps involved in three major soft lithography techniques [31]. Copyright © 2010 Springer Nature.

2.4.2 Nanofabrication techniques

Nanofabrication utilizes similar principles to those of microfabrication to achieve features at the nanoscale range.

Lithography

Different lithographic techniques have been proposed to accomplish this miniaturization and improved quality of the fabricated elements for different purposes.

- **Electron beam/ion lithography (EBL/EIL)**

EBL [32] utilizes an electron beam to pattern a resist while EIL [26] utilizes ions in place of electrons; both are called energy beams. Energy beam techniques introduce surface and sub-surface damage to the workpieces, which reduces their performance. As the electron/ion beam is exposed to a desired region of the resist, the solubility of the resist will be changed. By immersing the resulting film into a developer, selective removal of the resist is achieved.

Specifically, the focused energy beam is used to directly draw custom shapes on an electron/ion-sensitive resist covered surface [32–35]. However, issues of extensive time consumption and high-cost arise.

- **Colloid monolayer lithography**

Colloid monolayer lithography is an economic alternative to energy beam lithographic methods. It utilizes self-organized one- or 2D colloidal layers to fabricate nanostructures [36]. The colloidal layer can be either removed or kept in place afterwards based on application.

The spatial distribution array depends on the size and geometry of the colloidal particles, colloid concentration, and other parameters.

Colloidal silica spheres can also act as lenses, intensifying the laser beam effect on the substrate, used for high throughput patterning of nanoholes [37].

- **X-ray lithography**

This technique employs soft X-rays to transfer a desired pattern from a mask to a substrate [26].

- **Ion projection lithography**

Ion projection lithography employs a mask to prevent exposure of the designed region from hydrogen or helium ions [26].

- **Nano imprint lithography**

Nanoimprint lithography (NIL) has attracted considerable attention as one of the most prominent lithographic techniques. NIL uses a mold to define the nanoscale deformation of a resist, cured either by heat (thermoplastic) or UV (photocuring resist). After removal of the mold, the patterned resist can be used as is or treated with subsequent techniques to generate either a final device or a new mold for further processing.

The earliest form of NIL proposed by Chou et al. [39–41], based on thermoplastic polymers as resist materials, as a new nonconventional lithographic nanostructure manufacturing method, which has been developed and investigated since.

Principle

Standard thermoplastic NIL has three basic steps, as shown in Figure 2.5. In the first step, a mold predefined with topological patterns is pressed against the thermoplastic resist spin-coated substrate with increased temperature and elevated pressure. Above the glass transition temperature, the resist becomes a viscous liquid and can therefore be readily deformed into the mold. The pattern on the mold is transferred onto the softened resist, and after being cooled down, the resist hardens.

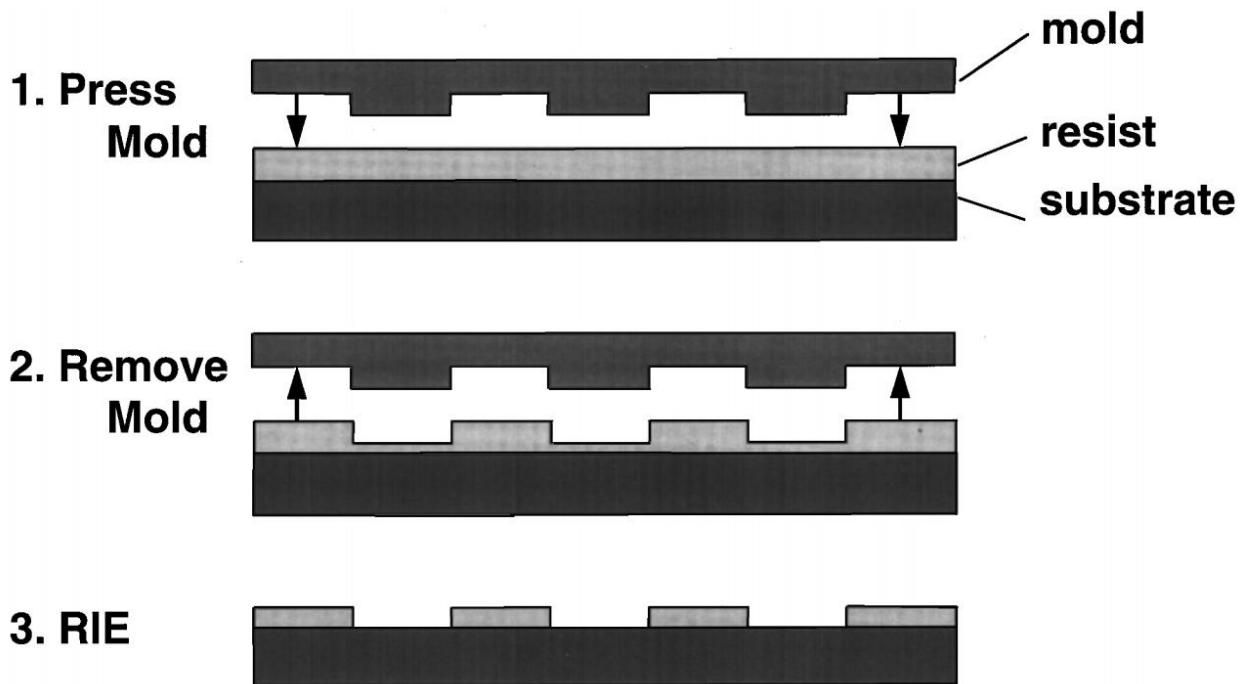


Figure 2.5 Schematic process of nanoimprint lithography [40]. Copyright © 1996 American Vacuum Society.

The mechanical deformation creates a thick contrast pattern in the resist, which enables grayscale lithography with only a single patterning step. No other conventional lithography techniques are able to achieve this [43]. The patterned resist remains on the substrate after removing the mold. In the third step, the pattern is transferred using an anisotropic etching method.

NIL does not utilize energetic beams; thus, it is more of a physical than chemical process, and is fundamentally different from stamping using a monolayer of self-assembled molecules. Therefore, the resolution of NIL is not limited by issues such as wave diffraction, scattering and interference in a resist and backscattering from a substrate.

Since the initial idea of NIL was proposed, numerous studies and improvements have been suggested; these studies have maximized its effectiveness in patterning

by minimizing its limitations. Specifically, photo-NIL has been proposed in order to substitute the high temperature required to soften the thermoplastic resist with UV-light to harden the resist for pattern transferring [44–50]. Based on these two hardening methods, three different types of nanoimprint lithography methods have been suggested in order to achieve high resolution, large-area, and low-cost patterns with different advantages and disadvantages: soft-mold NIL, hard-mold NIL, and hybrid-mold NIL, as shown in Table 2.3. A summary of various soft mold materials in detail is shown in Table 2.4. Micro lens arrays with two focal lengths fabricated using NIL is shown in Figure 2.6.

Table 2.3 Pros, cons, and research improvements for NIL based on hard mold, soft mold, and hybrid molds [38]. Copyright © 2016 B. Kwon and Jong H. Kim.

Lithography types	Example	Pros	Cons	Improvements
Hard mold	Silicon, Quartz	High resolution (<100 nm), high chemical stability, high mechanical strength for high aspect-ratio features	Low defect accommodation, high-cost, breakage of the mold during demolding, difficult fabrication process for the working molds	Use of blade for demolding to minimize the breakage of the molds, use of hydrophobic silane layers to coat the molds to avoid accumulation of resist
Soft mold	ETFE, PDMS, PFPE, PET	Generous defect accommodation, easiness of fabricating working molds, flexibility for nonflat surface, high chemical stability, cost-effectiveness	Low resolution (>150 nm), relatively low mechanical strength for high aspect-ratio features	Development of various types of functional polymers in order to enhance the mechanical strength and chemical stability for resolution improvement
Hybrid mold	MINS, Ormostamp, I-UVM-100	Combination of advantages of hard and soft molds	Relatively longer fabrication process compared to soft working molds	Introduction of the hydrophobic silane chain to the molds in order to reduce coating time to avoid resist accumulation

Chapter 2 Micro-Nano fabrication

Table 2.4 Summary of various soft mold materials adapted from [42], Copyright © 2013 Lan; licensee InTech.

Item	Sub-class	Young's Modulus (MPa)	Surface Energy (mN/m)	Viscosity (mPa.s)	Curing mode	
PDMS-based materials	s-PDMS	< 2	21-24	~3900	Thermal	
	h-PDMS	8-12	~20	Tunable	Thermal	
	X-PDMS	~80			Thermal	
	hv-PDMS	~3-4	~20		UV-Light	
Fluorinated polymer materials	PFPE-based materials	PFPE	4	12		UV-Light
		HPFPE	4-5.4	17-22	300-900	UV-Light
		a-PFPE	10.5	~18.5	60 cps at 25 °C	UV light
		PFPE-DMA	4	16.3	360	UV light
	ETFE	~1.2GPa	15.6			Thermal
	Teflon AF 2400	1.6 GPa	~16			Thermal
UV curable materials	PUA	2.7 GPa	23			UV light
	Modulus-tunable UV-curable materials	Tunable 19.8-320				UV light
	Ormostamp	650		750		UV-curable

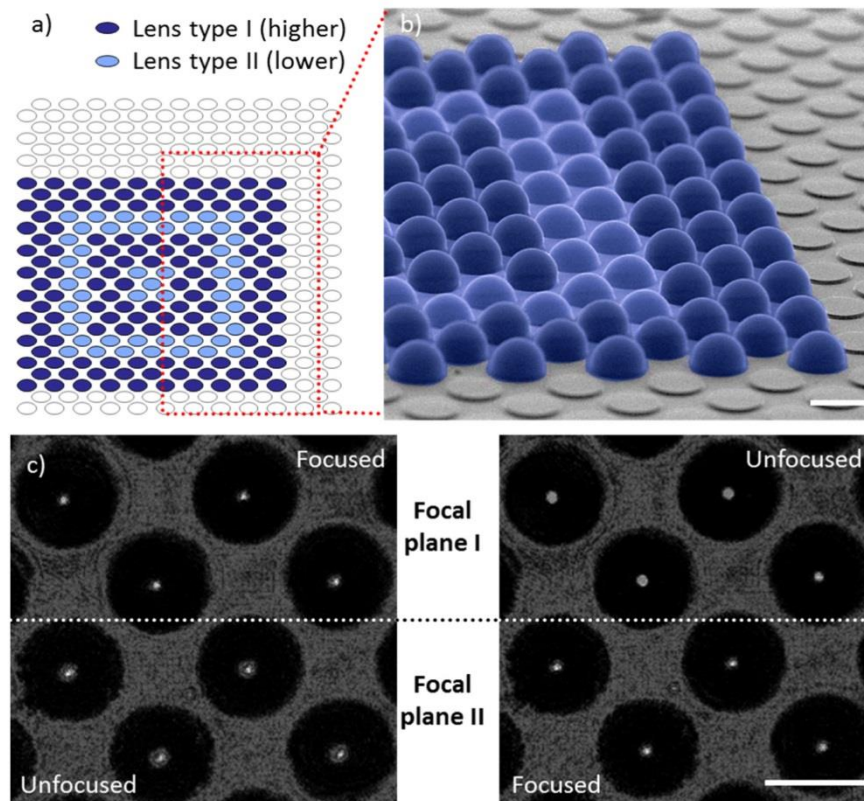


Figure 2.6 Micro lens arrays with two focal lengths fabricated using NIL. a) Schematic and b) SEM images of micro lens arrays of varying shapes patterned by NIL. c) Optical images of the lens type 1 (left) and type 2 (right) in black & white. Scale bars are 100 μm . Reproduced from [51], Copyright © 2015 Optical Society of America.

Molecular self-assembly

Molecular self-assembly is based on thermodynamically favored interactions of organic or inorganic molecules [52,53], namely DNA, proteins and peptides, to control pattern formation at the sub-nanometer scale. Molecules are brought together into energetically stable conformations. This spontaneous movement is favored by noncovalent forces, such as hydrophobic, electrostatic interactions, van der Waals, hydrogen bonding, etc.

Electrically induced nanopatterning

Electrically induced nanopatterning consists of two electrodes separated by an air gap δ as indicated, in Figure 2.7. A thin dielectric material liquid film is applied to the bottom electrode. When exposed to an external magnetic field, an electric field gradient is generated. The technique utilizes electrostatic interactions between the film and the gradient to produce nanoscale lateral patterns and structures [54]. Porous template for nanowire array with high densities can be fabricated using the technique [55].

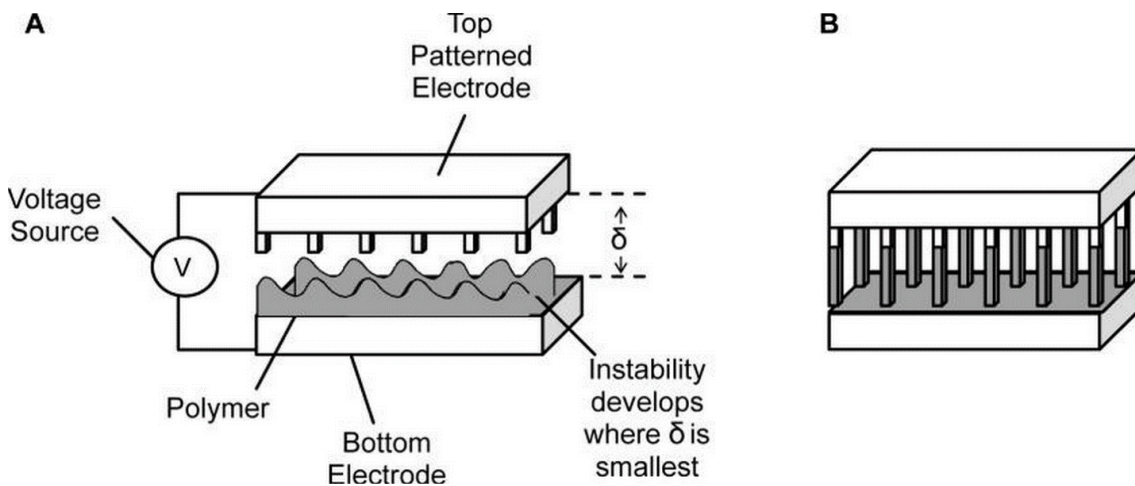


Figure 2.7 Schematic of electrically-induced nanopatterning process. Based on a figure from [54], Copyright © 2000 Springer Nature.

Rapid prototyping

The overall process – from the generation of complex geometrical patterns to the fabrication of functional multi-layered structures, structures with chemical functionality [37,56] and scaffolds for tissue engineering [57] – is referred to as 'rapid prototyping' [58].

2.4.3 Materials for Desktop MNF and applications

Remarkable advances of material sciences and technologies have helped to transition MNF from a cleanroom environment to a desktop setup. In addition to the conventional silicone-based materials, a rapidly growing number of new functional materials, as listed in Table 2.5 [59], have been introduced to MNF society [60].

For instance, environmentally responsive materials can find their applications in biosensing and bio-manipulation platforms [61], identifying changes in pressure, temperature, or target molecules, controlling release systems to analyze their environment, controlling the release of therapeutic agents, modifying the targeting and release properties of biodegradable nanoparticles [62,63], and functionalizing biological micro-nanosystems [64] made out of flexible polymers. Also, nanoscale building elements form scaffolds for tissue engineering [65,66].

Table 2.5 Different materials used in MNF, adapted from [59], Copyright © 2010 Tingrui Pan, Wei Wang, open access at Springerlink.com.

Material categories	Representative materials	Typical micro-nanofabrication methods	Biocompatibility and toxicity	Biomedical applications
Thermoset polymers	PDMS	Molding	Biocompatible	Used in almost all microfluidic and bio-/nanopatterning applications
	PMMA	Hot embossing	Biocompatible	Construct for microfluidics
Thermoplastic polymers	COC	Hot embossing	Biocompatible	Used in optofluidic applications primarily
	Polystyrene/polyolefin	Heat-activated	Biocompatible	Device packaging; pattern transfer; cell culture

Chapter 2 Micro-Nano fabrication

		shrinkage		platform
	SU8	Lithography	Toxic	Master for microfluidics and bio/nanopatterning
	KMPR			
	Dry film	Lithography	Biocompatible	Master for microfluidics and bio/nanopatterning
Photopatternable polymers	PEG	Lithography	Biocompatible	Used in cellular and biomolecular investigations and implantations
	Thiolene	Lithography	Biocompatible	Solvent-resistant for biocompatible applications
	Photopatternable PDMS	Lithography, molding	Usually toxic due to the additive chemicals	Construct for microfluidics; device packaging
	Nanoparticles	Self-assembly	Under study	Nanofluidics, nanosensing, nanomanipulation
Nanomaterials	Nanofiber	Electrospinning	Depended on the used polymer, usually biocompatible	2D/3D cell culture scaffold
	Nanocomposites	Molding	Depended on the functional components	Providing conductive, hydrophobic properties
	Silk	Electrospinning	Biocompatible after surface treatment	2D/3D cell culture scaffold, implantation
Biological materials	DNA	Self assembly	Biocompatible	Nanomachinery, 3D nanostructures
	Virus	Self assembly	Biocompatible	Nanomachine, nanostructure synthesis
	Chitosan	Electrodeposition	Biocompatible	Bioactive coating

Nanofabrication utilizes cutting edge technology and is prominent in the high end manufacture industry, for instance, high-tech microchips and microcontrollers using different materials. It has attracted scientists working in the military, aerospace and medical industries. It deals with the composition and properties of atoms in a material, managing to save space, time and money.

Integrated circuits

The introduction of nanofabrication has revolutionized integrated circuits (ICs), a crucial part of electronic devices industry for many decades. The programmable nanomachines allows for fabrication of circuits atom by atom, analogous to the construction of a building brick by brick.

Biomedical research

In addition, MNF opens up doors to the study and manipulate molecules, cells, and tissues. It allows for the investigation of pathological mechanisms and novel treatment options by constructing new synthetic systems. Physiological responses can also be altered through MNF. Figure 2.8 shows the MNF application in biomedical research, which is a 3D microfluidic on the paper-based substrate for point of care. Point-of-care diagnostics, integrated cell culture as well as micro-nanosopic bio-manipulation have advanced greatly thanks to MNF techniques.

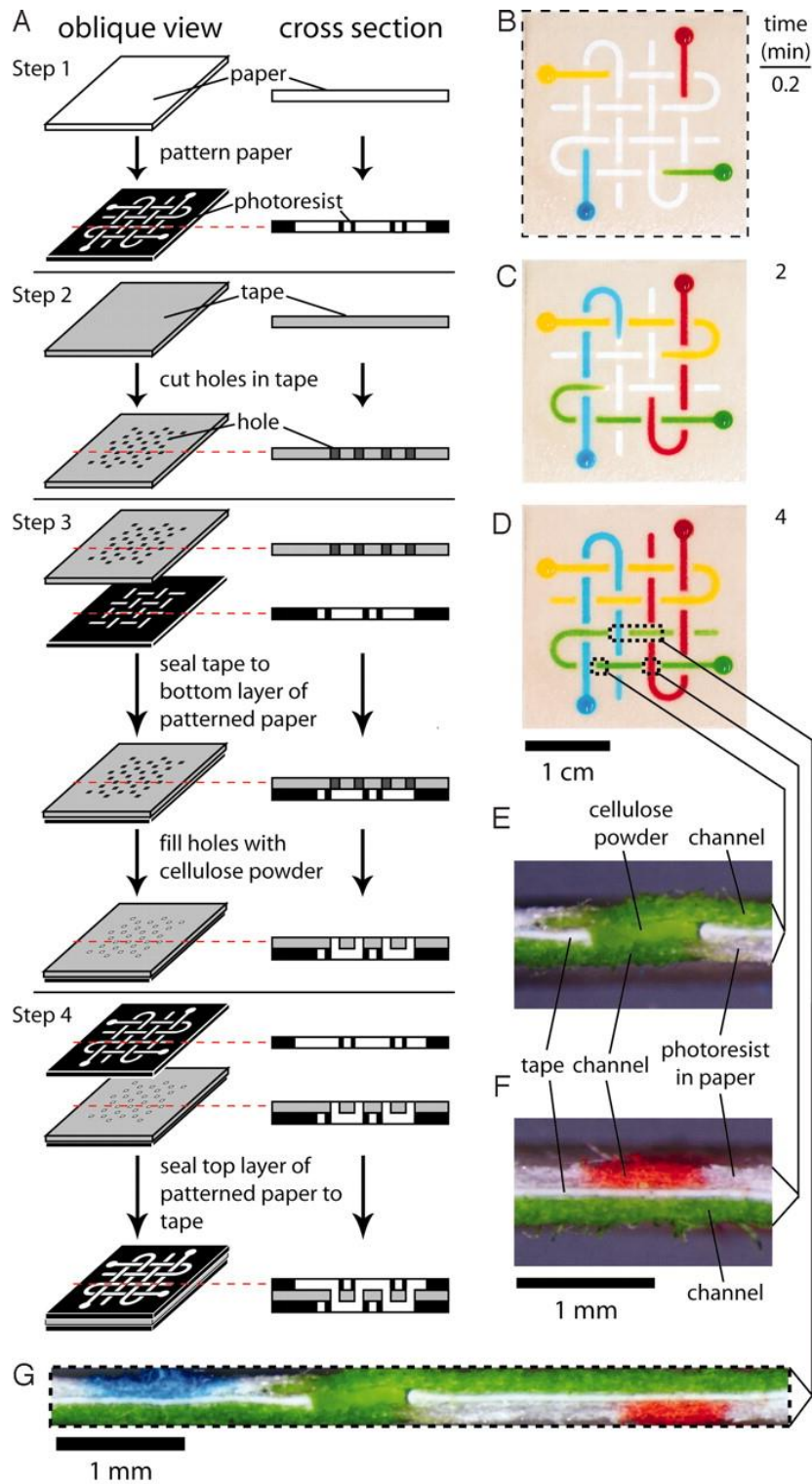


Figure 2.8 Application of MNF in biomedical research. 3D microfluidic on the paper-based substrate adapted from [71]. Copyright © 2008 National Academy of Sciences. U.S.A.

Drug delivery devices

MNF produces drug delivery vehicles with capabilities surpassing the current drug delivery systems by accurate control their size, topography, architecture, and functionality. Those drug delivery vehicles functionalize in a highly predictable manner, both *in vitro* and *in vivo*.

Drug delivery systems include injectable micro- and nanodevices, implantable, transdermal devices (stents for drug delivery), and microfabricated bio- and muco-adhesive systems; microneedles for transdermal drug delivery devices [67–69] are also described [20]. Figure 2.9 shows an example of RIE fabricated solid silicon microneedles.

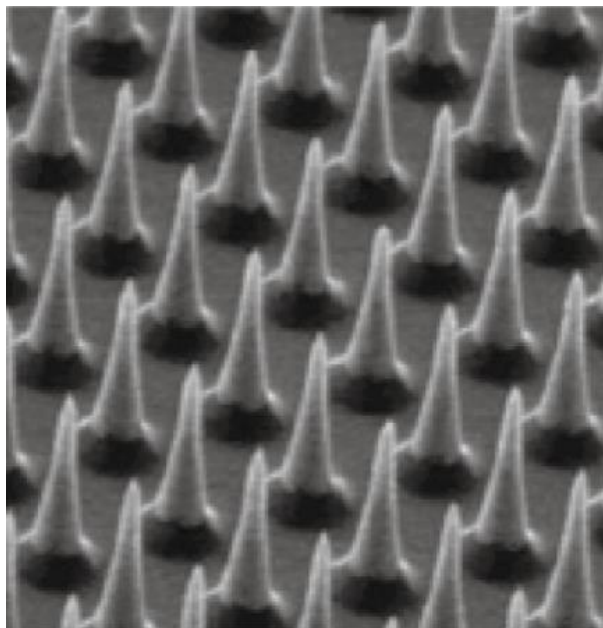


Figure 2.9 RIE prepared silicon microneedles (25 μ m in height) for transdermal drug delivery. Reproduced from [70]. Copyright © 2003 National Academy of Sciences, U.S.A.

References

- [1] biotechnology G W-N and 2003 undefined The'right'size in nanobiotechnology *nature.com*
- [2] Madou M J 2002 *Fundamentals of microfabrication: the science of miniaturization* (CRC Press)
- [3] Moore G E 1965 Cramming more components onto integrated circuits (Reprinted from Electronics, pg 114-117, April 19, 1965) *Proc. Ieee* **86** 82–5
- [4] Moore G E 2005 Excerpts from A Conversation with Gordon Moore: Moore's Law *Intel* 1–2
- [5] Ghosh A Scaling Laws, doi:10.1007/978-1-4419-9601-5_2.
- [6] Kardaun O J W F 2005 *Classical methods of statistics : with applications in fusion-oriented plasma physics* (Springer)
- [7] Machinery M 2018 Nanosystems : Molecular Machinery , Manufacturing , and Computation Detailed Table of Contents : 1–9
- [8] Jakeway S C, de Mello A J and Russell E L Miniaturized total analysis systems for biological analysis. *Fresenius. J. Anal. Chem.* **366** 525–39
- [9] Reynolds O 1883 An Experimental Investigation of the Circumstances Which Determine Whether the Motion of Water Shall Be Direct or Sinuous, and of the Law of Resistance in Parallel Channels *Philos. Trans. R. Soc. London* **174** 935–82
- [10] Kron C P A J 1994 Method for performing amplification of nucleic acid with two primers bound to a single solid support
- [11] Sommerfeld A 1908 Ein beitrag zur hydrodynamischen erklaerung der turbulenten fluessigkeitsbewegungen *Atti del* **4** 116–24
- [12] Moore G E 1995 Lithography and the future of Moore's law, doi:10.1117/12.209195.
- [13] H. Park and M. Kraatz et al. 2009 *Advanced Nanoscale ULSI Interconnects: Fundamentals and Applications* vol 49
- [14] Haselman M and Hauck S 2010 The Future of Integrated Circuits: A Survey of Nanoelectronics *Proc. IEEE* **98** 11–38
- [15] Zhan D, Han L, Zhang J, He Q, Tian Z-W and Tian Z-Q 2017 Electrochemical micro/nano-machining: principles and practices *Chem. Soc. Rev.* **46** 1526–44

Chapter 2 Micro-Nano fabrication

- [16] Torsten Villkner †, Dirk Janasek ‡ and Andreas Manz* ‡ 2004 Micro Total Analysis Systems. Recent Developments
- [17] Suleski T J and Kolste R D T 2005 Fabrication trends for free-space microoptics *J. Light. Technol.* **23** 633–46
- [18] Voldman J, Gray M L and Schmidt M A 1999 Microfabrication in Biology and Medicine *Annu. Rev. Biomed. Eng.* **1** 401–25
- [19] Li N, Tourovskaia A and Folch A 2003 Biology on a chip: microfabrication for studying the behavior of cultured cells. *Crit. Rev. Biomed. Eng.* **31** 423–88
- [20] Betancourt T and Brannon-Peppas L 2006 Micro-and nanofabrication methods in nanotechnological medical and pharmaceutical devices *Int. J. Nanomedicine* **1** 483–95
- [21] Becker H and Gärtner C 2000 Polymer microfabrication methods for microfluidic analytical applications *Electrophoresis* **21** 12–26
- [22] Chance T A L W 1988 Reduced mask manufacture of semiconductor memory devices
- [23] Yablonovitch E and Vrijen R B 1999 Optical projection lithography at half the Rayleigh resolution limit by two-photon exposure *Opt. Eng.* **38** 334
- [24] Xia Y and Whitesides G M 1998 SOFT LITHOGRAPHY *Annu. Rev. Mater. Sci.* **28** 153–84
- [25] Xia Y and Whitesides G M 1998 Soft Lithography *Angew. Chemie Int. Ed.* **37** 550–75
- [26] Chen Y and Pépin A 2001 Nanofabrication: Conventional and nonconventional methods *Electrophoresis* **22** 187–207
- [27] Curtis A and Wilkinson C 2001 Nanotechniques and approaches in biotechnology. *Trends Biotechnol.* **19** 97–101
- [28] Xia Y, McClelland J J, Gupta R, Qin D, Zhao X-M, Sohn L L, Celotta R J and Whitesides G M 1997 Replica molding using polymeric materials: A practical step toward nanomanufacturing *Adv. Mater.* **9** 147–9
- [29] King E, Xia Y, Zhao X-M and Whitesides G M 1997 Solvent-assisted microcontact molding: A convenient method for fabricating three-dimensional structures on surfaces of polymers *Adv. Mater.* **9** 651–4
- [30] Xia Y, Zhao X-M, Kim E and Whitesides G M 1995 A Selective Etching Solution for Use with Patterned Self-Assembled Monolayers of Alkanethiolates on Gold *Chem. Mater.* **7** 2332–7

- [31] Qin D, Xia Y and Whitesides G M 2010 Soft lithography for micro- and nanoscale patterning *Nat. Protoc.* **5** 491–502
- [32] Gates B D, Xu Q, Stewart M, Ryan D, Willson C G and Whitesides G M 2005 New Approaches to Nanofabrication: Molding, Printing, and Other Techniques *Chem. Rev.* **105** 1171–96
- [33] Stewart M E, Mack N H, Malyarchuk V, Soares J A N T, Lee T-W, Gray S K, Nuzzo R G and Rogers J A 2006 Quantitative multispectral biosensing and 1D imaging using quasi-3D plasmonic crystals *Proc. Natl. Acad. Sci.* **103** 17143–8
- [34] Backofen U, Matysik F-M and Lunte C E 2002 A Chip-Based Electrophoresis System with Electrochemical Detection and Hydrodynamic Injection *Anal. Chem.* **74** 4054–9
- [35] Odom T W, Love J C, Wolfe D B, Paul K E and Whitesides G M 2002 Improved Pattern Transfer in Soft Lithography Using Composite Stamps *Langmuir* **18** 5314–20
- [36] Burmeister F, Badowsky W, Braun T, Wieprich S, Boneberg J and Leiderer P 1999 Colloid monolayer lithography - a flexible approach for nanostructuring of surfaces *Appl. Surf. Sci.* **144–145** 461–6
- [37] Lu Y and Chen S C 2004 Micro and nano-fabrication of biodegradable polymers for drug delivery *Adv. Drug Deliv. Rev.* **56** 1621–33
- [38] Kwon B and Kim J H 2016 Importance of Molds for Nanoimprint Lithography: Hard, Soft, and Hybrid Molds *J. Nanosci.* **2016** 1–12
- [39] Chou S Y, Krauss P R and Renstrom P J 1995 Imprint of sub-25 nm vias and trenches in polymers *Appl. Phys. Lett.* **67** 3114–6
- [40] Chou S Y, Krauss P R and Renstrom P J 1996 Nanoimprint lithography *J. Vac. Sci. Technol. B* **14** 4129–33
- [41] Chou S Y, Krauss P R and Renstrom P J 1996 Imprint Lithography with 25-Nanometer Resolution *Science (80-.)*. **272** 85–7
- [42] Lan H 2013 Soft UV Nanoimprint Lithography and Its Applications *Updates in Advanced Lithography*
- [43] Barcelo S and Li Z 2016 Nanoimprint lithography for nanodevice fabrication *Nano Converg.* **3** 21
- [44] Choi S-J, Yoo P J, Baek S J, Kim T W and Lee H H 2004 An Ultraviolet-Curable Mold for Sub-100-nm Lithography *J. Am. Chem. Soc.* **126** 7744–5
- [45] Ahn S H and Guo L J 2009 Large-Area Roll-to-Roll and Roll-to-Plate

Nanoimprint Lithography: A Step toward High-Throughput Application of Continuous Nanoimprinting *ACS Nano* **3** 2304–10

- [46] Ahn S H and Guo L J 2008 High-Speed Roll-to-Roll Nanoimprint Lithography on Flexible Plastic Substrates *Adv. Mater.* **20** 2044–9
- [47] Weiss D N, Meyers S T and Keszler D A 2010 All-inorganic thermal nanoimprint process *J. Vac. Sci. Technol. B, Nanotechnol. Microelectron. Mater. Process. Meas. Phenom.* **28** 823–8
- [48] Koo N, Plachetka U, Otto M, Bolten J, Jeong J, Lee E and Kurz H 2008 The fabrication of a flexible mold for high resolution soft ultraviolet nanoimprint lithography *Nanotechnology* **19** 225304
- [49] Koo N I, Bender M, Plachetka U, Fuchs A, Wahlbrink T, Bolten J and Kurz H 2007 Improved mold fabrication for the definition of high quality nanopatterns by soft UV-nanoimprint lithography using diluted PDMS material *Microelectron. Eng.* **84** 904–8
- [50] Guo L J 2004 Topical Review: Recent progress in nanoimprint technology and its applications *J. Phys. D Appl. Phys.* R123–41
- [51] Jacot-Descombes L, Cadarso V J, Schleunitz A, Grützner S, Klein J J, Brugger J, Schiff H and Grützner G 2015 Organic-inorganic-hybrid-polymer microlens arrays with tailored optical characteristics and multi-focal properties *Opt. Express* **23** 25365
- [52] Rajagopal K and Schneider J P 2004 Self-assembling peptides and proteins for nanotechnological applications *Curr. Opin. Struct. Biol.* **14** 480–6
- [53] science G D- and 1997 undefined Fuzzy nanoassemblies: toward layered polymeric multicomposites *science.sciencemag.org*
- [54] Schäffer E, Thurn-Albrecht T, Russell T P and Steiner U 2000 Electrically induced structure formation and pattern transfer *Nature* **403** 874–7
- [55] Thurn-Albrecht T, Schotter J, Kästle G A, Emley N, Shibauchi T, Krusin-Elbaum L, Guarini K, Black C T, Tuominen M T and Russell T P 2000 Ultrahigh-density nanowire arrays grown in self-assembled diblock copolymer templates. *Science* **290** 2126–9
- [56] Fan H, Lu Y, Stump A, Reed S T, Baer T, Schunk R, Perez-Luna V, López G P and Brinker C J 2000 Rapid prototyping of patterned functional nanostructures *Nature* **405** 56–60
- [57] Yeong W-Y, Chua C-K, Leong K-F and Chandrasekaran M 2004 Rapid prototyping in tissue engineering: challenges and potential *Trends Biotechnol.* **22** 643–52

Chapter 2 Micro-Nano fabrication

- [58] Qin D, Xia Y, Materials G W-A and 1996 undefined Rapid prototyping of complex structures with feature sizes larger than 20 μm *Wiley Online Libr.*
- [59] Pan T and Wang W 2011 From Cleanroom to Desktop: Emerging Micro-Nanofabrication Technology for Biomedical Applications *Ann. Biomed. Eng.* **39** 600–20
- [60] Quake S R and Scherer A 2000 From micro- to nanofabrication with soft materials. *Science* **290** 1536–40
- [61] Mendes P M 2008 Stimuli-responsive surfaces for bio-applications *Chem. Soc. Rev.* **37** 2512
- [62] Blanchette J, Kavimandan N and Peppas N A 2004 Principles of transmucosal delivery of therapeutic agents *Biomed. Pharmacother.* **58** 142–51
- [63] Brannon-Peppas L and Blanchette J O 2004 Nanoparticle and targeted systems for cancer therapy *Adv. Drug Deliv. Rev.* **56** 1649–59
- [64] Liu C 2007 Recent Developments in Polymer MEMS *Adv. Mater.* **19** 3783–90
- [65] Seidlits S K, Lee J Y and Schmidt C E 2008 Nanostructured scaffolds for neural applications *Nanomedicine* **3** 183–99
- [66] Zhang L, today T W-N and 2009 undefined Nanotechnology and nanomaterials: promises for improved tissue regeneration *Elsevier*
- [67] Henry S, McAllister D V, Allen M G and Prausnitz M R 1998 Microfabricated microneedles: a novel approach to transdermal drug delivery. *J. Pharm. Sci.* **87** 922–5
- [68] Kaushik S, Hord A H, Denson D D, McAllister D V, Smitra S, Allen M G and Prausnitz M R 2001 Lack of pain associated with microfabricated microneedles. *Anesth. Analg.* **92** 502–4
- [69] Tao S L and Desai T A 2003 Microfabricated drug delivery systems: from particles to pores. *Adv. Drug Deliv. Rev.* **55** 315–28
- [70] McAllister D V, Wang P M, Davis S P, Park J-H, Canatella P J, Allen M G and Prausnitz M R 2003 Microfabricated needles for transdermal delivery of macromolecules and nanoparticles: fabrication methods and transport studies. *Proc. Natl. Acad. Sci. U. S. A.* **100** 13755–60
- [71] Martinez A W, Phillips S T and Whitesides G M 2008 Three-dimensional microfluidic devices fabricated in layered paper and tape. *Proc. Natl. Acad. Sci. U. S. A.* **105** 19606–11

Chapter 3

Microfluidic systems and “lab-on-a-chip”

Microfluidic systems or “lab-on-a-chip” (LOC) is a subset of microelectromechanical system (MEMS) devices and are often referred to as “micro total analysis systems” (μ TAS) or miniaturized analysis systems. Since its inception [1,2], it has revolutionized many aspects of quantitative biochemistry and analytical chemistry. The concept of μ TAS was proposed by Manz et.al. [3], in which sample pre-treatment, separation and detection were incorporated into silicon chip analyzers.

Both the growing number and improved quality of published scientific articles and patents reflect the importance of μ TAS, spanning from basic research to commercial applications [4]. It is highly multidisciplinary and serves as a focal point to bring together multidisciplinary research fields, including electronics, physics, chemistry and biology, among others. It deals with the precise control and manipulation of the behavior of fluids that are constrained on a single integrated chip with size from mm to a few square cm.

Typical advantages [5–7] are summarized in Table 3.1.

Table 3.1 Typical advantages of microfluidics systems

Compactness of the systems, allowing massive parallelization, leading to high throughput
Low fluid volumes consumption and cost effectiveness
Faster analysis and response times which leading to better process control and part quality verification [8]
Cost-effective disposable chips, allowing fabrication in mass production [9]

Chapter 3 Microfluidic systems and “lab-on-a-chip”

The most prominent disadvantages [10] are summarized in Table 3.2.

Table 3.2 Typical disadvantages of microfluidics systems

The micro-manufacturing process can be complex and labor intensive [11]
Most LOCs are novel proof of concepts, fully developed for widespread use needs time [12]
Effects of micro domain [12], making lab processes replication quite challenging and more complex

Advances in microfluidics technology have revolutionized molecular biology procedures for DNA analysis, e.g. polymerase chain reaction (PCR) and DNA sequencing; LOC systems for synthesis and analysis; microchips for drug screening [13] and cell culture. The basic idea of microfluidic biochips involves integrating the total sequence of lab processes, such as assay operations including sample preparation, pre-treatment and detection on a single chip [14]. In this thesis, the focus is put on PCR, where PCR is analyzed from analogue to digital and from the microscale to nanoscale.

3.1 Microfluidic Sanger sequencing

With the development of microfluidics, Sanger sequencing, described earlier, was performed on a microfluidic platform to reduce reagent usage as well as cost. The entire amplification as well as the separation of DNA fragments is integrated on a single glass wafer [15]. Microchips were applied to increase the throughput of conventional sequencing [16].

3.2 Polymerase chain reaction

Polymerase chain reaction (PCR) is a reliable way to repeatedly replicate a particular DNA sequence across several orders of magnitude in a short time with sufficient reaction components, including double-stranded DNA (dsDNA), $MgCl_2$, Tris-Cl, and four deoxynucleoside triphosphates (A, T, C, G), as well as primers. The method was conceived in the spring of 1983 by Kary Mullis [17–20] and is applicable to a large number of fields in modern biology and related sciences [21], such as biomedical research, criminal forensics, and molecular archaeology [22]. A schematic diagram of PCR is shown in Figure 3.1, where T_m denotes melting temperature.

Chapter 3 Microfluidic systems and “lab-on-a-chip”

Polymerase Chain Reaction - PCR

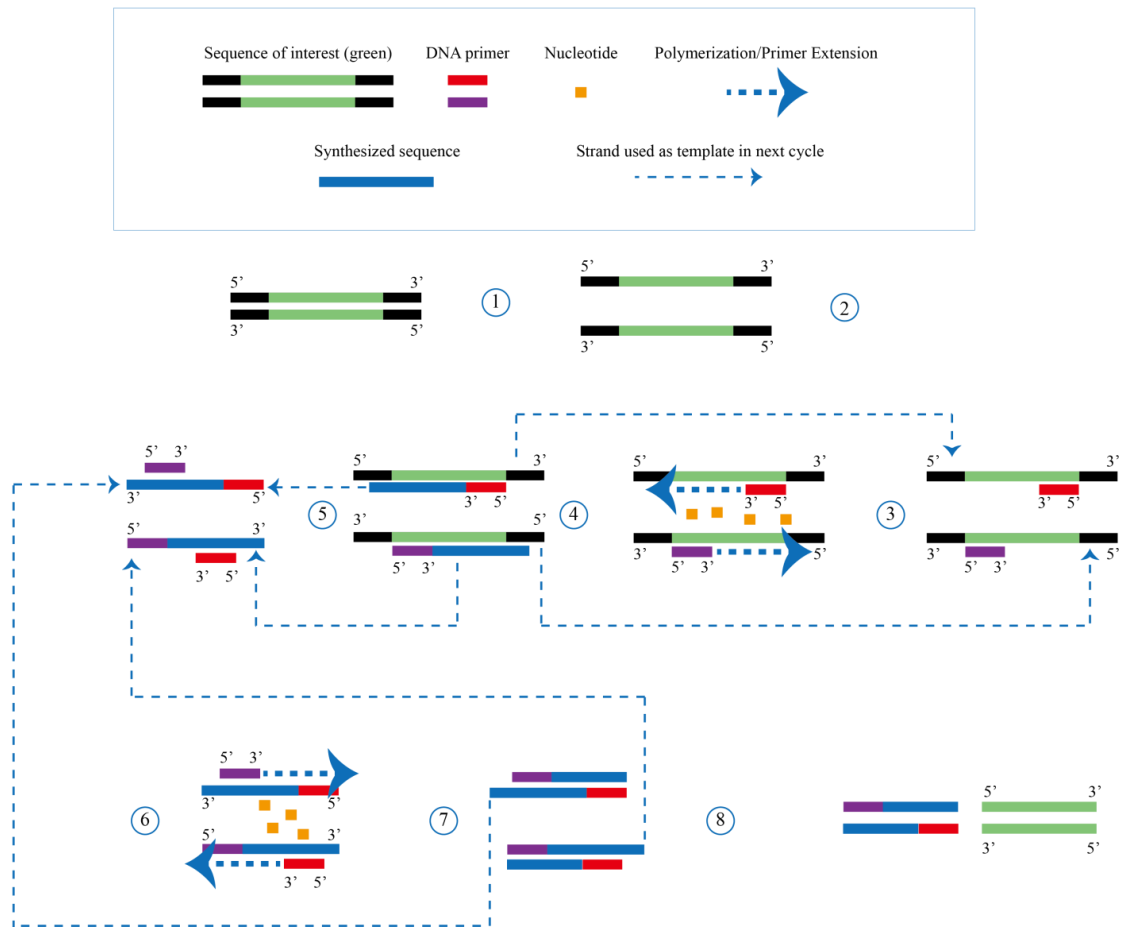


Figure 3.1 Color-coded diagram of PCR, 1. The DNA double helix is denatured at around 95°C and the strands separate. 2. The temperature is decreased to slightly below the melting temperature of the primers being used. Both primers hybridize to the complementary single-strand of DNA. These primers are supplied in excess to ensure that the strands do not re-anneal to one another. 3. Polymerization (extension) occurs via a DNA polymerase in the 5' to 3' direction on each strand. 4. The incorporated nucleotides give rise to new strands that extend past the sequence of interest. 5. The previously polymerized strands act as a template for the other primer (see the blue, thin dotted arrow). 6. Polymerization occurs via DNA polymerase in the 5' to 3' direction on each strand, this time stopping at the end of the sequence of interest. 7. The incorporated nucleotides give rise to new strands that encode the sequence of interest. 8. The synthesized strands encoding the sequence of interest anneal to one another to form the end product.

Chapter 3 Microfluidic systems and “lab-on-a-chip”

An important observation can be seen in Figure 3.1, where the original template will denature to a new single stranded DNA (ssDNA) of indefinite length [19] limited by the length of the template. The ssDNA of indefinite length in the subsequent cycles will produce ssDNA of length defined by the forward and reverse primers. As a result, the amount of indefinite length product increases linearly with cycle number while the amount of amplicon with a length defined by primers increases exponentially [23]. The product with an indefinite length can be negligible compared to the exponential growth of the desired fragment of DNA; subsequent detection methods using gel electrophoresis, an Agilent BioAnalyzer or melting curve analysis (MCA).

3.2.1 Quantification of DNA

Gel electrophoresis

Gel electrophoresis is a method used to separate and analyze DNA, RNA, proteins and their fragments [24], or as a preparative technique prior to mass spectrometry (MS), DNA sequencing, or Southern blotting for further characterization.

Gel electrophoresis is usually performed for analytical purposes. Before the invention of real-time PCR, DNA gel electrophoresis was often performed to analyze the amplification results of PCR, in terms of specificity, relative amounts and length. This involves using an electric field to move the charged molecules through a matrix of agarose or other substances, based on their size and charge [25].

Since DNA is negatively charged, a mixed population of DNA fragments will be separated when pulled toward the positively charged end of the gel. It can be used to estimate the size of DNA and check the specificity of PCR result. Figure 3.2 shows an example of gel analysis with each band denoting a specific size of DNA.

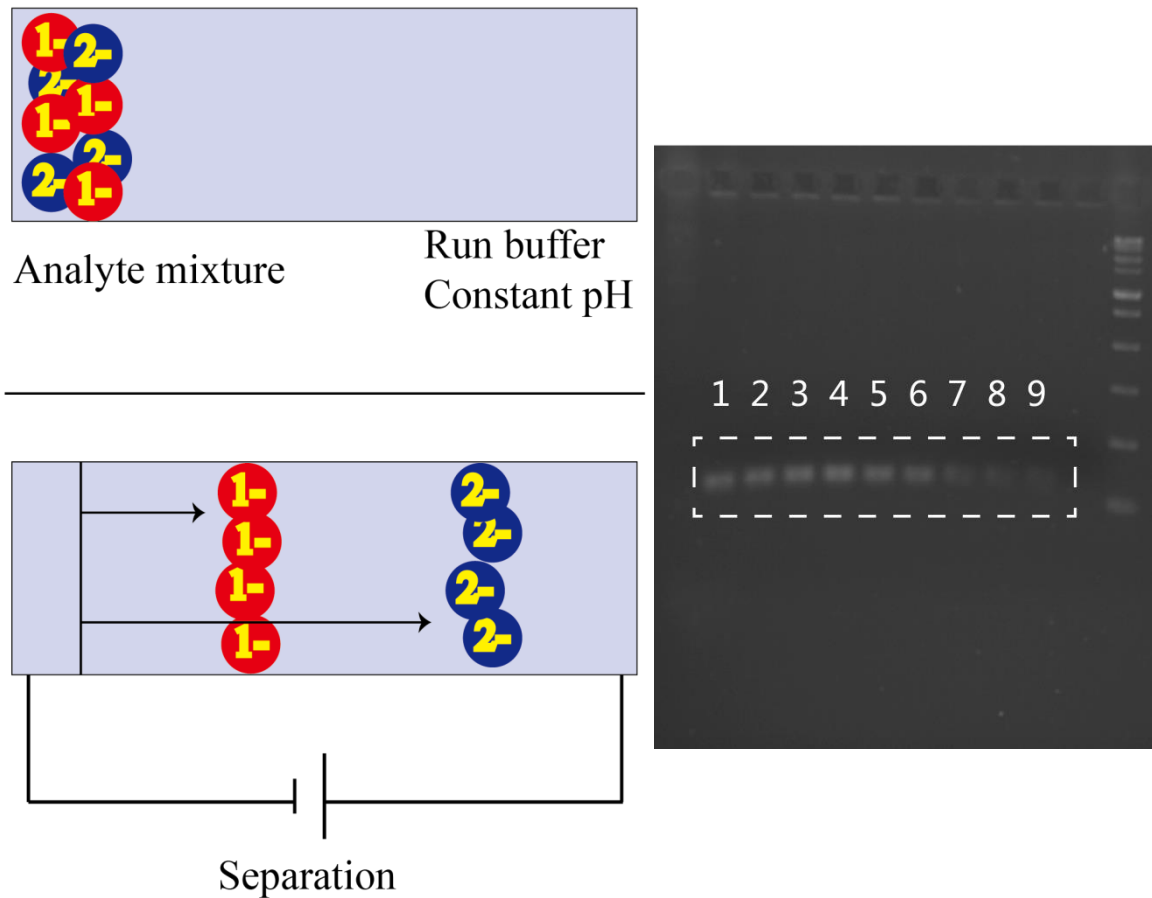


Figure 3.2 left: Separation principle of electrophoresis; right: gel electrophoresis picture taken by Bio-Rad imager.

Agilent 2100 system

The Agilent 2100 Bioanalyzer DNA assay allows the analysis of PCR products, with high resolution and sensitivity [26].

When analyzing PCR products with DNA kits designed for a Bioanalyzer, these kits outperform traditional slab gels, providing extra information about each fragment’s precise size and concentration. In addition, a large linear dynamic range of analysis allows for the discrimination of minute differences in the amplified

Chapter 3 Microfluidic systems and “lab-on-a-chip”

products. Figure 3.3 shows the DNA 1000 kit ladder, used as a calibration standard for PCR products.

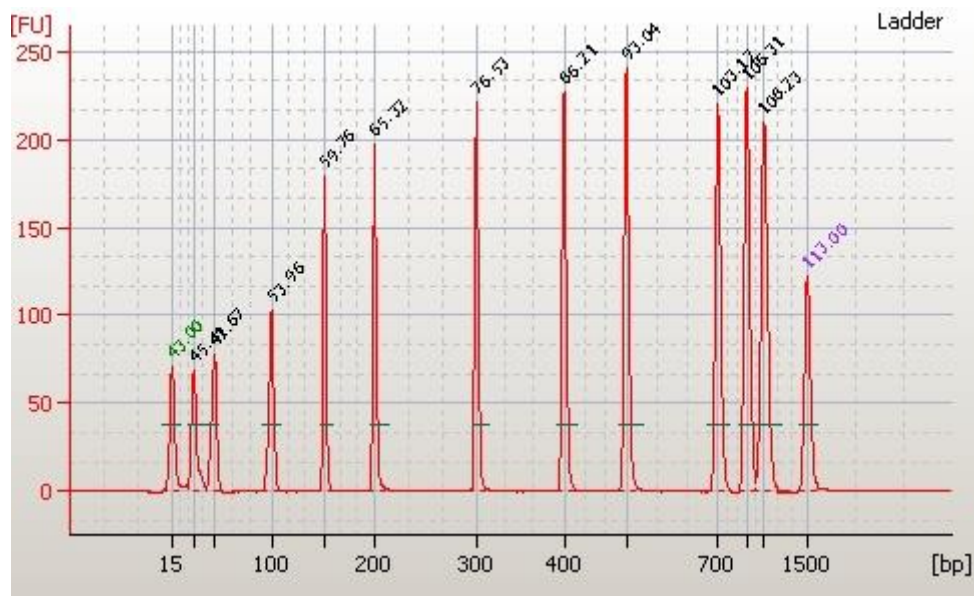


Figure 3.3 Agilent BioAnalyzer DNA 1000 kit ladder

3.2.2 Real-time PCR

As described in previous sections, a gel or a commercial analyzer is used to access samples after PCR thermal cycling. To improve the efficiency of post-PCR analysis, experiments with fluorescent markers are employed. One of the first examples is [27], where the primers used for PCR were modified at the 5'-end with a fluorescent dye. This pre-fluorescent modification eliminated the requirement for post-analysis labelling. The advancement increased the specificity of the detection and provided the information about the amplification in real-time. Furthermore, the detection of single nucleotide polymorphism (SNPs) is enabled as long as these are spanned by the primers.

Chapter 3 Microfluidic systems and “lab-on-a-chip”

A couple of years later, a group of scientists led by Russel Higuchi experimented with the addition of ethidium bromide (EtBr) for real-time purposes [28]. EtBr is an intercalating dye that selectively binds to dsDNA in a reversible manner and only expresses fluorescence when bound to dsDNA, retained non-specifically between the two strands. Therefore, information regarding the concentration of dsDNA in real-time during thermal cycling can be obtained simply through fluorescence measurements [29]. The method is called real-time PCR, also referred to as quantitative PCR (qPCR) [30], because fluorescence data are gathered while the synthesis process is taking place.

Since EtBr is considered as carcinogen [31], other intercalating dyes, such as SYBR Green I and Eva green are often used as a replacement. SYBR Green I absorbs blue light ($\lambda_{\text{max}} = 497 \text{ nm}$) and emits green light ($\lambda_{\text{max}} = 520 \text{ nm}$), the assay chemistry is shown in Figure 3.4(a).

Another method for the simultaneous detection and quantification of DNA involves fluorescently-labelled probes encoding a specific sequence, called the TaqMan assay; this is, shown in Figure 3.4(b).

Chapter 3 Microfluidic systems and “lab-on-a-chip”

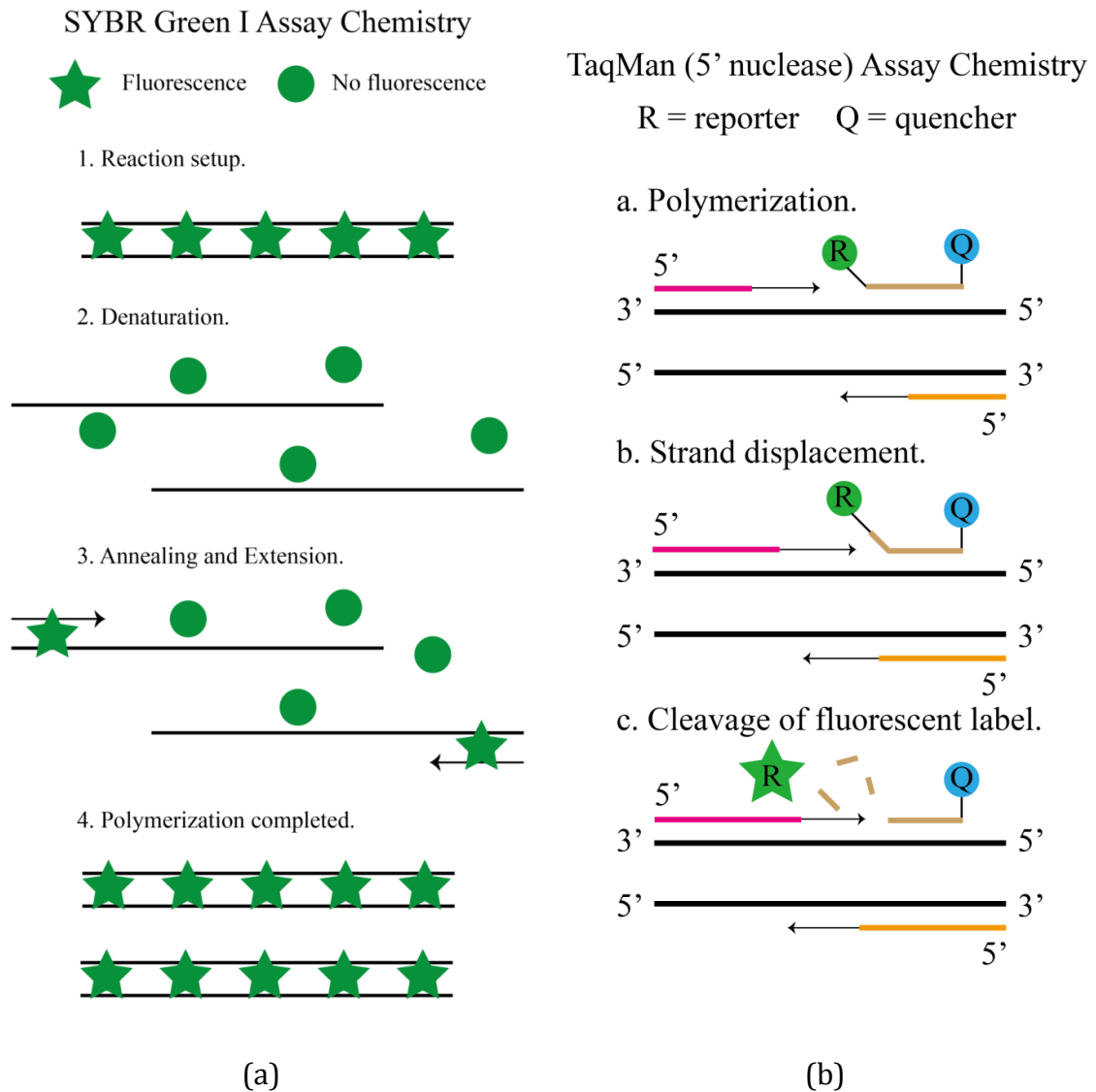


Figure 3.4 (a) SYBR Green dye assay chemistry. In the first step, SYBR Green I binds to the dsDNA and fluoresces. During denaturation, it is released and the fluorescence is drastically reduced. The third step is polymerization, during which primers anneal and extension begins. When polymerization is complete, SYBR Green I binds to the dsDNA, resulting in a net increase in fluorescence. (b) TaqMan assay chemistry. At first the reporter (R) is quenched by the quencher (Q), with further extension R is cleaved from the Q, reveals the fluorescence.

Melting Curve Analysis

With the development of real-time PCR using fluorescent markers, this allowed the observation of PCR amplification and analysis required for sequential operations. In [32], the fluorescence of SYBR Green I was continuously observed throughout thermal cycles. A rapid loss of fluorescence happened at the denaturation of the template during one thermal cycle. The temperature, at which the rapid loss occurred, or at which 50% of DNA is denatured, called melting temperature (T_m), is a characteristic of the template. It is influenced by the length, GC content and sequence of the DNA fragment. Melting curve analysis (MCA) is an assessment of the dissociation-characteristics of dsDNA in response to thermal heating. Ririe et al. [32] exploited the characteristics of PCR products by running a group of linear temperatures from extension to denaturation while continuously recording fluorescence signals. Afterwards, background fluorescence was removed. A plot with respect to temperature against the fluorescence signal recorded correspond to the temperature was drawn, called a melting curve. The first negative derivative of the melting curve was plotted, from which melting peaks can be obtained. Melting peaks allow the differentiation of different DNA fragments or fragments of the same length but with different sequences or GC contents. In contrast, gel electrophoresis is unable to differentiate between fragments of the same length. Melting peaks can also be used to assess the specificity of the amplified products, contamination caused by manual manipulations or primer dimers. The method is able to differentiate between T_m values of less than 2°C. The information from which the presence and identity of SNPs can be inferred gives vital clues to a molecule's mode of interaction. An exemplar MCA figure is shown in ***Chapter 4***.

3.2.3 Optimization

Several years later after the invention, PCR was improved with usage of a polymerase extracted from *Thermus aquaticus* (Taq) [33]. Unlike the polymerase from *Escherichia coli* used in original PCR method, Taq polymerase does not deactivate at high temperatures of around 95°C, which is a requirement of the denaturation step. Thus, there is no subsequent addition at every extension step, saving labor and removing an error-prone step.

The temperature chosen for the annealing and extension step was also optimized to improve the specificity and throughput of the amplicon. In thermal cycled PCR, temperature plays a very important role in each step. In particular, the hybridization step is where highly-matched primer-template hybridizes together, while poorly matched primer-templates dissociate. Due to the short length of the fragments, the extension step is usually omitted in real-time PCR as the enzyme is able to perform extension during the transition between the alignment stage and the denaturing stage [34,35]. For more detailed information and an explanation please refer to the **Chapter 4** of the thesis, where a temperature-dependent dye is employed as a temperature calibrator to optimize the multiple annealing temperatures in a single run, leading to great time and cost savings. Figure 3.5 shows the commercial machines in house and used in this work.

Chapter 3 Microfluidic systems and “lab-on-a-chip”

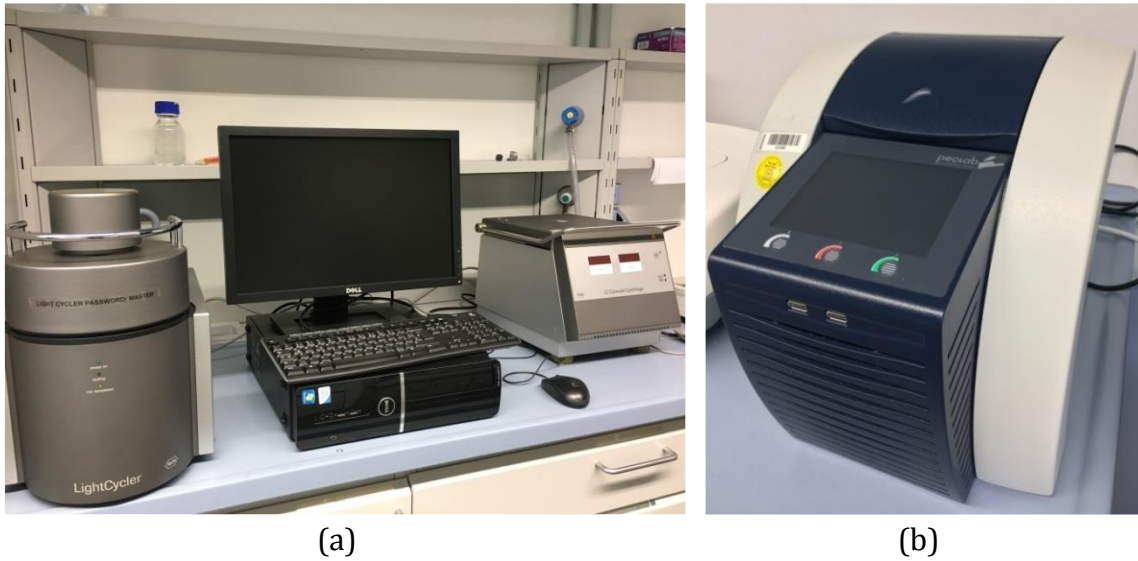


Figure 3.5 Commercial LightCycler and gradient PCR machine

PCR applications

-Medical applications

PCR is very popular in medical applications, as summarized in Table 3.3.

Table 3.3 Medical applications of PCR

The isolation and amplification of tumor suppressors [36]
Detect translocation-specific malignant cells at a high sensitivity [37]
Quantify and analyze single cells [30]
prenatal testing [38]
preimplantation genetic diagnosis [39]
tissue typing, vital to organ transplantation [40]
Study alterations to oncogenes , customize individual therapy regimens [41]
Early diagnosis of malignant diseases [42]

Chapter 3 Microfluidic systems and “lab-on-a-chip”

-Infectious disease applications

PCR is very instrumental in facilitating the diagnosis and treatment of infectious diseases. Detailed applications can be seen in Table 3.4.

Table 3.4 Infectious disease applications of PCR

Rapid and highly specific diagnosis of infectious diseases [43], allowing immediate and effective therapy
Permits identification of non-cultivable or slow-growing microorganisms or viruses [44]
Detection of infectious agents and the discrimination of non-pathogenic from pathogenic [43,45].
The human immunodeficiency virus (or HIV) [46]
Tuberculosis [47]
Detect viral DNA
Detect antibiotic resistance effects of therapy [48]
Monitor the spread of a disease organism [49]
Detect the sequences that are within the pertussis toxin gene [50]

-Forensic applications

Since PCR can generate millions copies of desired DNA fragments in short time, it is very helpful for forensic analysis with small amounts of samples, as summarized in Table 3.5.

Table 3.5 Forensic applications of PCR

Forensic analysis with extremely small amounts of sample
High discriminative power to identify genetic relationships between individuals [51]
Determine evolutionary relationships among organisms [52]
Real time sex determination, both ancient specimens and current suspects [53]

Chapter 3 Microfluidic systems and “lab-on-a-chip”

-Research applications

PCR has a variety of research applications, as can be seen in Table 3.6.

Table 3.6 Research applications of PCR

Generating hybridization probes for Southern or northern blot hybridization and DNA cloning [54]
Allows isolation of DNA fragments from genomic DNA
Extract segments from a completely unknown genome, or can generate just a single strand of an area of interest [55]
Facilitate DNA sequencing
Expedite recombinant DNA technologies [56]
Sequence-tagged sites [57]
Analysis of ancient DNA [58]
The phylogenic analysis of DNA from ancient sources [59]
The study of patterns of gene expression [60]
Enhanced the more traditional task of genetic mapping [61]

3.3 Digital PCR

In addition to closed-channel continuous systems, novel open structures are used as an alternative. In open structures, those discrete droplets are manipulated independently on a substrate, or encapsulated by another immiscible liquid to prevent evaporation or cross contamination. The approach is referred to as digital microfluidics following the analogy of digital microelectronics. In [23], four aqueous droplets were encapsulated by oil to form a virtual reaction chamber (VRC) for PCR, while in [62], VRC was employed for DNA pyrosequencing by controlling droplets movement using a magnet. Moving droplets using capillary sources on a digital track was pioneered in [63]. Other manipulation techniques

Chapter 3 Microfluidic systems and “lab-on-a-chip”

such as surface acoustic waves and mechanical actuation [64,65] have also been demonstrated. Because each droplet is controlled independently [23,62,63], giving the systems a dynamic reconfigurability, as well as high flexibility and fault-tolerance capability.

In conventional PCR, where the amplification is exponential, nucleic acids are quantified based on the number of amplification cycles and the final amount of PCR product for a reference sample. Nevertheless, this calculation creates uncertainties and inaccuracies due to a number of factors, including non-exponential initial amplification cycles, an uncertain number of cycles prior to reaching PCR plateaus, and detectable sensitivities. Last but not the least is the fact that the PCR efficiency between a sample of interest and that of reference sample could be different. The validity and precision of the results are greatly impacted due to the exponential nature of PCR.

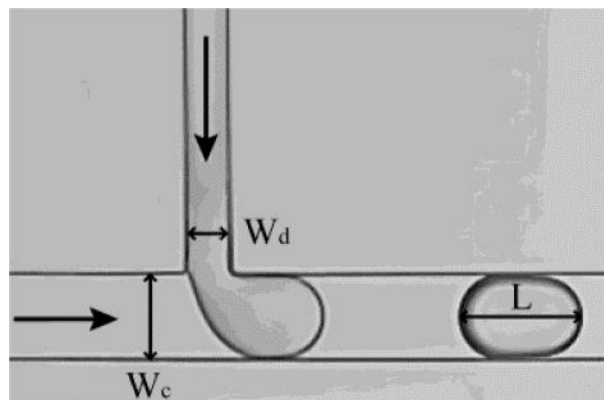
Digital PCR (dPCR) is a refinement of qPCR that is used to directly quantify nucleic acid strands, transferring the exponential profile of PCR into a linear, digital format. It does not rely on a calibration curve for target quantification; neither reference standards nor endogenous controls are needed. dPCR is carried out in such a way that the sample is divided into a large number of compartments prior to amplification. The partitions allow for a more reliable collection and sensitive measurements of nucleic acid amounts, although it is also more prone to error if operated by inexperienced users [66]. The reaction is then carried out in each individual compartment independently, resulting in a binary readout of either 1 or 0.

The method relies on the assumption that sample partitioning follows a Poisson distribution resulting in single or zero copy of target per partition. The presence or absence of fluorescence in each partition is counted after amplification. By performing a Poisson statistical analysis on the number of “yes” and “no” responses, the absolute concentration of target present in the initial sample is

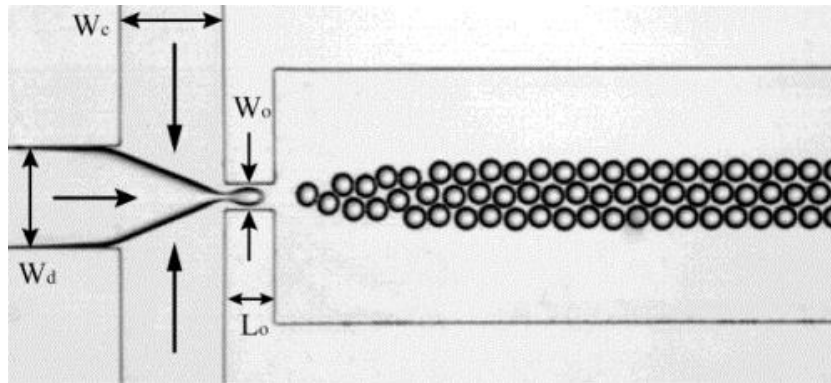
determined. This provides a sensitive and reproducible way of measuring the amount of nucleic acid present in a sample.

3.3.1 Droplet microfluidics

Droplet microfluidics is a subcategory of microfluidics where discrete volumes (from μL to fL) of fluids in immiscible phases are manipulated. The fluids follow laminar flow regimes and have low Reynolds numbers if droplets are to be formed. This further expands microfluidics into research applications in a digital format, such as dPCR, sorting and sensing, single cell analysis, etc. It is well suited for high throughput experiments [67], generating a large number of isolated compartments in short time, and provides better mixing and encapsulation. A well understanding from droplet generation [64] to droplet sorting, merging and breakup [68–70] is required if more benefits are to be exploited. Two most common techniques used for droplet generation are T-junction [71] and flow focusing [71,72]. In Figure 3.6, the widths of the dispersed phase and continuous phase channels are indicated as W_d , and W_c . W_o is the width of the orifice, and L_o the length of the orifice. Figure 3.7 shows the working flow of Bio rad QX100 for ddPCR, with Figure 3.8 shows a model of ddPCR at different nucleic acids concentrations.



(a) Droplet formation in a T-junction. $W_d = 50 \mu\text{m}$; $W_c = 100 \mu\text{m}$.



(b) Droplet formation in flow focusing device. $W_d = W_c = 200 \mu\text{m}$; $W_o = 50 \mu\text{m}$. $L_o = 100 \mu\text{m}$.

Figure 3.6 Droplet formation using T-junction and flow focusing [71]. Copyright © 2011 by Hao Gu et al. licensee MDPI, Basel, Switzerland.

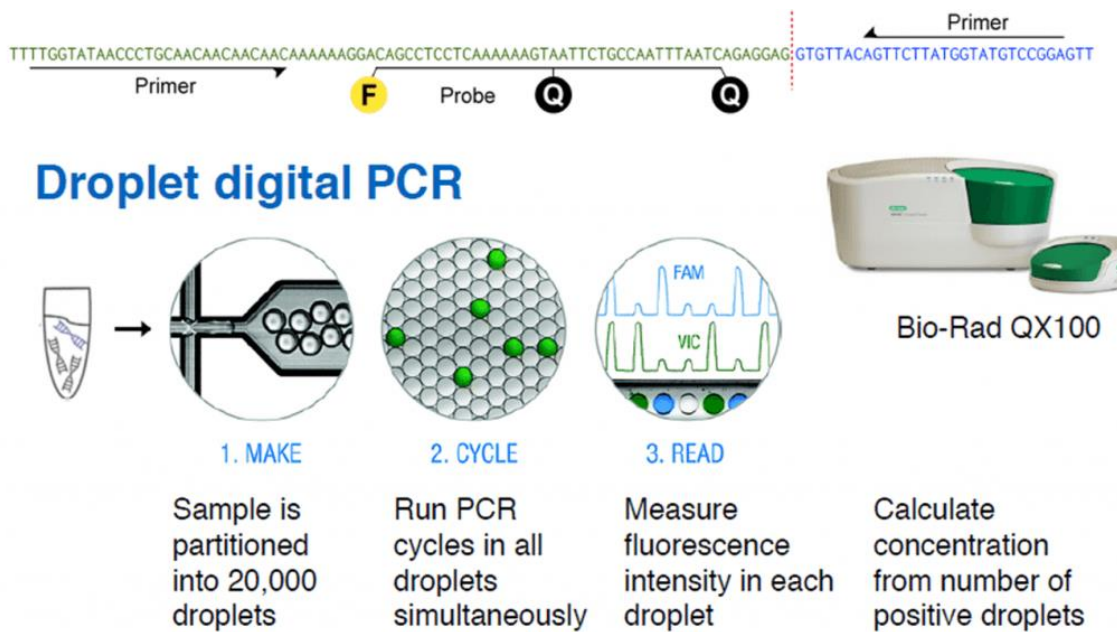


Figure 3.7 Bio Rad QX100 working flow, adapted from [73], Credit: Christof Winter.

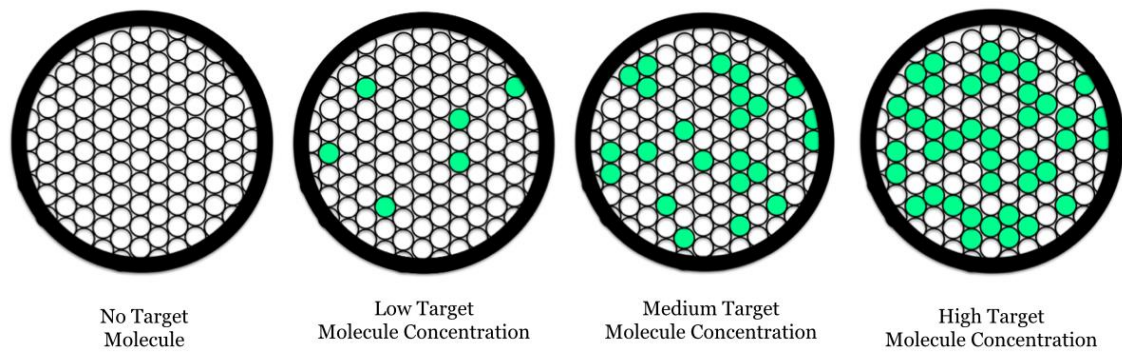


Figure 3.8 Adapted from [74], oil droplets containing fluorescent PCR target molecule.

3.3.2 Recombinase Polymerase Amplification

RPA is an isothermal alternative to PCR [75] developed and launched by TwistDx Ltd, a biotechnology company based in the UK. It aims to simplify the laboratory instrumentation required for PCR. Figure 3.9 shows an RPA cycle where all steps are operated at a low constant optimum temperature – 37°C. Figure 3.9 is the diagram created by TwistDx Ltd showing how RPA works. Starting with the formation of recombinase and oligonucleotide primer complexes, this technique targets homologous DNA. Then, strand exchange with a single-stranded DNA binding protein (SSB) forms a D-loop with SSB and binds the displaced strand of DNA, thereby preventing the dissociation of primers [76]. This is followed by polymerase synthesis. Parental strands separate and synthesis continues until two duplexes are formed. This is called a cycle.

The guidelines for primer and probe design for RPA are less established compared to PCR; a certain degree of trial and error may be taken. Recent results demonstrate that standard PCR primers can work just as well [77]. PCR probes should not be used for RPA, as most popular PCR probe systems are not suited for use with the TwistAmp® process. Most PCR probes employ the 5' to 3' nuclease activity of polymerases, the activity of which is fundamentally incompatible with

Chapter 3 Microfluidic systems and “lab-on-a-chip”

the RPA biochemistry. For example, RPA is not compatible with TaqMan probes (RPA polymerase is strand-displacing) or molecular beacons (RPA reactions contain single-stranded binding proteins that linearize them).

Unlike PCR, which is initiated by a “hot-start”, RPA is initiated by a chemical initiator (magnesium acetate) instead. Upon the addition of magnesium acetate, RPA starts immediately, albeit more slowly, at room temperature. The best temperatures for RPA are 37–42°C, at which the reaction progresses rapidly with specific amplification results. Since RPA does not require thermal cycling or relative control units, and can rapidly amplify a few target copies to detectable levels, makes it a promising candidate for the rapid detection of viral genomic DNA or RNA [78–83], pathogenic bacterial genomic DNA [84,85], and short length aptamer DNA [86]. By adding a reverse transcriptase enzyme, RPA can detect RNA as well as DNA, no need for a separate step to produce cDNA [78–80]. In short, RPA is an excellent choice when it comes to develop low-cost, rapid, point-of-care tests.

Figure 3.10 shows dRPA performed in a SlipChip, where the simultaneous initiation of all compartments with magnesium acetate occurs by a simple slipping step after pipette loading [87].

The RPA Cycle

All steps operate at low constant temperature (optimum 37°C)

a. Recombinase / oligonucleotide primer complexes form and target homologous DNA

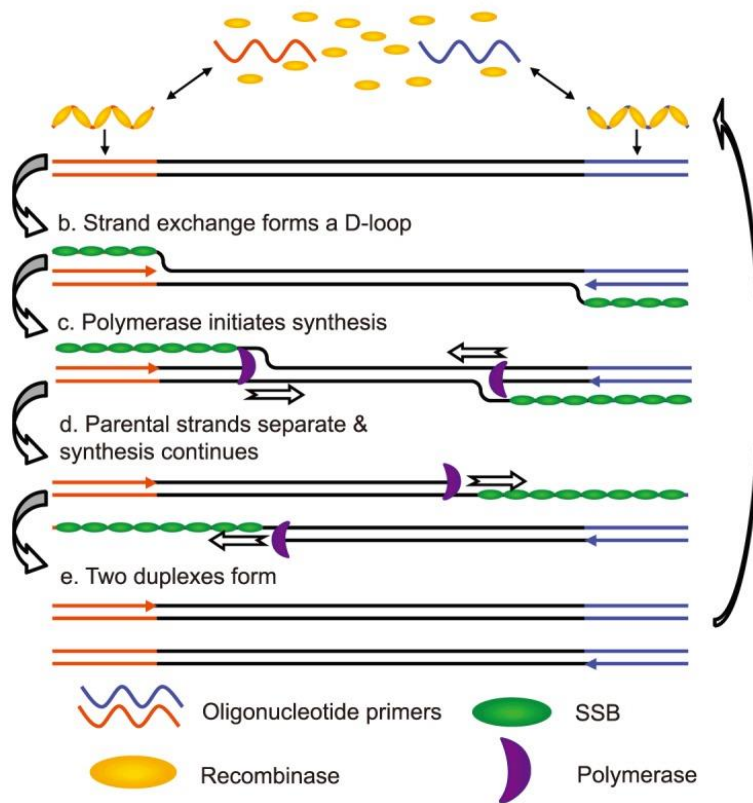


Figure 3.9 DNA amplification by Recombinase Polymerase Amplification. Credit: TwistDx Ltd.
http://www.twistdx.co.uk/our_technology/

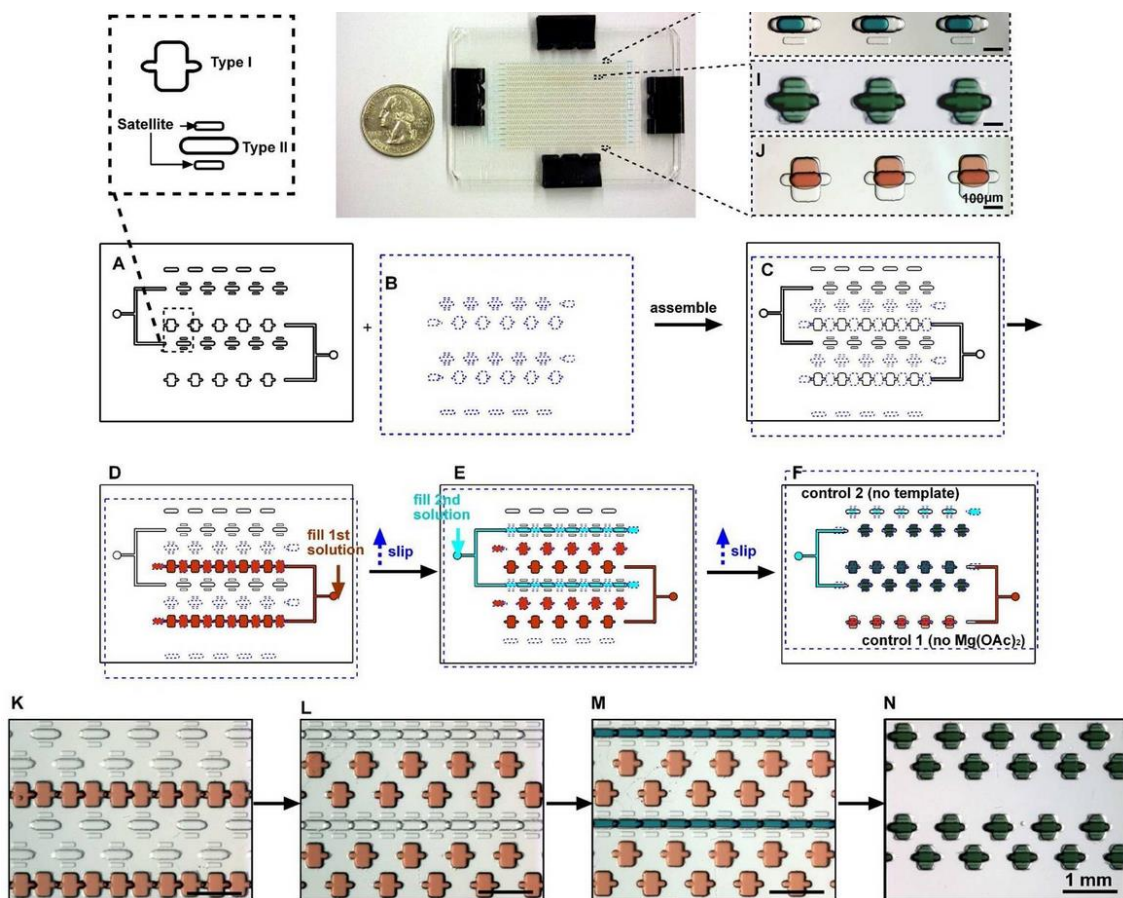


Figure 3.10 Schematic drawing of the two-step SlipChip for digital RPA. Adapted from [87].
Copyright © 2011 American Chemical Society.

3.4 Biomimetics

Nature as a guide

Ever since life is believed to have appeared on Earth, nature has gone through eons of evolution, natural selection and any other unguided natural progresses. For example, lotus leaves [88] show a self-cleaning effect, while rice leaves [89] exhibit anisotropic de-wetting behavior; a water strider’s leg [90] exerts super

Chapter 3 Microfluidic systems and “lab-on-a-chip”

hydrophobic forces, while geckos [91] have an interesting attachment mechanism. The understanding of the properties of biological materials and surfaces found in nature has guided scientists to imitate and produce those functions, using building blocks as small as possible to improve the variety and intelligence.

The complex interplay between surface morphology and physical/chemical properties endorse unique micro-and nanostructures of surfaces [92–98].

In past decades, increasing efforts have been put into engineering and designing those bioinspired artificial, smart materials, and processes (e.g., software), paving the way for real-world applications [99–105], e.g., biomimetic fins [106], neural memory devices [107], smart micro-/nanocontainers for drug delivery [108] and therapeutic purposes [109,110], various biosensors with biorecognitive properties [102,111,112].

Biologically inspired design or adaption or derivation [113–118] from nature is referred to as “biomimetics”. The word biomimetics first appeared in Webster’s dictionary in 1974, with the definition: *‘the study of formation, structure or function of biologically produced substances and materials (as enzymes or silk) and biological mechanisms and processes (as protein synthesis or photosynthesis) especially for the purpose of synthesizing similar products by artificial mechanisms which mimic nature ones’* [119,120].

The well-ordered multiscale structures [121] lend themselves to the creation of complex functionalities in bioinspired materials. Figure 3.11 shows plant leaves used as mold for microvascular network fabricated using PDMS. Figure 3.12 shows an overview of various objects from nature and their selected functions [119].

Resist-free antireflective nanostructured films fabricated using thermal NIL based on moth-eye shape were optimized in [122,123]. The highly enhanced AR properties demonstrate the potential for panel application.

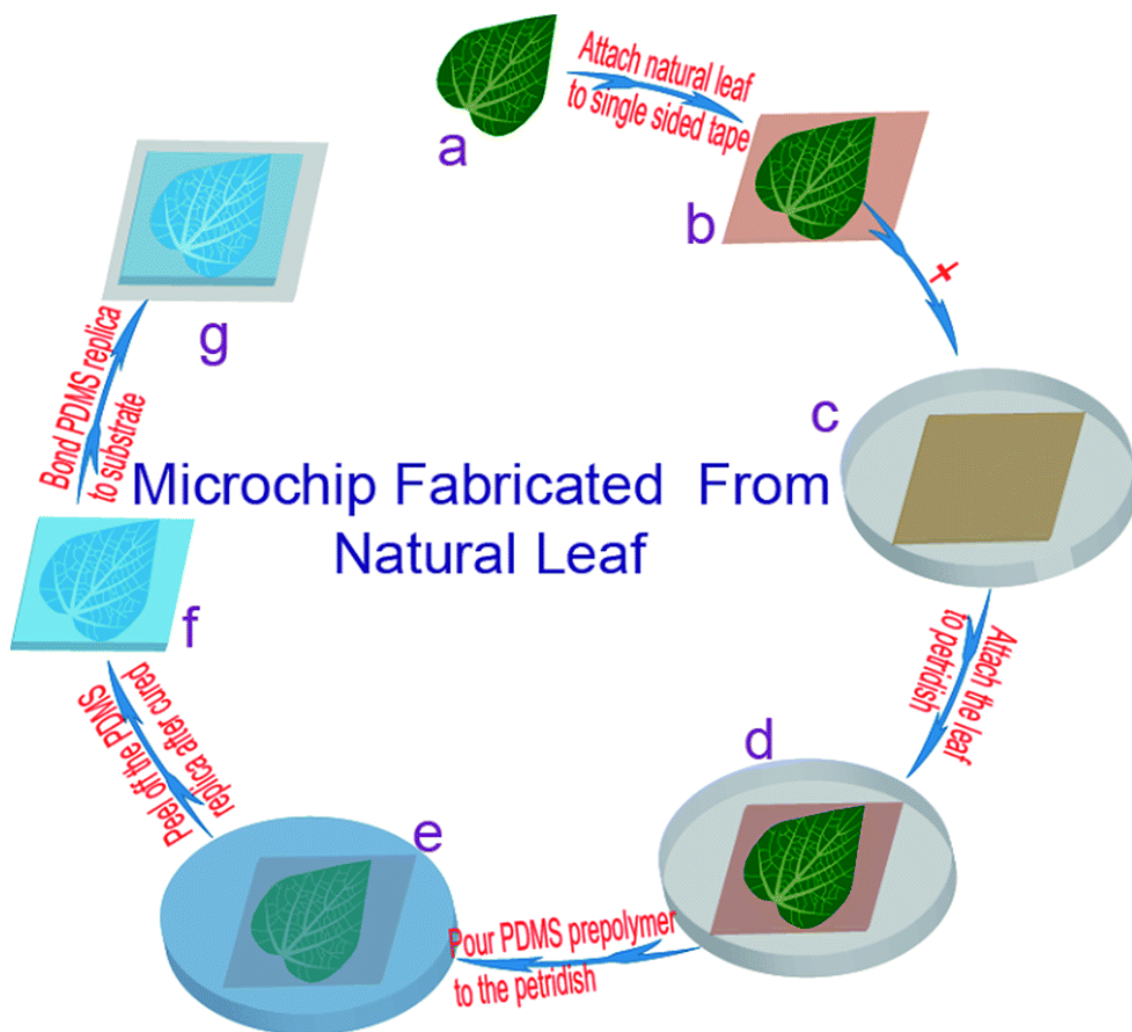


Figure 3.11 Schematic steps of using natural leaves as a mold for microvascular networks [RSC] [124]. Copyright © 2016 The Royal Society of Chemistry.

Chapter 3 Microfluidic systems and “lab-on-a-chip”

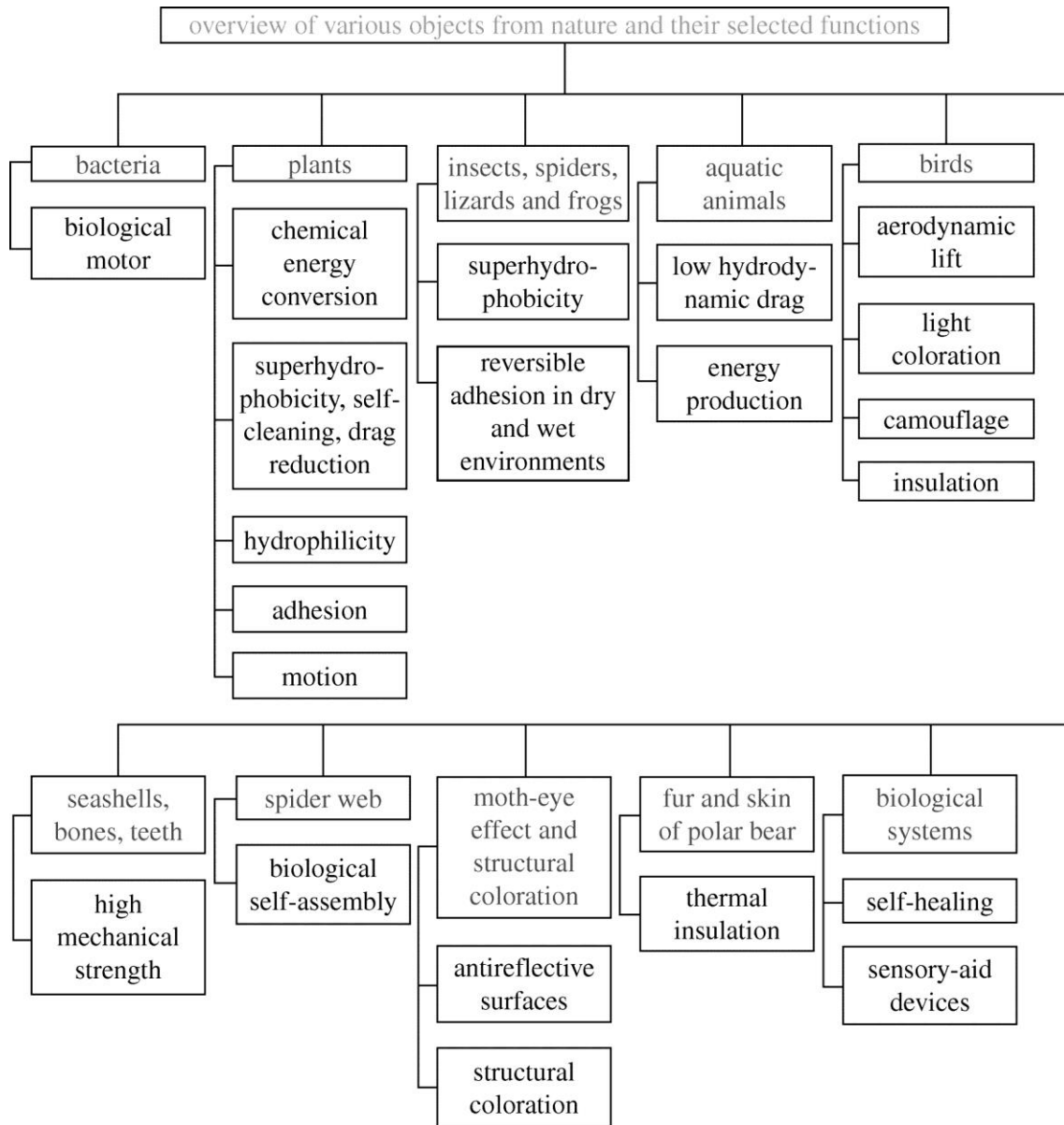


Figure 3.12 An overview of various objects from nature and their selected functions. Reproduced from [119]. Copyright © 2009 The Royal Society.

The cicada, an insect which is abundant in nature, exhibits a highly organized hexagonal nanopillar structures over its transparent wings. Initially, the wing struck scientists as a perfect design for self-cleaning applications. Many publications have mimicked the design to obtain anti-fouling surfaces. Figure 3.13

Chapter 3 Microfluidic systems and “lab-on-a-chip”

(a) shows SEM and AFM image of Cicada wing and (b) Bioinspired structure of Cicada wing.

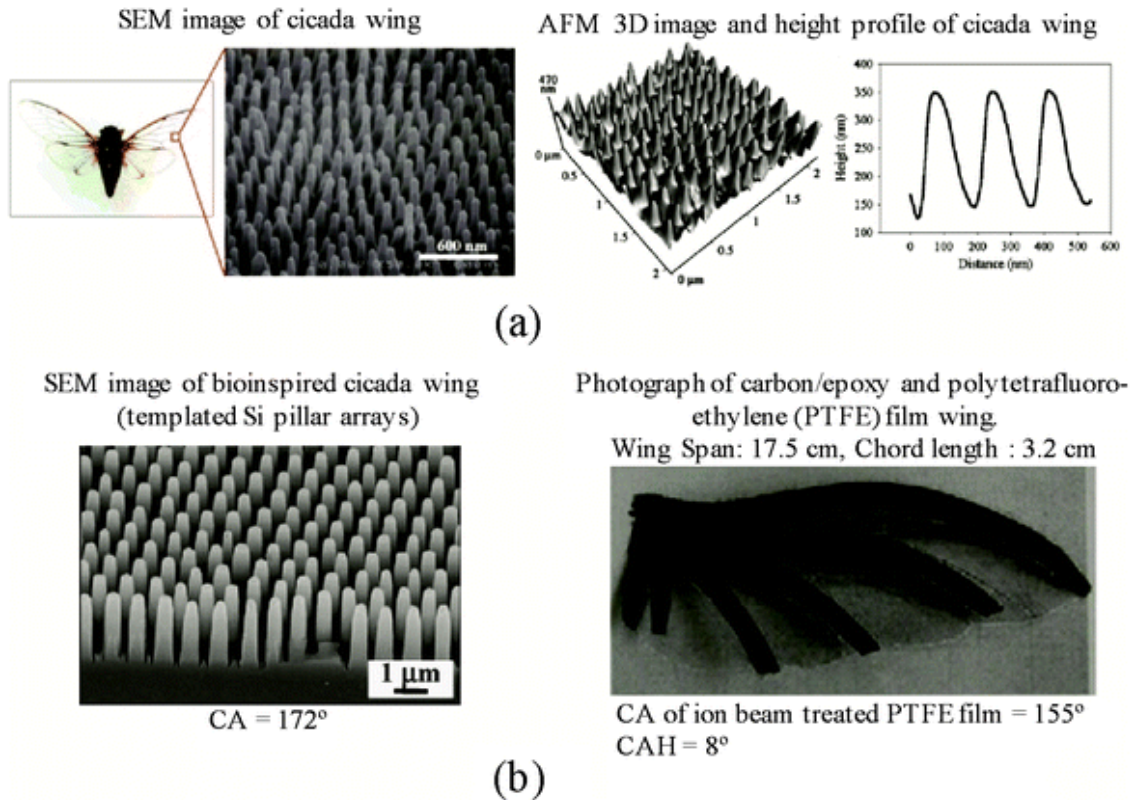


Figure 3.13 (a) Reproduced images and surface height maps for a cicada wing; left image reproduced from [125] (Copyright © 2004 American Chemical Society) and right image reproduced from [126] (Copyright © 2008 The Biophysical Society. Published by Elsevier Inc). (b) Bioinspired cicada wing surfaces; left image reproduced from [127] (Copyright © 2008 WILEY-VCH Verlag GmbH & Co. KGaA, Weinheim) and right image reproduced from [128] (Copyright © 2009 Jilin University. Published by Elsevier Ltd.).

As stated earlier in the thesis, dPCR can be performed in multiple formats, including wells, droplets, etc. Therefore, the fascinating nanopillar structure strikes me, instead, as a perfect mold for dPCR. By exploiting those highly

Chapter 3 Microfluidic systems and “lab-on-a-chip”

organized nanopillars, dPCR reactions run in those tiny nanowell arrays comes to mind. Therefore, the question is how to replicate these transparent wings as a stamp for imprinting? As can be seen, the wings are very thin and the structures are tiny.

With a trial in cleanrooms and knowledge from related published scientific papers, a duplex imprint technique with solid replication results out of a cleanroom is proposed in **Chapter 6** in this thesis. The well duplicated nanowell structures were first used to perform self-assembly experiments, in which 50 nm particles are easier to manipulate and visible. Further experiments on dPCR are still ongoing.

References

- [1] Terry S C and C. S 1975 A gas chromatography system fabricated on a silicon wafer using integrated circuit technology *Ph.D. Thesis Stanford Univ., CA*.
- [2] Terry S C, Herman J H and Angell J B 1979 A gas chromatographic air analyzer fabricated on a silicon wafer *IEEE Trans. Electron Devices* **26** 1880–6
- [3] Manz A, Graber N and Widmer H M 1990 Miniaturized total chemical analysis systems: A novel concept for chemical sensing *Sensors Actuators B Chem.* **1** 244–8
- [4] Arora A, Simone G, Salieb-Beugelaar G B, Kim J T and Manz A 2010 Latest Developments in Micro Total Analysis Systems *Anal. Chem.* **82** 4830–47
- [5] Darwin R. Reyes, Dimitri Iossifidis, Pierre-Alain Auroux † and and Manz* A 2002 Micro Total Analysis Systems. 1. Introduction, Theory, and Technology
- [6] Pierre-Alain Auroux †, Dimitri Iossifidis, Darwin R. Reyes and and Manz* A 2002 Micro Total Analysis Systems. 2. Analytical Standard Operations and Applications
- [7] Ghallab Y and Badawy W 2004 Sensing methods for dielectrophoresis phenomenon: from bulky instruments to lab-on-a-chip *IEEE Circuits Syst. Mag.* **4** 5–15

Chapter 3 Microfluidic systems and “lab-on-a-chip”

- [8] Pawell R S, Taylor R A, Morris K V. and Barber T J 2015 Automating microfluidic part verification *Microfluid. Nanofluidics* **18** 657–65
- [9] Pawell R S, Inglis D W, Barber T J and Taylor R A 2013 Manufacturing and wetting low-cost microfluidic cell separation devices *Biomicrofluidics* **7** 56501
- [10] Engel U and Eckstein R 2002 Microforming—from basic research to its realization *J. Mater. Process. Technol.* **125–126** 35–44
- [11] Sanchez-Salmeron A J, Lopez-Tarazon R, Guzman-Diana R and Ricolfe-Viala C 2005 Recent development in micro-handling systems for micro-manufacturing *J. Mater. Process. Technol.* **167** 499–507
- [12] Tay F E H 2002 *Microfluidics and BioMEMS applications* vol 10, ed F E H Tay (Boston, MA: Springer US)
- [13] Cui H-F, Ye J-S, Chen Y, Chong S-C and Sheu F-S 2006 Microelectrode Array Biochip: Tool for In Vitro Drug Screening Based on the Detection of a Drug Effect on Dopamine Release from PC12 Cells *Anal. Chem.* **78** 6347–55
- [14] Lee H and Cho D 2009 Lab on a chip technology *Lab Chip* **1** 409
- [15] Beres S B, Carroll R K, Shea P R, Sitkiewicz I, Martinez-Gutierrez J C, Low D E, McGeer A, Willey B M, Green K, Tyrrell G J, Goldman T D, Feldgarden M, Birren B W, Fofanov Y, Boos J, Wheaton W D, Honisch C and Musser J M 2010 Molecular complexity of successive bacterial epidemics deconvoluted by comparative pathogenomics. *Proc. Natl. Acad. Sci. U. S. A.* **107** 4371–6
- [16] Kan C-W, Fredlake C P, Doherty E A S and Barron A E 2004 DNA sequencing and genotyping in miniaturized electrophoresis systems *Electrophoresis* **25** 3564–88
- [17] Mullis K, Faloona F, Scharf S, Saiki R, Horn G and Erlich H 1986 Specific enzymatic amplification of DNA in vitro: the polymerase chain reaction. *Cold Spring Harb. Symp. Quant. Biol.* **51 Pt 1** 263–73
- [18] Hills W, Glenn T, Saiki R K and Scharf S J 1987 Process for amplifying, detecting, and/or-cloning nucleic acid sequences
- [19] Mullis K B and Faloona F A 1987 Specific synthesis of DNA in vitro via a polymerase-catalyzed chain reaction. *Methods Enzymol.* **155** 335–50
- [20] Bartlett J M S and Stirling D 2003 A Short History of the Polymerase Chain Reaction *PCR Protocols* (New Jersey: Humana Press) pp 3–6
- [21] PCR, <http://learn.genetics.utah.edu/content/labs/pcr/>, accessed 2018-04-24

Chapter 3 Microfluidic systems and “lab-on-a-chip”

- [22] Saiki R 1987 Amplification of a Short DNA Stretch by Repeated Cycles of In Vitro DNA Polymerization *Am. Assoc. Adv. Sci.* **155** 335–50
- [23] Publikationen der UdS: Virtual reaction chambers as a tool for polymerase chain reaction and protein thermal shift assays,
<https://publikationen.sulb.uni-saarland.de/handle/20.500.11880/23200;jsessionid=B7D4B0801FC6F099377C913775641A05?locale=en>. Accessed April 24, 2018.
- [24] Kryndushkin D S, Alexandrov I M, Ter-Avanesyan M D and Kushnirov V V 2003 Yeast [PSI⁺] prion aggregates are formed by small Sup35 polymers fragmented by Hsp104. *J. Biol. Chem.* **278** 49636–43
- [25] Sambrook J and Russell D W (David W 2001 *Molecular cloning : a laboratory manual* (Cold Spring Harbor Laboratory Press)
- [26] Agilent T and Dna B Agilent DNA Kits for the 2100 Bioanalyzer System A smart solution for nucleic acid analysis 0–1
- [27] Chehab F F and Kan Y W 1989 Detection of specific DNA sequences by fluorescence amplification: a color complementation assay. *Proc. Natl. Acad. Sci. U. S. A.* **86** 9178–82
- [28] Higuchi R, Dollinger G, Walsh P S and Griffith R 1992 Simultaneous Amplification and Detection of Specific DNA Sequences *Bio/Technology* **10** 413–7
- [29] Higuchi R, Fockler C, Dollinger G and Watson R 1993 Kinetic PCR Analysis: Real-time Monitoring of DNA Amplification Reactions *Nat. Biotechnol.* **11** 1026–30
- [30] Garibyan L and Avashia N 2013 Polymerase chain reaction. *J. Invest. Dermatol.* **133** 1–4
- [31] Elliott W 1963 The effects of antimicrobial agents on deoxyribonucleic acid polymerase *Biochem. J.* **86** 562–7
- [32] Ririe K M, Rasmussen R P and Wittwer C T 1997 Product differentiation by analysis of DNA melting curves during the polymerase chain reaction. *Anal. Biochem.* **245** 154–60
- [33] Saiki R K, Gelfand D H, Stoffel S, Scharf S J, Higuchi R, Horn G T, Mullis K B and Erlich H A 1988 Primer-directed enzymatic amplification of DNA with a thermostable DNA polymerase. *Science* **239** 487–91
- [34] Rapid PCR, https://dna.utah.edu/RapidPCR/Top_Rapid_PCR.html. Accessed April 26, 2018.

Chapter 3 Microfluidic systems and “lab-on-a-chip”

- [35] Li X, Wu W and Manz A 2017 Thermal gradient for fluorometric optimization of droplet PCR in virtual reaction chambers *Microchim. Acta* **1**–7
- [36] Knopf A, Lempart J, Bas M, Slotta-Huspenina J, Mansour N and Fritsche M K 2015 Oncogenes and tumor suppressor genes in squamous cell carcinoma of the tongue in young patients. *Oncotarget* **6** 3443–51
- [37] Tomar R S 2010 Molecular markers and plant biotechnology (New India Pub. Agency)
- [38] Chang M Y, Ahn S, Kim M Y, Han J H, Park H-R, Seo H K, Yoon J, Lee S, Oh D-Y, Kang C and Choi B Y 2018 One-step noninvasive prenatal testing (NIPT) for autosomal recessive homozygous point mutations using digital PCR *Sci. Rep.* **8** 2877
- [39] Dreesen J, Drusedau M, Smeets H, de Die-Smulders C, Coonen E, Dumoulin J, Gielen M, Evers J, Herbergs J and Geraedts J 2008 Validation of preimplantation genetic diagnosis by PCR analysis: genotype comparison of the blastomere and corresponding embryo, implications for clinical practice *Mol. Hum. Reprod.* **14** 573–9
- [40] Nazahah M and Koh M B C 2015 Tissue typing and its role in transplantation *ISBT Sci. Ser.* **10** 115–23
- [41] Bogdanov K V., Nikulina T S, Lomaia E G, Slyadnev M N and Zaritskey A Y 2017 Identification of oncogene mutations in leukemia patients using microchip-based PCR analysis *Russ. J. Bioorganic Chem.* **43** 544–51
- [42] Pfitzner T, Engert A, Wittor H, Schinköthe T, Oberhäuser F, Schulz H, Diehl V and Barth S 2000 A real-time PCR assay for the quantification of residual malignant cells in B cell chronic lymphatic leukemia. *Leukemia* **14** 754–66
- [43] Cai H Y, Caswell J L and Prescott J F 2014 Nonculture Molecular Techniques for Diagnosis of Bacterial Disease in Animals: A Diagnostic Laboratory Perspective <http://dx.doi.org/10.1177/0300985813511132>
- [44] Grif K, Heller I, Prodinger W M, Lechleitner K, Lass-Flörl C and Orth D 2012 Improvement of detection of bacterial pathogens in normally sterile body sites with a focus on orthopedic samples by use of a commercial 16S rRNA broad-range PCR and sequence analysis. *J. Clin. Microbiol.* **50** 2250–4
- [45] Logan J (Julie M J ., Edwards K (Kirstin J . and Saunders N (Nick A . 2009 *Real-time PCR : current technology and applications* (Caister Academic Press)
- [46] Sherman G G, Cooper P A, Coovadia A H, Puren A J, Jones S A, Mokhachane M and Bolton K D 2005 Polymerase chain reaction for diagnosis of human immunodeficiency virus infection in infancy in low resource settings. *Pediatr.*

Chapter 3 Microfluidic systems and “lab-on-a-chip”

Infect. Dis. J. **24** 993–7

- [47] Amin I, Idrees M, Awan Z, Shahid M, Afzal S and Hussain A 2011 PCR could be a method of choice for identification of both pulmonary and extra-pulmonary tuberculosis. *BMC Res. Notes* **4** 332
- [48] Rôças I N and Siqueira J F 2013 Detection of antibiotic resistance genes in samples from acute and chronic endodontic infections and after treatment *Arch. Oral Biol.* **58** 1123–8
- [49] Speers D J 2006 Clinical applications of molecular biology for infectious diseases. *Clin. Biochem. Rev.* **27** 39–51
- [50] Kolodkina V, Martinov V and Babenko A 2014 Multiplex real-time PCR assay for detection and differentiation of *Bordetella pertussis* and *Bordetella parapertussis*. *Iran. J. Microbiol.* **6** 140–8
- [51] Yoon J-M 2016 Genetic Distances in Three Ascidian Species determined by PCR Technique. *Dev. Reprod.* **20** 379–85
- [52] Lawrence J G, Ochman H and Hartl D L 1991 Molecular and evolutionary relationships among enteric bacteria *J. Gen. Microbiol.* **137** 191–1
- [53] Alonso A, Martín P, Albarrán C, García P, García O, Fernández De Simón L, García-Hirschfeld J, Sancho M, De La Rúa C and Fernández-Piqueras J 2004 Real-time PCR designs to estimate nuclear and mitochondrial DNA copy number in forensic and ancient DNA studies *Forensic Sci. Int.* **139** 141–9
- [54] de Muro M A 2008 Probe design, production, and applications 41–53
- [55] Alberts B, Johnsons A L J et al. 2002 Isolating , Cloning , and Sequencing DNA *Molecular Biology of the Cell* (Garland Science) pp 1–15
- [56] Ahmed S and Khosa A N An introduction to dna technologies and their role in livestock production: a review *Plant Sci* **20**
- [57] Talbert L E, Blake N K, Chee P W, Blake T K and Magyar G M 1994 Evaluation of “sequence-tagged-site” PCR products as molecular markers in wheat *Theor. Appl. Genet. Int. J. Plant Breed. Res.* **87** 789–94
- [58] Iñiguez A M, Araújo A, Ferreira L F and Vicente A C P 2003 Analysis of ancient DNA from coprolites: a perspective with random amplified polymorphic DNA-polymerase chain reaction approach. *Mem. Inst. Oswaldo Cruz* **98 Suppl 1** 63–5
- [59] Rizzi E, Lari M, Gigli E, De Bellis G and Caramelli D 2012 Ancient DNA studies: new perspectives on old samples *Genet. Sel. Evol.* **44** 21
- [60] Tomancak P, Beaton A, Weizsmann R, Kwan E, Shu S, Lewis S E, Richards S,

Chapter 3 Microfluidic systems and “lab-on-a-chip”

- Ashburner M, Hartenstein V, Celniker S E and Rubin G M 2002 Systematic determination of patterns of gene expression during *Drosophila* embryogenesis. *Genome Biol.* **3**RESEARCH0088
- [61] Kazianis S, Morizot D C, McEntire B B, Nairn R S and Borowsky R L 1996 Genetic mapping in *Xiphophorus* hybrid fish: assignment of 43 AP-PCR/RAPD and isozyme markers to multipoint linkage groups. *Genome Res.* **6** 280–9
- [62] Publikationen der UdS: Virtual reaction chambers as a tool for DNA sequencing,
<https://publikationen.sulb.uni-saarland.de/handle/20.500.11880/26906>.
Accessed April 30, 2018.
- [63] Pesant J, Hareng M, Mourey B and Perbet J 1986 Electrodes for a device operating by electrically controlled fluid displacement
- [64] Chokkalingam V, Herminghaus S and Seemann R 2008 Self-synchronizing pairwise production of monodisperse droplets by microfluidic step emulsification *Appl. Phys. Lett.* **93** 254101
- [65] Shemesh J, Bransky A, Khoury M and Levenberg S 2010 Advanced microfluidic droplet manipulation based on piezoelectric actuation *Biomed. Microdevices* **12** 907–14
- [66] TechNews Guiding our pcr experiments, <https://www.future-science.com/doi/pdf/10.2144/000114283>. Accessed April 25, 2018.
- [67] Chokkalingam V, Tel J, Wimmers F, Liu X, Semenov S, Thiele J, Figdor C G and Huck W T S 2013 Probing cellular heterogeneity in cytokine-secreting immune cells using droplet-based microfluidics *Lab Chip* **13** 4740
- [68] Teh S-Y, Lin R, Hung L-H and Lee A P 2008 Droplet microfluidics *Lab Chip* **8** 198
- [69] Prakash M and Gershenfeld N 2007 Microfluidic Bubble Logic *Science (80-)*. **315** 832–5
- [70] Samie M, Salari A and Shafii M B 2013 Breakup of microdroplets in asymmetric T junctions *Phys. Rev. E* **87** 53003
- [71] Gu H, Duits M H G and Mugele F 2011 Droplets formation and merging in two-phase flow microfluidics. *Int. J. Mol. Sci.* **12** 2572–97
- [72] Churchman A H, Mico V, de Pablo J G, Peyman S A, Freear S and Evans S D 2018 Combined flow-focus and self-assembly routes for the formation of lipid stabilized oil-shelled microbubbles *Microsystems Nanoeng.* **4** 17087

Chapter 3 Microfluidic systems and “lab-on-a-chip”

- [73] Droplet Digital PCR to Measure Tumor Load | Labcritics, <http://www.labcritics.com/droplet-digital-pcr-to-measure-tumor-load-6498/>. Accessed April 27, 2018.
- [74] File:Oil droplets containing fluorescent PCR target molecule.jpg - Wikimedia Commons, https://commons.wikimedia.org/wiki/File:Oil_droplets_containing_fluorescent_PCR_target_molecule.jpg. Accessed April 25, 2018.
- [75] Piepenburg O, Williams C H, Stemple D L and Armes N A 2006 DNA Detection Using Recombination Proteins ed J Haber *PLoS Biol.* **4** e204
- [76] Li Z, Liu Y, Wei Q, Liu Y, Liu W, Zhang X and Yu Y 2016 Picoliter Well Array Chip-Based Digital Recombinase Polymerase Amplification for Absolute Quantification of Nucleic Acids ed V M Ugaz *PLoS One* **11** e0153359
- [77] Using PCR primers with Recombinase Polymerase Amplification, <https://www.twistdx.co.uk/en/rpa/using-pcr-primers>. Accessed April 26, 2018.
- [78] Euler M, Wang Y, Nentwich O, Piepenburg O, Hufert F T and Weidmann M 2012 Recombinase polymerase amplification assay for rapid detection of Rift Valley fever virus. *J. Clin. Virol.* **54** 308–12
- [79] Amer H M, Abd El Wahed A, Shalaby M A, Almajhdi F N, Hufert F T and Weidmann M 2013 A new approach for diagnosis of bovine coronavirus using a reverse transcription recombinase polymerase amplification assay *J. Virol. Methods* **193** 337–40
- [80] Abd El Wahed A, El-Deeb A, El-Tholoth M, Abd El Kader H, Ahmed A, Hassan S, Hoffmann B, Haas B, Shalaby M A, Hufert F T and Weidmann M 2013 A Portable Reverse Transcription Recombinase Polymerase Amplification Assay for Rapid Detection of Foot-and-Mouth Disease Virus ed X-J Meng *PLoS One* **8** e71642
- [81] Boyle D S, Lehman D A, Lillis L, Peterson D, Singhal M, Armes N, Parker M, Piepenburg O and Overbaugh J 2013 Rapid detection of HIV-1 proviral DNA for early infant diagnosis using recombinase polymerase amplification. *MBio* **4** e00135-13
- [82] Euler M, Wang Y, Otto P, Tomaso H, Escudero R, Anda P, Hufert F T and Weidmann M 2012 Recombinase polymerase amplification assay for rapid detection of *Francisella tularensis*. *J. Clin. Microbiol.* **50** 2234–8
- [83] Euler M, Wang Y, Heidenreich D, Patel P, Strohmeier O, Hakenberg S, Niedrig M, Hufert F T and Weidmann M 2013 Development of a panel of recombinase polymerase amplification assays for detection of biothreat agents. *J. Clin. Microbiol.* **51** 1110–7

Chapter 3 Microfluidic systems and “lab-on-a-chip”

- [84] Kersting S, Rausch V, Bier F F and von Nickisch-Rosenegk M 2014 Multiplex isothermal solid-phase recombinase polymerase amplification for the specific and fast DNA-based detection of three bacterial pathogens *Microchim. Acta* **181** 1715–23
- [85] Santiago-Felipe S, Tortajada-Genaro L A, Morais S, Puchades R and Maquieira Á 2015 Isothermal DNA amplification strategies for duplex microorganism detection *Food Chem.* **174** 509–15
- [86] Loo J F C, Lau P M, Ho H P and Kong S K 2013 An aptamer-based bio-barcode assay with isothermal recombinase polymerase amplification for cytochrome-c detection and anti-cancer drug screening *Talanta* **115** 159–65
- [87] Shen F, Davydova E K, Du W, Kreutz J E, Piepenburg O and Ismagilov R F 2011 Digital Isothermal Quantification of Nucleic Acids via Simultaneous Chemical Initiation of Recombinase Polymerase Amplification Reactions on SlipChip *Anal. Chem.* **83** 3533–40
- [88] Liu Y, Tang J, Wang R, Lu H, Li L, Kong Y, Qi K and Xin J H 2007 Artificial lotus leaf structures from assembling carbon nanotubes and their applications in hydrophobic textiles *J. Mater. Chem.* **17** 1071–8
- [89] Feng L, Li S, Li Y, Li H, Zhang L, Zhai J, Song Y, Liu B, Jiang L and Zhu D 2002 Super-Hydrophobic Surfaces: From Natural to Artificial *Adv. Mater.* **14** 1857–60
- [90] Shi F, Niu J, Liu J, Liu F, Wang Z, Feng X-Q and Zhang X 2007 Towards Understanding Why a Superhydrophobic Coating Is Needed by Water Striders *Adv. Mater.* **19** 2257–61
- [91] Lee H, Lee B P and Messersmith P B 2007 A reversible wet/dry adhesive inspired by mussels and geckos *Nature* **448** 338–41
- [92] Li X-M, Reinhoudt D and Crego-Calama M 2007 What do we need for a superhydrophobic surface? A review on the recent progress in the preparation of superhydrophobic surfaces *Chem. Soc. Rev.* **36** 1350
- [93] Zhang X, Shi F, Niu J, Jiang Y and Wang Z 2008 Superhydrophobic surfaces: from structural control to functional application *J. Mater. Chem.* **18** 621–33
- [94] Lee Y, Park S-H, Kim K-B and Lee J-K 2007 Fabrication of Hierarchical Structures on a Polymer Surface to Mimic Natural Superhydrophobic Surfaces *Adv. Mater.* **19** 2330–5
- [95] Parker A R and Townley H E 2007 Biomimetics of photonic nanostructures *Nat. Nanotechnol.* **2** 347–53
- [96] Zhou B . 2000 Bio-inspired study of structural materials *Mater. Sci. Eng. C* **11**

Chapter 3 Microfluidic systems and “lab-on-a-chip”

13–8

- [97] Feng X J and Jiang L 2006 Design and Creation of Superwetting/Antiwetting Surfaces *Adv. Mater.* **18** 3063–78
- [98] Nishimoto S, Bhushan B, Koch K, Walzel P, Ochiai T, Murakami T, Fujishima A, Nakata K, Sakai H, Murakami T, Abe M, Komine T and Fujishima A 2013 Bioinspired self-cleaning surfaces with superhydrophobicity, superoleophobicity, and superhydrophilicity *RSC Adv.* **3** 671–90
- [99] Behl M and Lendlein A 2007 Actively moving polymers *Soft Matter* **3** 58–67
- [100] Liu J and Lu Y 2006 Smart Nanomaterials Responsive to Multiple Chemical Stimuli with Controllable Cooperativity *Adv. Mater.* **18** 1667–71
- [101] Willet N, Gohy J-F, Lei L, Heinrich M, Auvray L, Varshney S, Jérôme R and Leyh B 2007 Fast Multiresponsive Micellar Gels from a Smart ABC Triblock Copolymer *Angew. Chemie Int. Ed.* **46** 7988–92
- [102] Bayley H and Cremer P S 2001 Stochastic sensors inspired by biology *Nature* **413** 226–30
- [103] Maeda S, Hara Y, Sakai T, Yoshida R and Hashimoto S 2007 Self-Walking Gel *Adv. Mater.* **19** 3480–4
- [104] Feng L, Sun T and Feng L I N 2005 Bioinspired Surfaces with Special Wettability Bioinspired Surfaces with Special Wettability *Acc. Chem. Res.* **38** 644–652
- [105] Chan E P, Smith E J, Hayward R C and Crosby A J 2008 Surface Wrinkles for Smart Adhesion *Adv. Mater.* **20** 711–6
- [106] Wang Z, Hang G, Wang Y, Li J and Du W 2008 Embedded SMA wire actuated biomimetic fin: a module for biomimetic underwater propulsion *Smart Mater. Struct.* **17** 25039
- [107] Winter J O, Liu T Y, Korgel B A and Schmidt C E 2001 Recognition Molecule Directed Interfacing Between Semiconductor Quantum Dots and Nerve Cells *Adv. Mater.* **13** 1673–7
- [108] Ibarz G, Dähne L, Donath E and Möhwald H 2001 Smart Micro- and Nanocontainers for Storage, Transport, and Release *Adv. Mater.* **13** 1324
- [109] Betancourt T and Brannon-Peppas L 2006 Micro-and nanofabrication methods in nanotechnological medical and pharmaceutical devices *Int. J. Nanomedicine* **1** 483–95
- [110] Hilt J Z and Byrne M E 2004 Configurational biomimesis in drug delivery: molecular imprinting of biologically significant molecules *Adv. Drug Deliv.*

Chapter 3 Microfluidic systems and “lab-on-a-chip”

Rev. **56** 1599–620

- [111] Kim S-R and Abbott N L 2001 Rubbed Films of Functionalized Bovine Serum Albumin as Substrates for the Imaging of Protein-Receptor Interactions Using Liquid Crystals *Adv. Mater.* **13** 1445–9
- [112] Bontidean I, Kumar A, Csöregi E, Galaev I Y and Mattiasson B 2001 Highly Sensitive Novel Biosensor Based on an Immobilized lac Repressor *Angew. Chemie Int. Ed.* **40** 2676–8
- [113] Hosoda N and Kato T 2001 Thin-film formation of calcium carbonate crystals: Effects of functional groups of matrix polymers *Chem. Mater.* **13** 688–93
- [114] Orme C A, Noy A, Wierzbicki A, McBride M T, Grantham M, Teng H H, Dove P M and DeYoreo J J 2001 Formation of chiral morphologies through selective binding of amino acids to calcite surface steps *Nature* **411** 775–9
- [115] Niemeyer C M 2001 Nanoparticles, Proteins, and Nucleic Acids: Biotechnology Meets Materials Science *Angew. Chemie Int. Ed.* **40** 4128–58
- [116] Tomsia A P, Saiz E, Song J and Bertozzi C R 2005 Biomimetic Bonelike Composites and Novel Bioactive Glass Coatings *Adv. Eng. Mater.* **7** 999–1004
- [117] Lu Y and Liu J 2007 Smart Nanomaterials Inspired by Biology: Dynamic Assembly of Error-Free Nanomaterials in Response to Multiple Chemical and Biological Stimuli *Acc. Chem. Res.* **40** 315–23
- [118] Kinbara K and Aida T 2005 Toward intelligent molecular machines: Directed motions of biological and artificial molecules and assemblies *Chem. Rev.* **105** 1377–400
- [119] Bhushan B Biomimetics: lessons from nature – an overview,
doi:10.1098/rsta.2009.0011.
- [120] Bhushan B 2013 *Introduction to Tribology* (The Atrium, Southern Gate, Chichester, West Sussex, PO19 8SQ, UK: John Wiley & Sons, Ltd),
doi:10.1002/adma.200800836.
- [121] Xia F and Jiang L 2008 Bio-Inspired, Smart, Multiscale Interfacial Materials *Adv. Mater.* **20** 2842–58
- [122] Kang Y H, Han J H, Cho S Y and Choi C-G 2014 Resist-free antireflective nanostructured film fabricated by thermal-NIL *Nano Converg.* **1** 19
- [123] Kim J K, Park S-J, Kim S, Park H-H, Kim K, Choi J-H, Lee J, Choi D-G, Suh K Y and Jeong J-H 2012 Fabrication of ZrO₂ nanopatterns for biomimetic

Chapter 3 Microfluidic systems and “lab-on-a-chip”

antireflection by thermal nanoimprint lithography *Microelectron. Eng.* **100** 12–5

- [124] Wu W, Guijt R M, Silina Y E, Koch M, Manz A, Lee L P, Chiesl T N, Barron A E, Lu Y, Mirkin C, Liu C, Marxa U, Horland R and Marx U 2016 Plant leaves as templates for soft lithography *RSC Adv.* **6** 22469–75
- [125] Lee W, Jin M, Yoo W and Lee J 2004 Nanostructuring of a Polymeric Substrate with Well-defined Nanometer-Scale Topography and Tailored Surface Wettability 7665–9
- [126] Watson G S, Myhra S, Cribb B W and Watson J A 2008 Putative functions and functional efficiency of ordered cuticular nanoarrays on insect wings. *Biophys. J.* **94** 3352–60
- [127] Min W-L, Jiang B and Jiang P 2008 Bioinspired Self-Cleaning Antireflection Coatings *Adv. Mater.* **20** 3914–8
- [128] Lee Y, Yoo Y, Kim J, Widhiarini S, Park B, Park H C, Yoon K J and Byun D 2009 Mimicking a Superhydrophobic Insect Wing by Argon and Oxygen Ion Beam Treatment on Polytetrafluoroethylene Film *J. Bionic Eng.* **6** 365–70

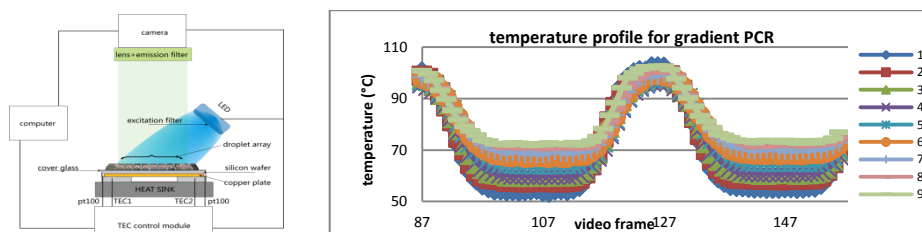
Chapter 4

Thermal gradient for fluorometric optimization of droplet PCR in virtual reaction chambers

This chapter is published in *Microchimica Acta*, doi:10.1007/s00604-017-2353-6.

Graphical Abstract

This paper aims to optimize polymerase chain reaction using a gradient feature in a single experiment, which will lead to great time savings and a reduction in reagent use. The exact temperature-time course of the sample is monitored through the use of Sulforhodamine B, which provides solution temperatures in real time throughout the thermal cycling required for the reaction. A proportional correlation between fluorescence intensity and product concentration was verified by commercial devices. There was no need for further post-analysis to determine the optimal temperature.



Chapter 4 Thermal gradient for fluorometric optimization of droplet PCR in virtual reaction chambers

Abstract

An open system with a thermal gradient is described for the optimization of polymerase chain reaction (PCR) optimization. Two thermal electric coolers were used as the heat source. The gradient is measured through encapsulated water-based beads of a temperature-dependent dye inside mineral oil, thereby forming virtual reaction chambers. Nine droplets (with typical volume of 0.7 μL) were used. Using the intrinsic fluorescence of a temperature-sensitive inert dye (sulforhodamine B), the process involves measurement of the fluorescence intensity at a known, uniform temperature together with the instrument-specific calibration constant to calculate an unknown, possibly non-uniform temperature. The results show that a nearly linear thermal gradient is obtained. This gradient function is a useful feature that can be used for optimization of a commonly used enzyme-activated reaction, viz. PCR. The emission spectra of fluorescent droplets during two-step PCR were monitored and the changes in fluorescence between 50 $^{\circ}\text{C}$ and 100 $^{\circ}\text{C}$ quantified. As the gradient feature allows for testing a range of annealing temperatures simultaneously, the optimal annealing temperature can be easily determined in a single experiment.

KEYWORDS

Microfluidics; droplet PCR; thermal gradient; fluorometric sensing; temperature-dependent dye; sulforhodamine B; virtual reaction chamber

4.1 Introduction

Microfluidic systems, or “labs-on-a-chip”, have revolutionized many aspects of quantitative biochemistry and analytical chemistry [1]. The potential advantages,

Chapter 4 Thermal gradient for fluorometric optimization of droplet PCR in virtual reaction chambers

including portability, speed, high efficiency, and reduced reagent consumption [1-4] have been explored by the miniaturization and integration of the various chemical operations. As in digital microfluidics where droplets are manipulated on an open, hydrophobic surface, the virtual reaction chamber (VRC) offers a simple way of exploiting the advantages of microfluidics and droplets while circumventing many of the practical problems. It is formed by encapsulating single aqueous sample droplets with volumes in the low microliter range within slight larger oil droplets [5-7].

Temperature is the most fundamental element in biochemical reactions [8], either in micro or macro scale. Therefore, to obtain robust, unique and clean products, optimization needs to be performed. This optimal temperature is often reaction dependent, or relies on other factors such as the physical characteristics of the molecules in a particular solvent or equipment characteristics. On the other hand, temperature may affect the rate or efficiency of the reaction. Accurate control of sample temperatures in microfluidic systems is often very important, particularly during the reaction and separation. The importance of temperature control in lab-on-a-chip devices has been demonstrated for enzyme-activated reactions [1,5,9-11].

One of these enzyme-activated reactions, polymerase chain reaction (PCR) [12], conducted by a deoxyribonucleic acid (DNA) polymerase, is introduced to illustrate the point. PCR utilizes biological and chemical components to orchestrate enzymatic amplification. It gives access to a method of amplifying DNA molecules across several orders of magnitude, which has substantially accelerated the pace of research in many fields of biology.

The sequence and length of PCR primers generally determine the annealing temperature of the thermal cycling reaction for a specific assay. Using too low an annealing temperature can produce non-specific priming of templated DNA or

Chapter 4 Thermal gradient for fluorometric optimization of droplet PCR in virtual reaction chambers

form primer-dimers, whereas if the temperature is too high, little or no product may be produced. Therefore, PCR yield is reduced. These problems can often be avoided by an annealing temperature optimization step [13-15].

Most groups have reported using a temperature sensor to measure the temperature of the substrate of a microfluidic system [6,7,9,16] or on the outside of capillaries [17,18]. This is perhaps the simplest and easiest way to measure temperature. However, it is not accurate considering the temperature discrepancy between the temperature on the outside of the system and the fluid inside the system. Besides, concerns caused by direct sensor contact within the solution, such as product contamination or inhibition, the added thermal mass of the sensor, and the obstruction of optical measurements become more acute as the sample volume decreases, forcing measurements external to the sample and compromising accuracy during rapid temperature transitions.

A simple solution for non-contact temperature measurement is to use a passive reference dye whose fluorescence varies with temperature but does not inhibit the reaction. The technique takes advantage of the temperature dependence of the fluorescence intensity of a dilute fluorophore added to the fluid [2]. Since the fluorescence of many dyes is temperature-dependent [19,20], a suitable dye has to be chosen for each specific application. Considering the repeated heating and cooling during thermal cycling, sulforhodamine B has been used for measuring temperature because of its reliable fluorescence over time [19-21]. Moreover, sulforhodamine B exhibits excellent temperature sensitivity.

4 parallel PCR reaction-stations were presented in [15] with a purpose of optimizing annealing temperature in the range of 50-68 °C. Our work, based on VRC, is capable of affording 9 thermal gradients, aiming to optimize PCR reaction in a single run and in more precise temperature scale. More thermal gradients can be obtained by smaller droplet size and tighter posited droplets. Commercially

Chapter 4 Thermal gradient for fluorometric optimization of droplet PCR in virtual reaction chambers

available gradient thermocyclers, such as the 96 Universal Gradient, PeQSTAR Mastercycler egradient (<http://www.labx.com>), and Chromo 4 usually require more than two temperature controlling modules to achieve the same temperature gradient. Most of them either have no real-time detection [22], or require large volumes of the PCR cocktail for the reaction [23]. Multi-zone temperature control may ensure accuracy. Nevertheless, more energy is consumed by multi-heater units. Meanwhile, the footprint is much bigger because of multi-heater units and corresponding control parts. A two-step thermal gradient for fluorometric optimization of droplet PCR in virtual reaction chambers is present here. Sulforhodamine B was used for real-time thermal gradient control and monitoring. The method incorporates a two-step protocol combining the annealing and elongation steps, which leads to significant time-savings and a reduction in reagent use during optimization and standard PCR experiments.

4.2. Materials and methods

4.2.1. Surface preparation

As described earlier, the glass surface for the VRC has to be hydrophobic as well as oleo phobic. Chemical vapor deposition method is applied to silanize glass coverslips. A self-assembly monolayer of a fluorosilane with a reproducible contact angle (Drop shape analysis system DAS 10 MK 2, <https://www.kruss.de>) around 109° was achieved. Coating stability was assessed by the INM institute (<http://www.leibniz-inm.de>). Detailed description on surface coating can be accessed in supplementary material.

4.2.2. Temperature calibration

Theoretically, given a small piece of highly thermally conductive material, a uniform thermal distribution can be reached in seconds or milliseconds. By applying two different temperatures to this material, points along the temperature difference direction should have temperatures in between.

To demonstrate the point, sulforhodamine B, a passive dye which exhibits excellent temperature sensitivity, was chosen for monitoring the temperature. For absolute intensity of the fluorescence to serve as a temperature monitor, the instrument and dye must be stable over time. Temperature calibration was performed at equilibrium temperatures, not while the temperature was changing.

Temperature can be related to fluorescence through a calibration constant:

$$C = \ln(I/I_{ref}) / (1/T - 1/T_{ref}) \quad (4.1)$$

Fluorescence intensities I were measured at temperatures T (in Kelvin) and related to reference fluorescence intensity I_{ref} at a reference temperature T_{ref} . Instrument-specific calibration constants are used to convert fluorescence to solution temperatures. Afterwards, the solution temperatures were converted into Celsius using the following formula:

$$t(^{\circ}C) = T(K) - 273.15 \quad (4.2)$$

Where t and T represent temperature in Celsius and Kelvin, respectively. Detailed temperature calibration description can be found in supplementary material.

4.2.3. Reagents

All buffers were made using deionized water from a Milli-Q ProgradT3 column (<http://www.merckmillipore.com/DE/de>). The fluorescence of sulforhodamine B (monosodium salt, <http://www.sigmaaldrich.com/germany.html>) was measured in a “mock” PCR solution (without polymerase) at a final concentration of 0.1 mM; see protocol below. The polymerase was replaced with deionized water.

The performance of the system was verified by performing real-time PCR to detect a DNA segment of an avian virus. The PCR primers for the chosen avian virus segment (detailed sequence can be found in supporting material) were designed by Primer Express 3.0. The sequence of the forward primer:

5-TGTACTCCCCAGTGTCATGATTG-3;

Reverse primer:

5-AAGGGAATAAGCGGCCATATC-3.

The melting temperature for the primer (Eurofins, Germany) is 60.6 °C.

The master mix was prepared by adding 3 µL of 25 mM MgCl₂, 9 µL 50 pM of each forward and reverse primer, and 4 µL of the LightCycler FastStart DNA Master SYBR Green I (<http://www.roche.de/>). 2 µL DNA templates were added to the reaction mixture to the total volume of 27 µL immediately before the onset of the reaction. The template concentration was around 10⁵ copies ·µL⁻¹.

4.2.4. On-chip PCR thermocycling

The instrument setup is shown in Figure 4.1. Thermocycling of the microfluidic device was achieved using two thermoelectric coolers (1TML10-21x21-10,

Chapter 4 Thermal gradient for fluorometric optimization of droplet PCR in virtual reaction chambers

<http://www.thermion-company.com/>) and a manufactured controller TEC-1122-SV (<http://www.meerstetter.ch/>). Temperature feedback was accomplished by inserting two 1 mm-thick 22x22 mm copper plates on top of each TEC unit with an embedded pt100 (<http://de.farnell.com/>) temperature sensor. Temperature control was performed by proportional integrated derivative (PID) feedback control. Optimized PID constants were used to achieve a fast yet stable control system. Then, another piece of 1.2 mm thick 20x65 mm copper plate was placed between the microfluidic device and two small copper plates to facilitate efficient heat transfer to achieve a uniform heat distribution. A custom-fabricated copper block was placed beneath the TEC device to dissipate waste heat. Finally, a 3-mm silicon wafer was placed between the copper plate and the microfluidic device to help equalize heat distribution and provide a better optical surface for imaging. The VRC used in this work was formed by a 0.7 μL sample, covered with 3 μL of M5904 mineral oil (Sigma-Aldrich, <http://www.sigmaaldrich.com/germany.html>) and placed on a 170 μm thick hydrophobic/oleo phobic microscope coverslip. Two-step PCR thermocycling was initiated with a 10 minute “hot start” at 95 °C to activate the Taq polymerase followed by 40 cycles of ramping between 50 °C and 95 °C using 10 seconds hold times and a thermal ramp rate of 5 °C \cdot s⁻¹. The total PCR thermocycling reaction time required \sim 45 minutes. The ability to perform on-chip thermal cycling of droplets is necessary to be able to perform real-time observation of the entire droplet reactor array during PCR amplification.

Chapter 4 Thermal gradient for fluorometric optimization of droplet PCR in virtual reaction chambers

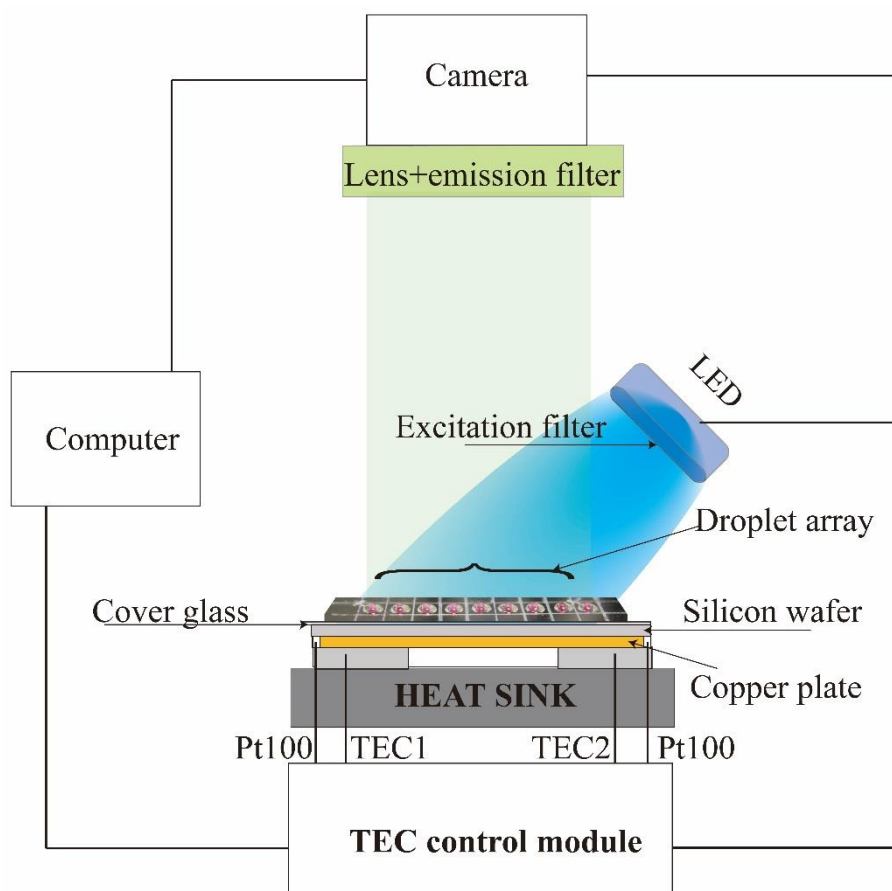


Figure 4.1 Instrument setup. The TEC control module sends out a signal to LED and camera at the same time at the end of the annealing step, making sure that the LED light is on while capturing the image.

To find the optimal annealing temperature for the reaction, a recommended temperature range ± 10 °C above and below the calculated melting temperature of the primers was used. Since the melting temperature for primer was 60.6 °C, the temperature gradient was set to 52 °C~72 °C for optimization.

4.2.5. Image acquisition and processing

Fluorescence imaging of the sulforhodamine B dye was performed using a ProgRes MF Cool CCD camera (<https://www.jenoptik.de/>). The camera gain was set manually to 1 and kept constant throughout the whole experiment. An appropriate filter set (ET546/22x, ET605/70m, www.ahf.de) was applied in front of the C-mount fixed focal lens HF 16HA-1B/1.4 (<http://fujifilm.jp>). Fluorescence imaging of the PCR reaction was the same as that for sulforhodamine B, except the filter set was different (MF469/35 <https://www.thorlabs.de/>, ET525/50 <https://www.chroma.com/>).

ImageJ software and custom Matlab code were used to systematically detect and quantify fluorescent droplets and analyze the size and the fluorescence intensity.

4.2.6. Melting analysis

Because SYBR Green I bind to all double-stranded DNA, it is necessary to check the specificity of the PCR assay by analyzing the amplified products. After each reaction, a melting curve analysis was run. A BioAnalyzer 2100 (<http://www.agilent.com/>) and gel electrophoresis were also used to check the specificity of the amplicon. Additional information on amplicon concentration can be accessed through the analysis from the BioAnalyzer. An optimized SYBR Green I PCR reaction should have a single peak in the melt curve, corresponding to a single band on the gel image. By comparing the gel image with the melt curve, one can identify peaks in the melt curve that correspond to specific products, additional non-specific bands and primer dimers.

4.2.7. Commercial instrument

Another group of experiments were performed on a commercial gradient machine, i.e. 96 Universal Gradient, PeQSTAR in house. Unfortunately, the device does not have a real-time function. Because of its large reaction volume, gel electrophoresis was carried out after the reaction. 5 μ L of each reaction product from the PeQSTAR commercial gradient machine was resolved on a 2% agarose gel for a period of 30 min at 100 V. 6X DNA Gel loading buffer was added at a ratio of 5:1. Gel images were taken by Bio-Rad (www.bio-rad.com). Gel lanes were processed using ImageJ.

4.3. Results

4.3.1. Temperature gradient

When two different temperatures were applied at the two ends of the chip, a group of nearly linear different temperatures was obtained, forming a thermal gradient. Figure 4.2 illustrates the different temperatures in color. Meanwhile, the thermal gradient is represented by color depth. From left to right, the droplets are numbered droplet 1 to 9. The fluorescence of sulforhodamine B decreased as the temperature increased.

Chapter 4 Thermal gradient for fluorometric optimization of droplet PCR in virtual reaction chambers

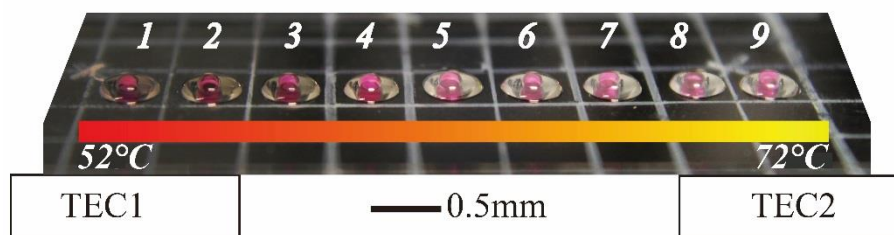


Figure 4.2 Droplet array with thermal gradient. From left to right, the temperature increases and the droplets are numbered as droplet 1 to 9.

After temperature calibration, a two-step thermal cycling was run with sulforhodamine B monitoring the temperature in real time. Figure 4.3 shows the instrument equilibration of sulforhodamine B assessed at 55 °C while 4.4 shows the temperature profile of each droplet during the PCR reaction, positioned exactly as shown in Figure 4.2. In order to demonstrate more clearly, the combined annealing and extension steps were set to 30 seconds. Each video frame denotes 2 seconds. The thermal gradient is clearly observable.

Chapter 4 Thermal gradient for fluorometric optimization of droplet PCR in virtual reaction chambers

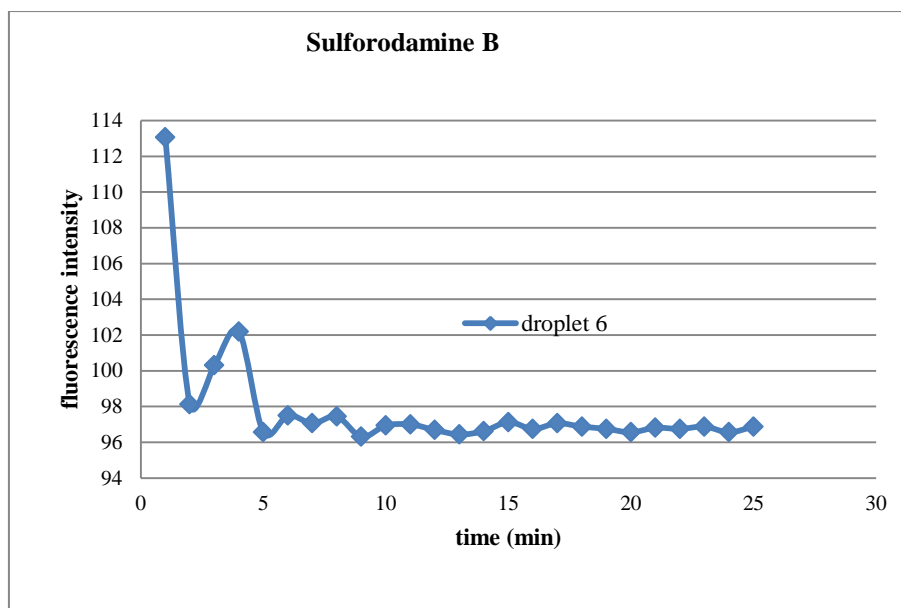


Figure 4.3 Instrument equilibration of sulforhodamine B assessed at 55 °C. After 20 min, no evident change in fluorescence as well as evidence of photo bleaching was observed.

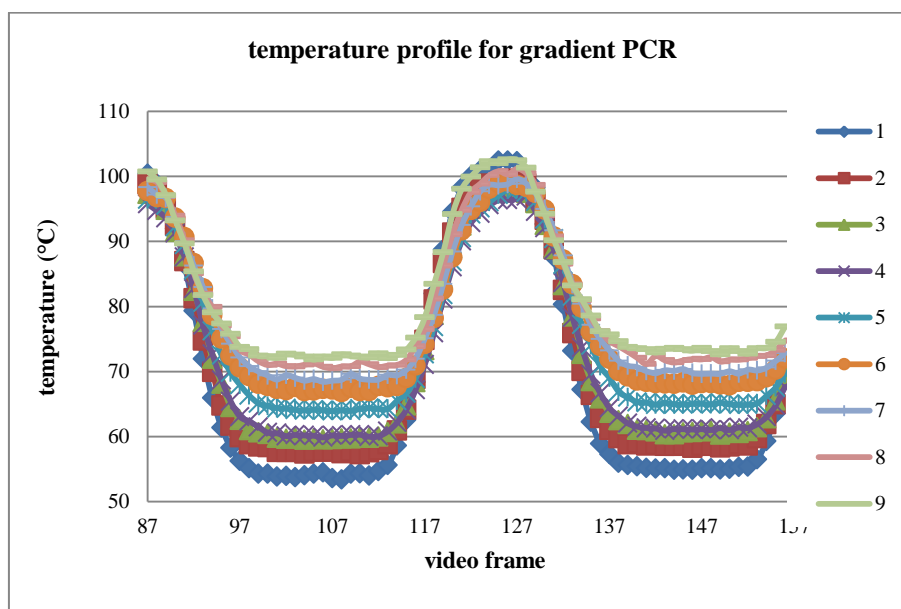


Figure 4.4 Temperature profile for gradient PCR. Each line denotes one sample as illustrated in Figure 4.2.

4.3.2. Gradient PCR

Nine droplets were prepared in each temperature zone. An additional droplet without template (NTC) was positioned in parallel with the fifth droplet, or can be placed anywhere on the chip except for spaces already taken up by the nine droplets. With a thermal gradient, PCR experiments can be optimized in a single run. The amplification curves of the reaction are shown in Figure 4.5. The intensity plots reveal that droplet 4 has the highest fluorescence intensity. The best yield of the product was acquired at 61.04 °C.

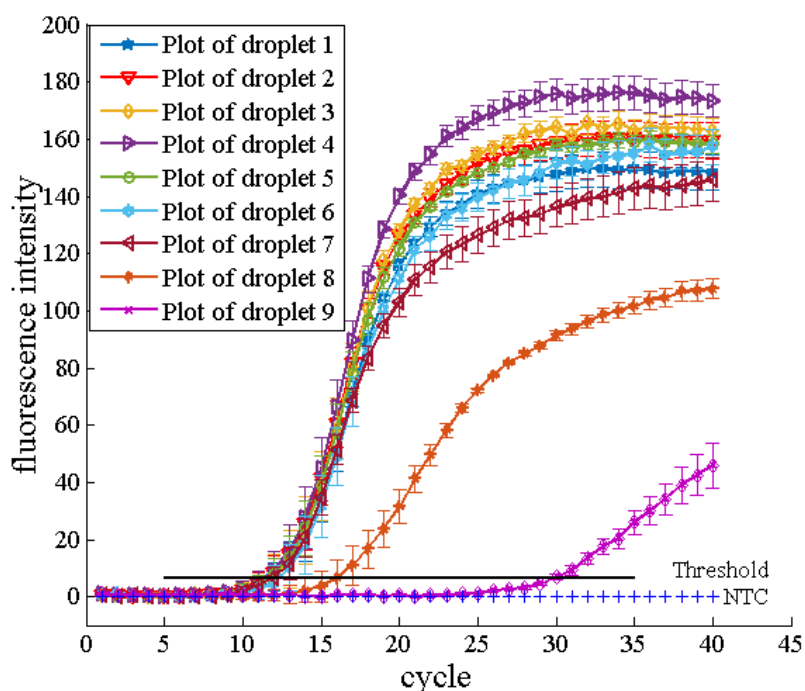


Figure 4.5 Amplification curves of gradient PCR. NTC denotes no template control.

Chapter 4 Thermal gradient for fluorometric optimization of droplet PCR in virtual reaction chambers

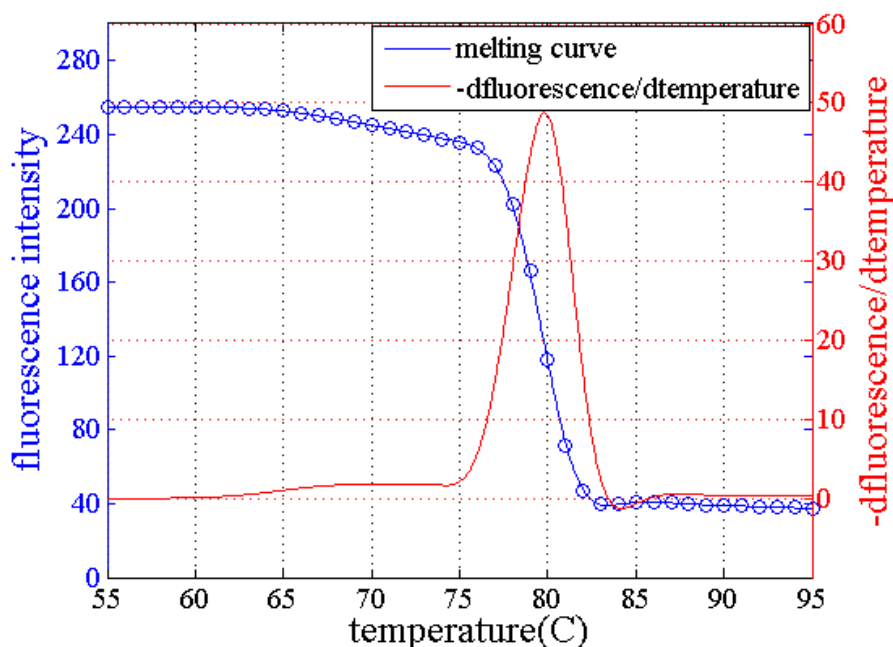


Figure 4.6 Melt curve analysis of droplet 4 with the first derivative of the change in fluorescence intensity as a function of the temperature; meanwhile, only a single peak corresponding to the PCR product is observed. The amplicon is clean and specific.

Melt curve analysis was run to testify the specificity of the product, as shown in Figure 4.6. Robust, unique, and clean products were obtained during the amplification, without any secondary products such as primer-dimers.

Another group of experiments was performed on 96 Universal Gradient, PeQSTAR. Since it is not a real-time machine, gel image of the results was taken by a Bio-Rad imager. The gel lanes of the gel image processed using ImageJ as shown in Figure 4.7 show that 61.6 °C was the optimal temperature. The result is in accordance with the result from our device.

Chapter 4 Thermal gradient for fluorometric optimization of droplet PCR in virtual reaction chambers

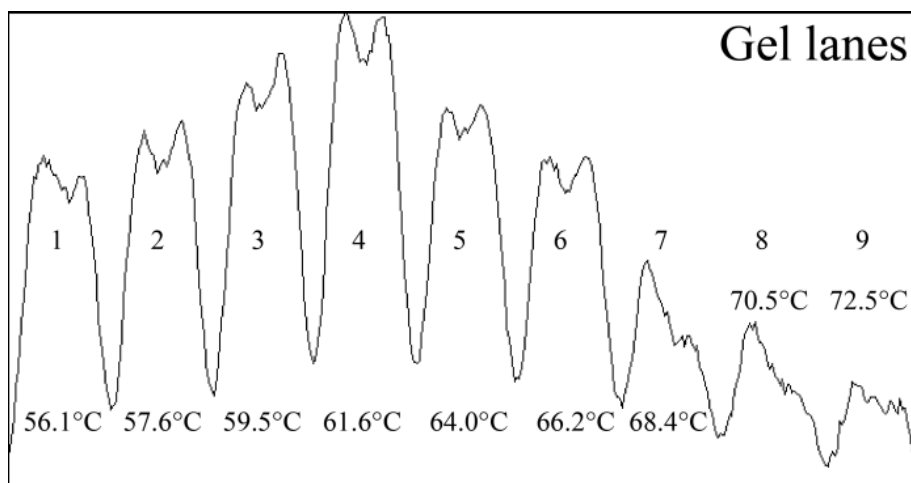


Figure 4.7 Agarose gel result of PCR run on a commercial 96 Universal Gradient, PeQSTAR. The columns are gel lanes of the target amplicons. Lane 4 has the best result.

Figure 4.8 shows the temperature calculated from the calibration constant (the blue curve). The red curve represents the temperature measured by direct contact of the temperature sensor of the chip without thermal loads. No temporal delay was taken into consideration. Both methods showed an almost linear thermal gradient. Since the droplet volume is small, and so is the temperature sensor size, the discrepancies between the two methods can be neglected. However, care must be taken when using a large volume (thermal loads) for the reaction (most commercial devices use large volumes).

In order to determine the relationship between fluorescence intensity and the final concentration, the results were transferred to a BioAnalyzer 2100 for further analysis. After running the analysis, a correlation analysis between the temperature gradient and the product concentration was performed in Figure 4.9. The y-axis is the BioAnalyzer analysis from the annealing temperature optimization experiment. The optimal temperature was 60.62°C.

Chapter 4 Thermal gradient for fluorometric optimization of droplet
PCR in virtual reaction chambers

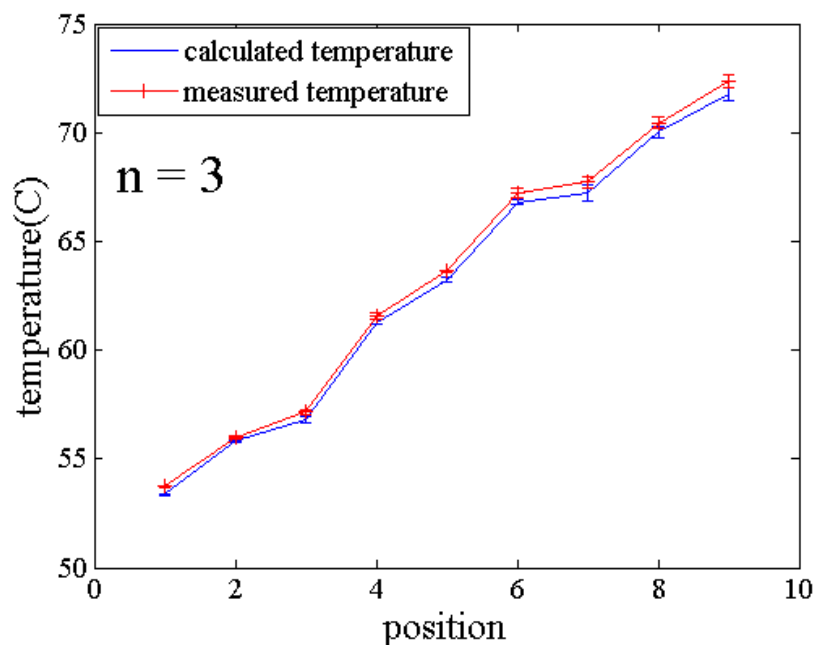


Figure 4.8 Thermal gradient formed from droplet 1 to 9.

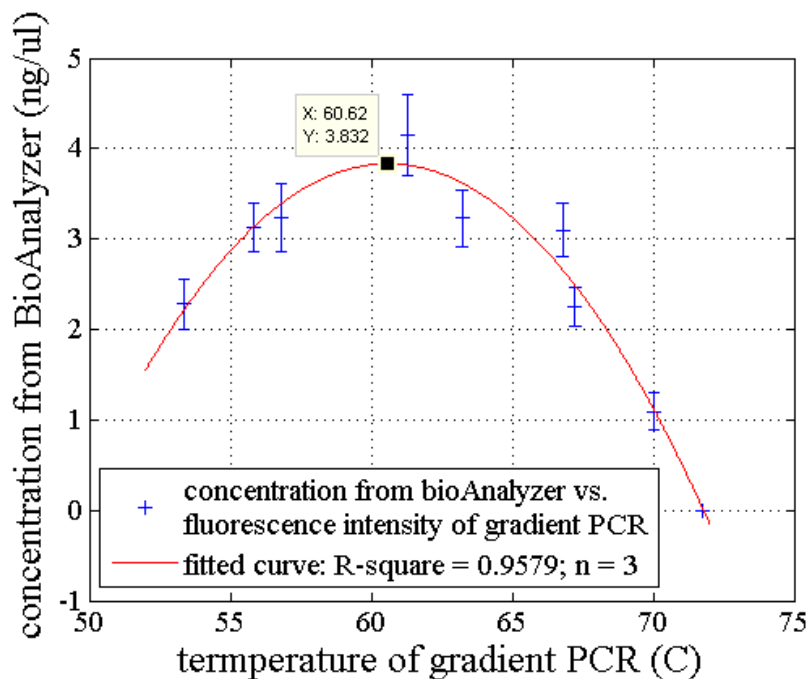


Figure 4.9 Correlation between the thermal gradient and the BioAnalyzer analysis of amplicon concentrations.

4.4. Discussion

Different dyes react differently to temperature changes. The fluorescence of most dyes decreases as the temperature is increased. The exact temperature-time course of the sample can be monitored through the use of a temperature-sensitive passive reference dye, which can provide solution temperatures in real time throughout the thermal cycling. Therefore potentially controls the solution temperature. Sulforhodamine B was chosen because of its high temperature sensitivity and stability over repeated heating and cooling cycles. In addition to evaporation and/or condensation, other potential artifacts include instrument drift, thermal degradation of the dye, and fluorescence quenching, all of which might affect fluorescence signal as well. To use fluorescence to monitor temperature, fluorescence variations must be attributable to temperature. After 20 min, no evident change in fluorescence was observed. In addition, no evidence of photo bleaching of sulforhodamine B was observed.

The calibration constant is dependent on the physical characteristics of the fluorescent molecules in a particular solvent. It provides a quantitative way of judging the overall temperature sensitivity of the dye and optics. Different calibration constants range from 1314 ~ 1487 K for sulforhodamine B, with an accuracy of $\pm 0.8 \sim 8\%$. Continuous acquisition throughout temperature cycling and melting was possible. A higher value of the calibration constant correlates to greater temperature sensitivity and system precision. Solution temperatures were determined using the calibration constant, I_{ref} and T_{ref} as shown in formula (4.1).

The reaction chamber was made by encapsulation of a water-based sample in mineral oil. As no solid cover or micro channels were required, device fabrications consisted only of deposition and patterning the substrate using chemical vapor deposition. The use of disposable glass slides prevents cross-contamination. The small droplet shape minimized the temperature gradient throughout the droplet.

Chapter 4 Thermal gradient for fluorometric optimization of droplet PCR in virtual reaction chambers

Furthermore, the disposable coverslip was not subject to any processing. The glass thermal conductivity coefficient is $1.1 \text{ Wm}^{-1}\text{K}^{-1}$, while the surrounding air has a thermal conductivity coefficient of only $0.025 \text{ Wm}^{-1}\text{K}^{-1}$. Therefore, the temperature of the glass will be determined only by the temperature of the silicon wafer attached to the thermoelectric coolers.

The outcome of optimizing the annealing temperature under a single gradient experiment with the primer set (melting temperature $60.6 \text{ }^\circ\text{C}$) was successful under a gradient range of $52 \text{ }^\circ\text{C}$ to $72 \text{ }^\circ\text{C}$. The primer set displayed a range of annealing temperatures that can successfully amplify the specific amplicon. The experiment demonstrates the possibility of optimizing a primer set using a single PCR protocol with a selected range of temperatures. This was also confirmed by running an experiment on a commercial gradient device in house. The gel electrophoresis of the products from the commercial device verified that our device works. PCR was optimized in a single run thanks to the thermal gradient generated based on a temperature-dependent dye. Furthermore, the optimal temperature was related to the relative fluorescence intensity of the gradient PCR, since the fluorescence intensity was proportional to the concentration. Hence, no further post-analysis using a gel or BioAnalyzer is required, saving a lot of time and effort. Moreover, because only a very small volume of the reagent mixture is needed for optimization, reagent costs and sample consumption can be highly reduced. Finally, the device is easy to operate. However, this system is not perfect, such as the droplet preparation and alignment have to be done manually.

4.5. Conclusion

A small and simple device with a thermal gradient to optimize PCR was designed, with real-time monitoring of the gradient based on a temperature-dependent dye.

Chapter 4 Thermal gradient for fluorometric optimization of droplet PCR in virtual reaction chambers

This was achieved with no direct contact of the temperature sensor, no time delay and no discrepancies between the device and the droplet inside the oil. The gradient feature greatly reduced the time devoted to determining the optimal annealing temperature. The device is cheap, easy to operate and time-saving. Moreover, more gradients can be obtained using smaller and more tightly arranged droplets. The gradient feature is not limited to the annealing step but also allows for the optimization of the denaturation or extension temperature in one experiment as well. We expect that this temperature gradient feature will be used to optimize many reactions in the future.

Acknowledgements

We would like to thank Christian Ahrberg (former KIST Europe employee) for help with data processing. We would like to thank Yuliya E. Silina (INM institute, Saarland University) for testing the stability of the coating method. We would like to thank Zhenjun Chang (Jiangsu University of Science and Technology) for the advice of revising the manuscript. This research was funded by the China Scholarship Council (File No. 201308330205).

Author contribution

Xiangping Li built the instrumental setup, conducted all the experiments and prepared the manuscript. Dr. Wenming Wu gave the idea of gradient PCR. Prof. Andreas Manz advised on experimental design and was also involved with discussions. All authors have reviewed the manuscript.

Electronic Supporting Information

Surface preparation

As described main text, the glass surface for the virtual reaction chamber has to be hydrophobic as well as oleo phobic. Chemical vapor deposition method was applied to silanize glass coverslips. First, the glass coverslips were cleaned in a boiling H_2SO_4/H_2O_2 (piranha solution) mixture for 20 min, then rinsed in deionized water, and dried under a flow of nitrogen. Second, the glass coverslips were placed into a room temperature vacuum oven with 50 μ L of fluorosilane solution trichloro (1H, 1H, 2H, 2H-perfluorooctyl) silane (FOTS) (Sigma-Aldrich, Germany). The oven was closed and evacuated by a conventional oil rotary pump to pressure below 0.1 Torr and flushed three times with nitrogen. The temperature inside the oven was then increased while the pump was still running. Once the temperature reached 150 °C, the system was kept steady for 20 min. Then, the oven was flushed again three times with nitrogen, the pump was switched off, and the oven was vented with nitrogen, before taking the glass out. A self-assembly monolayer of a fluorosilane with a reproducible contact angle (Drop shape analysis system DAS 10 MK 2, KRÜSS) around 109° was achieved. Coating stability was assessed by the INM institute (Saarland University, Germany).

Temperature calibration

For absolute fluorescence to serve as a temperature monitor, the instrument and dye must be stable over time. Temperature calibration was performed at equilibrium temperatures, not while the temperature was changing.

Temperature can be related to fluorescence through a calibration constant:

Chapter 4 Thermal gradient for fluorometric optimization of droplet PCR in virtual reaction chambers

$$C = \ln(I/I_{ref}) / (1/T - 1/T_{ref}) \quad (1)$$

Fluorescence intensities I were measured at temperatures T (in *Kelvin*) and related to reference fluorescence intensity I_{ref} at a reference temperature T_{ref} .

To determine the calibration constant, the two reference temperatures and their corresponding fluorescence intensity have to be chosen wisely. Room temperature (T_{ref}) was chosen as the first reference temperature. The fluorescence at room temperature (I_{ref1}) was kept record. The second reference temperature (T_m) was obtained on the Roche LightCycler Carousel-Based system (Roche Diagnostics, Germany). Increasing the temperature on the device slowly until reach this melting temperature, where fluorescence of intercalating SYBR I disappears. The fluorescence of Sulforhodamine B (I_{ref2}) was recorded at this melting temperature point on the device. The two reference temperatures with a good span ensured the accuracy of the calibration constant, thus the accuracy of the calibrated temperature curve. Bad reference temperatures can introduce the possibility of large systematic uncertainties, particularly at temperatures far from these reference temperatures. The corresponding fluorescence intensities were calculated through calibration images. Each calibration image was the average of 28 sequential video frames. For the calibration curve, the intensity at each temperature was determined by averaging the intensity value of all the pixels of the corresponding image.

Instrument-specific calibration constants were used to convert fluorescence to solution temperatures. Solution temperatures were determined from fluorescence using calibration constant C , the reference temperature and the reference fluorescence:

$$T = 1 / (\ln(I/I_{ref}) / C + 1/T_{ref}) \quad (2)$$

Chapter 4 Thermal gradient for fluorometric optimization of droplet PCR in virtual reaction chambers

Then, the solution temperatures were converted into *Celsius* using the following formula:

$$t(^{\circ}C) = T(K) - 273.15 \quad (3)$$

where t and T represent temperature in *Celsius* and *Kelvin*, respectively.

Temperature calibration raw data:

T_{ref} 26.7°C 299.85K (room temperature)

T_m 80°C 353.15K (melting temperature)

I_{ref} at room temperature

$I_{ref1} = 115.36128.47137.37157.80143.64145.87132.93129.12123.47$

I_{ref} at melting temperature

Average of 28 sequential video frames

$I_{ref2} = 55.79 58.50 60.77 70.79 64.09 66.83 61.80 62.53 63.09$

Calculate Calibration Constant C using T_{ref} , T_m , and their corresponding fluorescence intensity using the formula (2).

After temperature calibration, record the fluorescence signals during reaction and convert them into temperature using the following formula:

$$t(^{\circ}C) = 1/(\ln(I/I_{ref})/C + 1/T_{ref}) - 273.15 \quad (4)$$

Template and primer information

DNA amplicon (66 bp) of avian virus:

Chapter 4 Thermal gradient for fluorometric optimization of droplet PCR in virtual reaction chambers

TGTACTCCCCAGTGTCATGATTGATGATAAGAACACAGTCTTTCTGATATGGCCGCTTA
TTCCCTT.

The PCR primers for avian were designed by Primer Express 3.0. The sequence of the forward primer: 5-TGTACTCCCCAGTGTCATGATTG-3;

Reverse primer: 5-AAGGGAATAAGCGGCCATATC-3.

The melting temperature for the primer (Eurofins, Germany) is 60.6 °C.

References

- [1] Kopp M U, De Mello A J and Manz A 1998 Chemical amplification: continuous-flow PCR on a chip *Science* 280 1046-8
- [2] Ross D, Gaitan M and Locascio L E 2001 Temperature measurement in microfluidic systems using a temperature-dependent fluorescent dye *Analytical Chemistry* 73 4117-23
- [3] Wu J, Kodzius R, Cao W and Wen W 2014 Extraction, amplification and detection of DNA in microfluidic chip-based assays *Microchim Acta* 181 1611-31
- [4] Karle M, Vashist S K, Zengerle R and von Stetten F 2016 Microfluidic solutions enabling continuous processing and monitoring of biological samples: A review *Analytica chimica acta* 929 1-22
- [5] Neuzil P, Pipper J and Hsieh T M 2006 Disposable real-time microPCR device: lab-on-a-chip at a low cost *Molecular Biosystems* 2 292-8
- [6] Neuzil P, Sun W, Karásek T and Manz A 2015 Nanoliter-sized overheated reactor *Applied Physics Letters* 106 024104
- [7] Ahrberg C D, Ilic B R, Manz A and Neuzil P 2016 Handheld real-time PCR device *Lab Chip* 16 586-92
- [8] Wang X-d, Wolfbeis O S and Meier R J 2013 Luminescent probes and sensors for temperature *Chemical Society Reviews* 42 7834-69

Chapter 4 Thermal gradient for fluorometric optimization of droplet PCR in virtual reaction chambers

- [9] Vukusic P and Hooper I 2005 Directionally controlled fluorescence emission in butterflies *Science* 310 1151-
- [10] Hatch A C, Fisher J S, Tovar A R, Hsieh A T, Lin R, Pentoney S L, Yang D L and Lee A P 2011 1-Million droplet array with wide-field fluorescence imaging for digital PCR *Lab Chip* 11 3838-45
- [11] Ahrberg C D, Manz A and Chung B G 2016 Polymerase chain reaction in microfluidic devices *Lab Chip* 16 3866-84
- [12] Mullis K, Faloona F, Scharf S, Saiki R, Horn G and Erlich H 1986 Specific enzymatic amplification of DNA in vitro: the polymerase chain reaction. In: *Cold Spring Harbor Symp. Quant. Biol.*: Cold Spring Harbor Laboratory Press) pp 263-73
- [13] Kean O W Using the gradient technology of the Mastercycler pro to generate a single universal PCR protocol for multiple primer sets. (Malaysia: Eppendorf Asia Pacific Headquarters, Kuala Lumpur)
- [14] Lopez J and Prezioso V 2001 A better way to optimize: two-step gradient PCR *Eppendorf BioNews Appl Note* 16 3-4
- [15] Kim H, Park N and Hahn J H 2016 Parallel-processing continuous-flow device for optimization-free polymerase chain reaction *Analytical and bioanalytical chemistry* 408 6751-8
- [16] Lagally E, Medintz I and Mathies R 2001 Single-molecule DNA amplification and analysis in an integrated microfluidic device *Analytical Chemistry* 73 565-70
- [17] Terabe S, Otsuka K and Ando T 1985 Electrokinetic chromatography with micellar solution and open-tubular capillary *Analytical Chemistry* 57 834-41
- [18] LightCycler 2.0 Product specifications.
<https://lifescience.roche.com/shop/en/global/products/lightcycler14301-20-instrument>. Accessed 15 September 2015
- [19] Sanford L N and Wittwer C T 2014 Fluorescence-based temperature control for polymerase chain reaction *Analytical biochemistry* 448 75-81
- [20] Sanford L N and Wittwer C T 2013 Monitoring temperature with fluorescence during real-time PCR and melting analysis *Analytical biochemistry* 434 26-33

Chapter 4 Thermal gradient for fluorometric optimization of droplet PCR in virtual reaction chambers

- [21] Natrajan V and Christensen K 2008 Two-color laser-induced fluorescent thermometry for microfluidic systems *Measurement Science and Technology* 20 015401
- [22] Prime PCR Optimisation: Using a gradient. Application Note A01-001B. technehelp@bibby-scientific.com
- [23] Bio-Rad 2006 Real-Time PCR applications guide

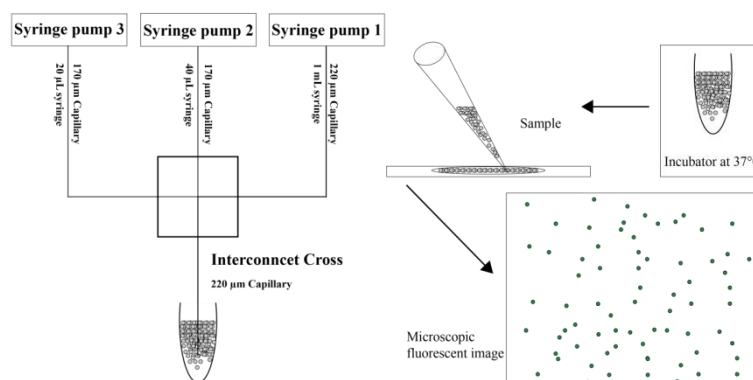
Chapter 5

Precise definition of starting time by capillary-based chemical initiation of digital isothermal DNA amplification

Manuscript in submission

Graphical abstract

A precise definition of the starting time of recombinase polymerase amplification (RPA) is proposed to achieve digital quantification of nucleic acids. Since the RPA reaction proceeds immediately, albeit slowly, at room temperature upon the addition of a chemical initiator, this increases the number of false positives at the single molecule level. A straightforward solution is to mix reagents after compartmentalization. A capillary-based setup is described controlling the initiation of RPA reactions by encapsulating the chemical initiator to each reaction compartment using shear force when passing through a cross connector. The performance of digital droplet RPA (ddRPA) was validated. Potential applications in clinical and academic research under resource-limited settings can be envisaged.



Chapter 5 Precise definition of starting time by capillary-based chemical initiation of digital isothermal DNA amplification

Abstract

Digital polymerase chain reaction is a sensitive and reproducible method to assess the presence or absence of the amplification of individual target molecules confined in isolated compartments; this is used for the quantification of nucleic acids. In this paper, the precise definition of the start time of recombinase polymerase amplification (RPA) is proposed to achieve the digital quantification of nucleic acids at the single molecule level. RPA is a sequence-specific isothermal amplification method. Since the reaction will start immediately albeit slowly at room temperature following the addition of the chemical initiator (magnesium acetate), the number of false positives in digital RPA is increased if all reagents are mixed prior to compartmentalization. A capillary-based setup is described here to control the initiation of digital droplet RPA (ddRPA) reactions by encapsulating the chemical initiator to each reaction partition using shear force when passed through a cross connector. Thousands of independent compartments are generated. The performance of ddRPA was validated by counting the positive application results of target molecules (Avian virus DNA) confined in the partitions. The ddRPA capillary-based setup provides a simple nucleic acid quantification method without thermal cycling. Potential applications in clinical and academic research under resource-limited settings can be envisaged. The ability to initiate chemical reaction compartments by the encapsulation of a chemical initiator using similar capillaries can be applied to a broader range of applications.

Keywords: RPA, Capillary, Avian virus, ddPCR, chemical initiator

5.1 Introduction

The quantitative analysis of nucleic acids is of great importance for studying gene expression [1] and molecular diagnostics [2–5], such as in the analysis of genomic diseases and cancer [6,7] and prenatal diagnostics [8,9]. Digital PCR (dPCR) is a method that is widely used for the quantitative analysis of nucleic acids. This method transfers the exponential nature of PCR amplification into a linear, digital format. Since its inception [6,10], dPCR has shown advantages over real-time PCR (or quantitative PCR) in terms of repeatability, reproducibility and linearity, without being dependent on the cycle threshold or external references, especially in rare variant diagnosis, molecule screening, and genome sequencing [11,12].

dPCR can be performed in various formats, namely well plates [9,13], microdroplets [14–16], pneumatic-controlled microchips [17], centrifugal force-driven setups [18,19], and the SlipChip [20,21]. By partitioning the diluted target molecules into a large number of isolated minute-volume partitions, single copy of nucleic acid templates will be confined in independent partitions and amplified by PCR. The number of compartments is usually much higher than the expected number of target molecules in the sample and all compartments are assumed to be of the same size. A statistical Poisson distribution analysis on the number of binary “yes” and “no” readout is performed after reaction to determine the number of target molecules in the sample.

A new version of dPCR [22,23] – digital droplet PCR (ddPCR), is enabled by droplet microfluidics. ddPCR consists of a huge number of aqueous droplets encapsulated in a carrier oil which are used to guarantee that one molecule or zero is present at the limit of dilution [24], resulting in the accurate quantification of target molecules. Aqueous micro-droplets have provided miniaturized reaction chambers for a large number of chemical, biochemical or pharmaceutical applications, etc. There are two most common techniques used for generating the monodisperse

Chapter 5 Precise definition of starting time by capillary-based chemical initiation of digital isothermal DNA amplification

homogenous droplets: T-junctions [16,25–27] and flow focusing [28,29]. T-junction chips consist of two perpendicularly joined inlets. The dispersed phase is pinched off at the junction by the flow of a continuous phase. Flow-focusing chips have three inlets. The dispersed liquid is intercepted by two other channels delivering the carrier phase. The joined flow then passes through a constriction where droplets are formed.

Although the process for generating a large number of monodisperse, small-volume reaction compartments has been considerably simplified, thermal cycling and accurate temperature control [30] is still an essential step for ddPCR methods. For chip-based ddPCRs in labs, the droplets easily settle down and coalesce to large ones during thermocycling in plate wells [13,31] or in PCR tubes [32,33], further worsening the situation. As a result, missing targets and random noise arises among amplicons.

In parallel to microfluidic chips, many sophisticated chip-free machines with high precision are used for biological analyses, such as HPLC [34]. The channels are basically capillaries assembled with their connectors, and usually work under high pressure. It has demonstrated that the capillary junctions (T and cross shape) can be used to generate droplets. The sizes of the droplets generated are close to those of conventional microfluidic chips or even smaller depending on the inner diameter of the capillaries and the fluids' speed, laying the foundation for setting up ddRPA on the basis of capillaries.

Recombinase polymerase amplification (RPA) is an isothermal DNA amplification technique, which works best at a low constant temperature of 37-42°C. RPA uses strand-displacing polymerases to copy the target sequence upon primer binding. It is tolerant to impure samples and uses lyophilized enzymes easy for storage and transport [35]. Digital isothermal amplification experiments have been shown

Chapter 5 Precise definition of starting time by capillary-based chemical initiation of digital isothermal DNA amplification

[19,21,34–36], where the mechanism of DNA amplification and fluorescence signal generation facilitated by RPA has been described.

For ddPCR, the PCR mix is usually compartmentalized into a large number of droplets after which amplification is triggered by a “hot-start”. In comparison, isothermal methods such as RPA cannot be triggered by a hot-start but will start immediately even at room temperature when a chemical initiator is added. Inspired by this, in this paper, a capillary-based setup is described to perform ddRPA. In [36], a pico-array chip was fabricated using a photolithography mask and deep reactive-ion etching. The results are comparable; however, the fabrication involves a lot of work. A simple setup using droplet microfluidics with a precise definition of the starting time of RPA is proposed in this contribution. The droplet generation is done using an inter-connect cross. In contrast to a T-junction, it has 3 inlet channels; it differs from flow focusing by introducing different liquids through each inlet. The technical advance illustrated in this work is the capability to confine individual target molecules and the chemical initiator into separate reaction compartments at the same time for precise starting time definition. The droplets are then put into an incubator to perform ddRPA. The amplified target molecule is detected by measuring the fluorescence emitted by SYBR Green I, which is more convenient to have on hand and less expensive. The setup can also be utilized to perform high-throughput chemical and biological reactions or screenings as initiating processes such as the confinement of one reagent with addition of another in isolated compartments are required.

5.2 Experimental

An integrated ddPCR system based on capillary is demonstrated in this section, where capillaries are associated with pumps and the junction. In this integrated ddRPA system, a cross-shaped interconnect junction serves as a droplet generator by introducing three different liquids to each inlet, thus confining one reagent with another in isolated compartments. Droplets are collected at the outlet. A stock solution of avian virus DNA [30] was chosen as the target molecule. The target molecules were diluted at various concentrations ranging from NTC to 2.6×10^3 copies/50 μ L.

5.2.1 Materials

The Labsmith μ Process Breadboard Model 3 R0 and SPS01 programmable syringe pump (Labsmith, Denmark) were bought from Labsmith. A syringe pump (World precision instruments (www.wpiinc.com)) was used to deliver the carrier oil phase. Microscope slides with a single cavity (VWR, Germany) for sample reading were purchased from VWR. All water used in the experiments was from a Milli-Q ProgradT3 column (<http://www.merckmillipore.com/DE/de>). Microscope Lens 2.5 x/0.075 NA (Epiplan-NEOFLUAR) was used to capture wide-field fluorescence image. Capillaries with inner/outer diameter of 220 μ m/363 μ m and 170 μ m/363 μ m VSD tubing (VWR, Germany) were purchased from VWR. Figure 5.1 shows some elements for building the setup.

Chapter 5 Precise definition of starting time by capillary-based chemical initiation of digital isothermal DNA amplification



Figure 5.1 Glass slide with a single cavity, one piece fitting, interconnect cross, 40 μ L syringe, a strand of capillary and SPS01 programmable syringe pump.

Chapter 5 Precise definition of starting time by capillary-based chemical initiation of digital isothermal DNA amplification

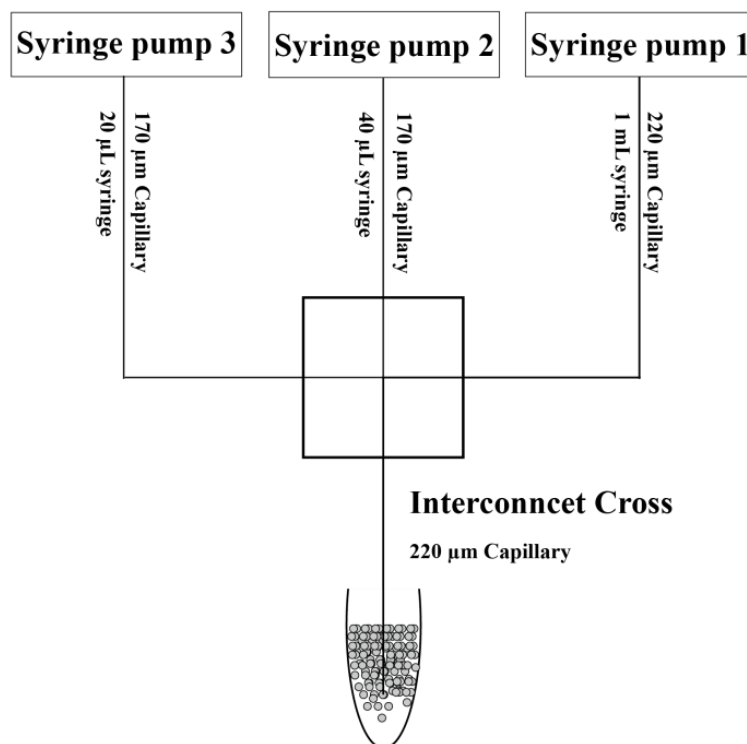


Figure 5.2 Sketches of the droplet generation. Syringe pump 1 is from world precision instruments. Syringe pump 2 and 3 are SPS01 programmable pumps. Pumps 2 and 3 were assembled on the Labsmith μ Process Breadboard.

5.2.2 PCR reagents

The TwistAmp exo+Campylocacter kit “improved formulation” for RPA was purchased from TwistDx Limited (Cambridge, United Kingdom). Glass slides with a cavity were purchased from VWR (Germany). SYBR was bought from Sigma-Aldrich (Germany). HFE-7500 3M Novec Engineered fluid was used as the continuous carrier oil phase.

Chapter 5 Precise definition of starting time by capillary-based chemical initiation of digital isothermal DNA amplification

Dilutions of DNA stock solution were performed in Eppendorf tubes using MilliQ water. Then, templates with various dilution factors were added to the pre-mixed PCR reagent.

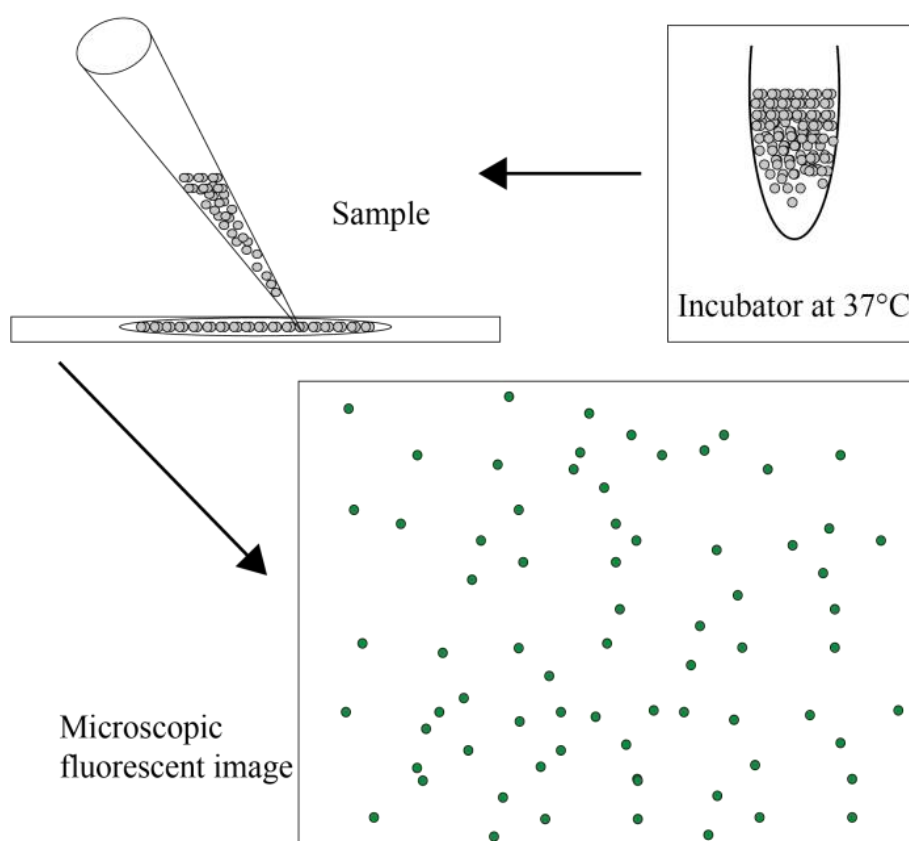


Figure 5.3 working flow of sample reading.

The RPA master mix was prepared according to the manufacturer's protocol, except for the addition of Mg^{2+} . The mixture was divided into two parts, as described. Mixture 1 consists of rehydrating the lyophilized enzyme in 29.5 μL of rehydration buffer, and then adding 5 μL each of primer, forward and reverse [30]

Chapter 5 Precise definition of starting time by capillary-based chemical initiation of digital isothermal DNA amplification

(100 pm/ μL). The solution was pulse-vortexed several times and then centrifuged briefly.

Mixture 2 consists of 5 μL of 280 mM of $\text{Mg}(\text{OAc})_2$ solution, 10 μL of Avian virus DNA and 2 μL of SYBR 100x. Reaction mixture 1 was introduced to a 40 μL syringe using a Labsmith Programmable syringe pump, while reaction mixture 2 was introduced to a 20 μL syringe, both at a speed of 20 $\mu\text{L}/\text{min}$. The oil phase was filled manually. The droplet generation setup is shown in Figure 5.2.

The dispensing rate of the three inputs was set to 3.5 $\mu\text{L}/\text{min}$ for reaction mixture 1, 1.5 $\mu\text{L}/\text{min}$ for reaction mixture 2 and 55 $\mu\text{L}/\text{min}$ for the continuous oil phase. The droplets collected were then put into a 37°C incubator for 1 hour. After incubation, 15 μL of each droplet samples was pipetted, with about half of the volume of fluorinated oil used to keep droplets from coalescence. The droplets were then pipetted into the cavity part of the microscope glass slide. A monolayer of droplets was assembled, floating on the top layer because of the lighter intensity. This enabled the subsequent imaging to count positive droplets. The work flow of sample reading is shown in Figure 5.3. All fluorescence images were acquired using a fluorescence microscope with a 2.5 X/0.075 NA objective. Each image frame has around 176 droplets with a droplet size of 11.67 nL, as shown in Figure 5.4.

5.3 Results and discussion

Unlike that which has been established in PCR, many isothermal amplification techniques are not triggered by a “hot-start”. Instead, the reaction is usually set off by a chemical initiator. For RPA, the mixture is prepared without the addition of a chemical initiator (e.g. Mg^{2+}) to keep the reaction from starting. However, the reaction begins immediately upon the addition of Mg^{2+} , albeit slowly at room

Chapter 5 Precise definition of starting time by capillary-based chemical initiation of digital isothermal DNA amplification

temperature (25°C). When ddRPA is performed in a digital format, this phenomenon would cause potential issues, leading to inaccurate results. Therefore, to avoid such false-positive errors, the ddRPA proposed in this contribution compartmentalized the magnesium acetate with the remaining components of RPA at the same time. In other words, the noninitiating components (Mg^{2+} - deprived solution 1) and initiating reaction mixture 2 (Mg^{2+}) were encapsulated simultaneously.

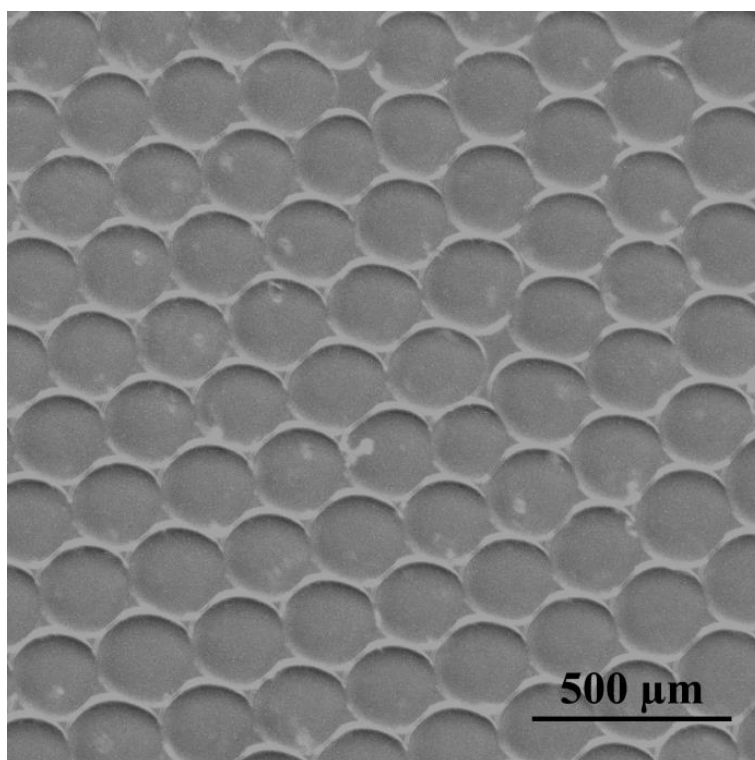


Figure 5.4 Droplet image taken using a 2.5x microscope lens. The droplet size is calculated to be 11.67 nL.

The design mentioned above first includes the two reagents in such a way that the reaction cannot be started automatically upon mixing. Then, the two mixtures are loaded separately into two independent syringes. The method is very straightforward and useful for defining the precise timing of the reaction by

Chapter 5 Precise definition of starting time by capillary-based chemical initiation of digital isothermal DNA amplification

allowing compartmentalization and mixing the two reagents afterwards. The incubation of compartments is performed after confining the target molecules inside.

While real-time PCR/RPA monitors the change in fluorescence signal over time, ddRPA relies on the end point binary fluorescence reading of either “0” or “1”. This end point readout is expected to be more accurate more tolerant to temperature fluctuations. Since the working temperature defines enzyme activity, real-time methods requiring accurate temperature control and quantitative analysis calibration are dramatically affected by temperature. Therefore, ddRPA is more applicable in point-of-care diagnostics, together with reliable and high resolution. It converts the exponential nature of the PCR to a linear signal profile; variations in the amplification efficiency are permitted, thus providing data with higher precision at measuring changes in samples.

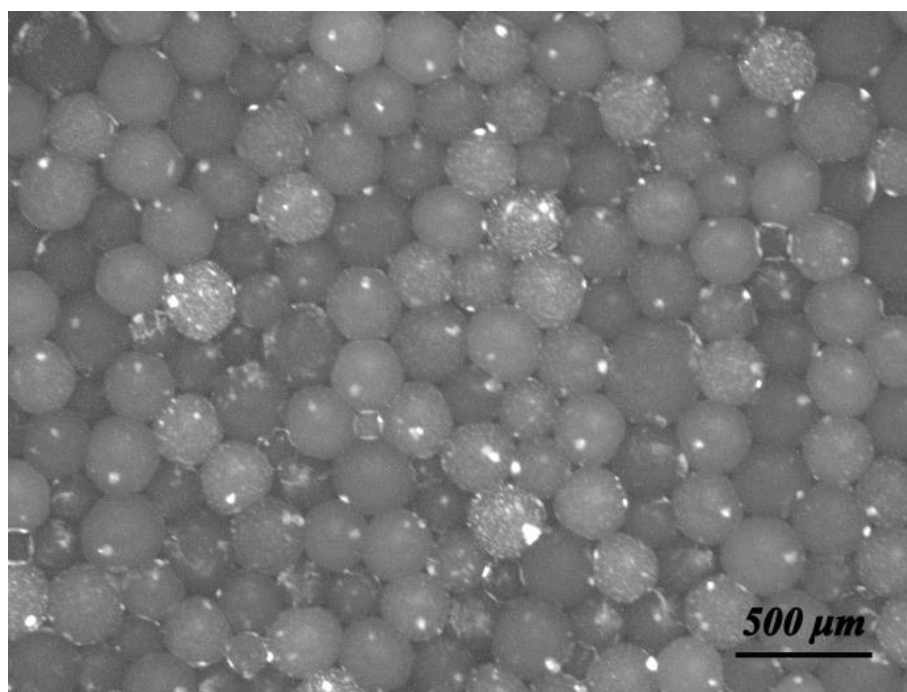


Figure 5.5 Original fluorescent image of ddRPA with an initial concentration 2.6×10^3 copies/50 μ L.

Chapter 5 Precise definition of starting time by capillary-based chemical initiation of digital isothermal DNA amplification

The performance of ddRPA was characterized by running a series of dilutions of the DNA stock solution from a previous work. Positive droplets exhibit increased fluorescence after incubation compared to negative ones, since at least one copy of the target DNA molecule was present, while there were 0 copies in negative droplets, as shown in Figure 5.5. False colored fluorescence images, with green indicating positive droplets and red indicating negative droplets, are shown in Figure 5.6. As the target DNA was diluted, the fraction of positive droplets of the sample reader decreased proportionally after incubation. The experiments were repeated four times at each diluted concentration to verify the robustness and reproducibility, as shown in figure 5.7. A regression fit of the linearized form of the Poisson equation (equation 5.1) [20][21], was utilized to statistically characterize the performance of the ddRPA experiments. In equation 5.1, p is the number of positive droplets, c is the initial concentration of target molecules prior to the dilution, x is the fractional dilution factor (in units of concentration⁻¹, e.g. 10 fold dilution corresponds to $x=0.1$), and t is the total number of droplets. The excellent regression fit obtained in Figure 5.8 indicates that the serially-diluted experiments produce self-consistent results that follow a Poisson distribution, supporting the appropriate use of the fit as a method of estimation. The initial stock concentration of Avian virus DNA is 2.6×10^3 copies/ 50 μ L. The expected results over the dilution range could then be calculated based on the fitting.

Chapter 5 Precise definition of starting time by capillary-based chemical initiation of digital isothermal DNA amplification

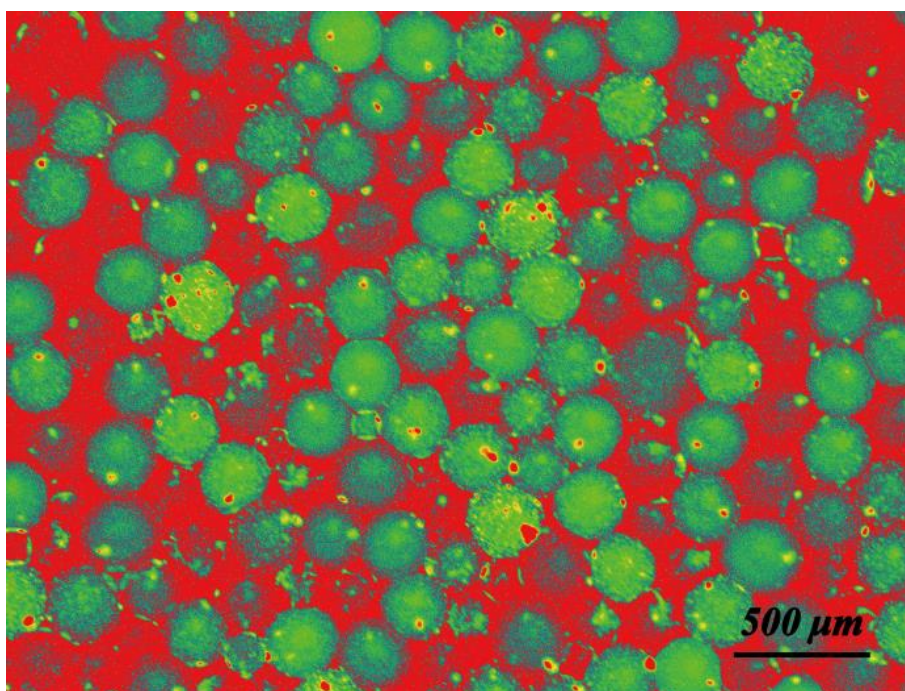


Figure 5.6 False colored fluorescence image, with green indicating positive droplets, and red indicating negative droplets.

$$\ln(t - p) = -c * x + \ln(t) \quad (5.1)$$

No false positive droplets were observed in the experiments due to the isolation in compartments prior to mixing all reagents. The applicability for the quantitative analysis of viral loads can be expanded by the incorporation of a reverse-transcription step. More broadly, this methodology can find numerous applications that need the precise definition of a start time of the reaction using a simple, chip-free setup, with only capillaries, thus saving the complex fabrication process, which is very attractive in resource-limited areas.

Chapter 5 Precise definition of starting time by capillary-based chemical initiation of digital isothermal DNA amplification

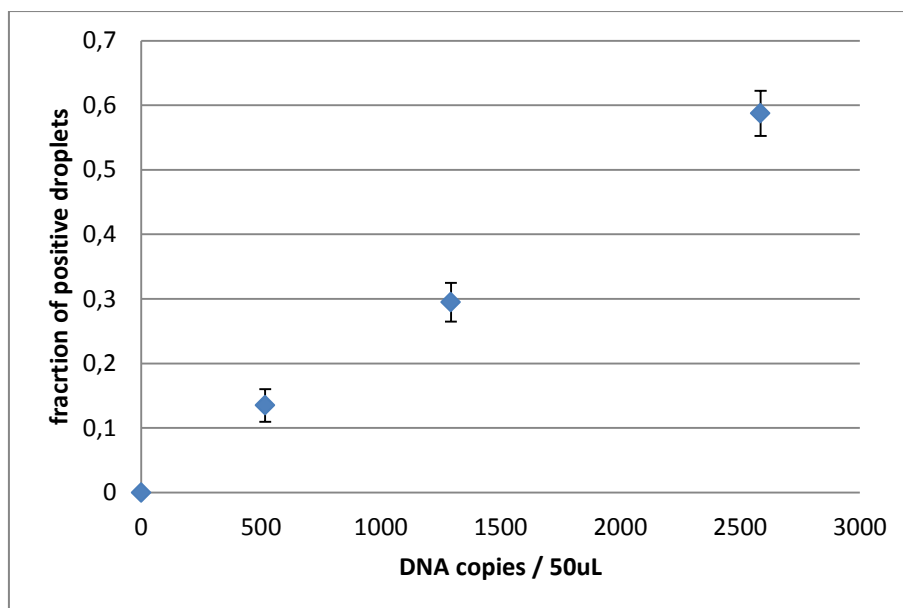


Figure 5.7 digital quantification of RPA experiments with different dilutions. Experimental average of the ratio of the number of positive droplets/droplets was plotted as a function of the diluted sample.

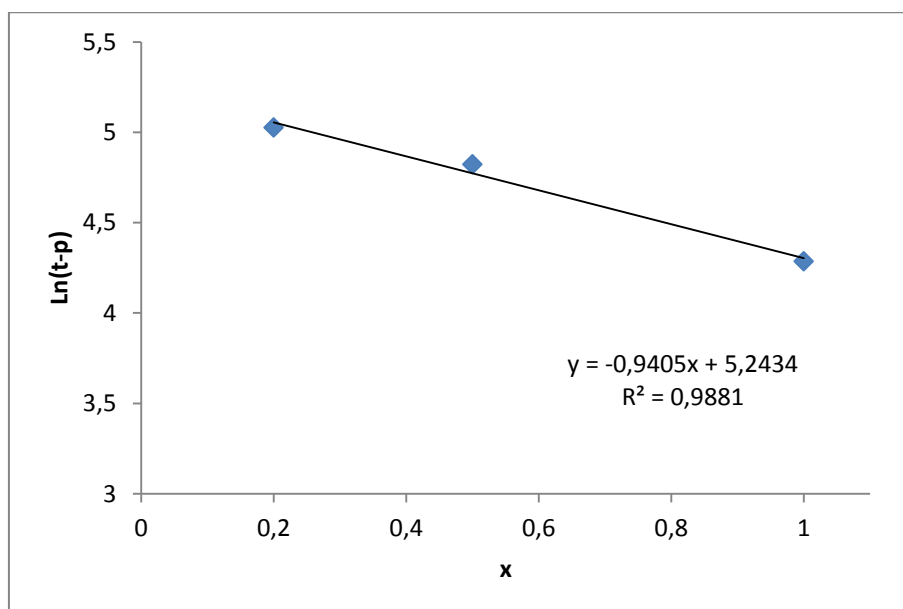


Figure 5.8 Regression fit of results of the three different concentrations according to equation 5.1.

5.4 Conclusion

In summary, a ddRPA system using capillaries with the precise definition of the start time of the amplification is proposed. It has demonstrated that the chemical initiation of RPA in compartmentalized partitions lends itself to nucleic acid quantification in a digital format.

Since the RPA reaction is initiated by magnesium acetate instead of the “hot-start” established in standard PCR, even at room temperature (25°C), this increases the number of false positives in ddRPA if all reagents are mixed prior to compartmentalization. Our ddRPA scheme addressed this issue by preparing the reaction mixture separately with one part containing no magnesium acetate. The two solutions, one containing Mg^{2+} and the Mg^{2+} – deprived solution, were then introduced through different syringes; the magnesium acetate was added to each single compartment by fluorinated oil using the sheer force when passing through an interconnect cross. Thanks to the isolated compartments, no false positive droplets of RPA were observed. In the meantime, the possibility of cross-contamination was eliminated, leading to a robust and reproducible result. The statistical analysis of results demonstrated that the capillary-based ddRPA system is of high performance in terms of simplicity and reliability. In short, the system shows a high linearity at a series of different dilutions ranging from NTC to 2.6×10^3 copies per 50 μ L, and the self-consistent performance follows a Poisson distribution. More broadly, a wider range of applications which rely on or require an initiation process can utilize this methodology.

Chapter 5 Precise definition of starting time by capillary-based chemical initiation of digital isothermal DNA amplification

Author contributions

Xiangping Li came with the idea of using capillary setup to precise control the starting time of PRA and conducted the experiments. Prof. Andreas Manz involved in experimental design and discussions. Both authors have reviewed the manuscript.

Reference

- [1] Livak K J and Schmittgen T D 2001 Analysis of Relative Gene Expression Data Using Real-Time Quantitative PCR and the $2^{-\Delta\Delta CT}$ Method *Methods* **25** 402–8
- [2] Mackay I M, Arden K E and Nitsche A 2002 Real-time PCR in virology. *Nucleic Acids Res.* **30** 1292–305
- [3] Jarvius J, Melin J, Göransson J, Stenberg J, Fredriksson S, Gonzalez-Rey C, Bertilsson S and Nilsson M 2006 Digital quantification using amplified single-molecule detection *Nat. Methods* **3** 725–7
- [4] Cheng B, Landay A and Miller V 2008 Research needs and challenges in the development of HIV diagnostic and treatment monitoring tests for use in resource-limited settings *Curr. Opin. HIV AIDS* **3** 495–503
- [5] Preiser W, Drexler J F and Drosten C 2006 HIV-1 Viral Load Assays for Resource-Limited Settings: Clades Matter *PLoS Med.* **3** e538
- [6] Vogelstein B and Kinzler K W 1999 Digital PCR. *Proc. Natl. Acad. Sci. U. S. A.* **96** 9236–41
- [7] Nacht M, Dracheva T, Gao Y, Fujii T, Chen Y, Player A, Akmaev V, Cook B, Dufault M, Zhang M, Zhang W, Guo M, Curran J, Han S, Sidransky D, Buetow K, Madden S L and Jen J 2001 Molecular characteristics of non-small cell lung cancer. *Proc. Natl. Acad. Sci. U. S. A.* **98** 15203–8
- [8] Fan H C and Quake S R 2007 Detection of aneuploidy with digital polymerase chain reaction *Anal. Chem.* **79** 7576–9

Chapter 5 Precise definition of starting time by capillary-based chemical initiation of digital isothermal DNA amplification

- [9] Dennis Lo Y M, Lun F M F, Chan K C A, Tsui N B Y, Chong K C, Lau T K, Leung T Y, Zee B C Y, Cantor C R and Chiu R W K Digital PCR for the molecular detection of fetal chromosomal aneuploidy
- [10] Sykes P J, Neoh S H, Brisco M J, Hughes E, Condon J and Morley A A 1992 Quantitation of targets for PCR by use of limiting dilution. *Biotechniques* **13** 444–9
- [11] Huggett J F, Foy C A, Benes V, Emslie K, Garson J A, Haynes R, Hellemans J, Kubista M, Mueller R D, Nolan T, Pfaffl M W, Shipley G L, Vandesompele J, Wittwer C T and Bustin S A The Digital MIQE Guidelines: Minimum Information for Publication of Quantitative Digital PCR Experiments
- [12] Hindson C M, Chevillet J R, Briggs H A, Gallichotte E N, Ruf I K, Hindson B J, Vessella R L and Tewari M 2013 Absolute quantification by droplet digital PCR versus analog real-time PCR *Nat. Methods* **10** 1003–5
- [13] Bian X, Jing F, Li G, Fan X, Jia C, Zhou H, Jin Q and Zhao J 2015 A microfluidic droplet digital PCR for simultaneous detection of pathogenic *Escherichia coli* O157 and *Listeria monocytogenes* *Biosens. Bioelectron.* **74** 770–7
- [14] Leng X, Zhang W, Wang C, Cui L and Yang C J 2010 Agarose droplet microfluidics for highly parallel and efficient single molecule emulsion PCR *Lab Chip* **10** 2841
- [15] Anon Droplet Digital™ PCR Droplet Digital™ PCR Applications Guide
- [16] Garstecki P, Fuerstman M J, Stone H A and Whitesides G M 2006 Formation of droplets and bubbles in a microfluidic T-junction—scaling and mechanism of break-up *Lab Chip* **6** 437
- [17] Ottesen E A, Hong J W, Quake S R and Leadbetter J R 2006 Microfluidic digital PCR enables multigene analysis of individual environmental bacteria. *Science* **314** 1464–7
- [18] Sundberg S O, Wittwer C T, Gao C and Gale B K 2010 Spinning Disk Platform for Microfluidic Digital Polymerase Chain Reaction *Anal. Chem.* **82** 1546–50
- [19] Schuler F, Schwemmer F, Trotter M, Wadle S, Zengerle R, von Stetten F and Paust N 2015 Centrifugal step emulsification applied for absolute quantification of nucleic acids by digital droplet RPA *Lab Chip* **15** 2759–66
- [20] Shen F, Du W, Kreutz J E, Fok A and Ismagilov R F 2010 Digital PCR on a SlipChip *Lab Chip* **10** 2666
- [21] Shen F, Davydova E K, Du W, Kreutz J E, Piepenburg O and Ismagilov R F

Chapter 5 Precise definition of starting time by capillary-based chemical initiation of digital isothermal DNA amplification

- 2011 Digital Isothermal Quantification of Nucleic Acids via Simultaneous Chemical Initiation of Recombinase Polymerase Amplification Reactions on SlipChip *Anal. Chem.* **83** 3533–40
- [22] Zhu P and Wang L 2017 Passive and active droplet generation with microfluidics: a review *Lab Chip* **17** 34–75
- [23] Wu T, Luo Z, Ding W, Cheng Z and He L 2017 Monodisperse droplets by impinging flow-focusing *Microfluid. Nanofluidics* **21** 129
- [24] Zilionis R, Nainys J, Veres A, Savova V, Zemmour D, Klein A M and Mazutis L 2016 Single-cell barcoding and sequencing using droplet microfluidics *Nat. Protoc.* **12** 44–73
- [25] Seemann R, Brinkmann M, Pfohl T and Herminghaus S 2012 Droplet based microfluidics *Reports Prog. Phys.* **75** 16601
- [26] Malsch D, Gleichmann N, Kielpinski M, Mayer G, Henkel T, Mueller D, van Steijn V, Kleijn C R and Kreutzer M T 2010 Dynamics of droplet formation at T-shaped nozzles with elastic feed lines *Microfluid. Nanofluidics* **8** 497–507
- [27] Thorsen T, Roberts R W, Arnold F H and Quake S R 2001 Dynamic Pattern Formation in a Vesicle-Generating Microfluidic Device *Phys. Rev. Lett.* **86** 4163–6
- [28] Gañán-Calvo A M 1998 Generation of Steady Liquid Microthreads and Micron-Sized Monodisperse Sprays in Gas Streams *Phys. Rev. Lett.* **80** 285–8
- [29] Anna S L, Bontoux N and Stone H A 2003 Formation of dispersions using “flow focusing” in microchannels *Appl. Phys. Lett.* **82** 364–6
- [30] Li X, Wu W and Manz A 2017 Thermal gradient for fluorometric optimization of droplet PCR in virtual reaction chambers *Microchim. Acta* 1–7
- [31] Beer N R, Hindson B J, Wheeler E K, Hall S B, Rose K A, Kennedy I M and Colston B W 2007 On-chip, real-time, single-copy polymerase chain reaction in picoliter droplets *Anal. Chem.* **79** 8471–5
- [32] Pekin D, Skhiri Y, Baret J-C, Le Corre D, Mazutis L, Ben Salem C, Millot F, El Harrak A, Hutchison J B, Larson J W, Link D R, Laurent-Puig P, Griffiths A D and Taly V 2011 Quantitative and sensitive detection of rare mutations using droplet-based microfluidics *Lab Chip* **11** 2156
- [33] Witte A K, Fister S, Mester P, Schoder D and Rossmanith P 2016 Evaluation of the performance of quantitative detection of the *Listeria monocytogenes*

Chapter 5 Precise definition of starting time by capillary-based chemical initiation of digital isothermal DNA amplification

prfA locus with droplet digital PCR *Anal. Bioanal. Chem.* **408** 7583–93

- [34] Chen J, Luo Z, Li L, He J, Li L, Zhu J, Wu P and He L 2018 Capillary-based integrated digital PCR in picoliter droplets *Lab Chip* **18** 412–21
- [35] Piepenburg O, Williams C H, Stemple D L and Armes N A 2006 DNA detection using recombination proteins ed J Haber *PLoS Biol.* **4** 1115–21
- [36] Li Z, Liu Y, Wei Q, Liu Y, Liu W, Zhang X and Yu Y 2016 Picoliter Well Array Chip-Based Digital Recombinase Polymerase Amplification for Absolute Quantification of Nucleic Acids ed V M Ugaz *PLoS One* **11** e0153359

Chapter 6

Duplex-imprinted Nano well arrays for promising nanoparticles assembly

This chapter has been published in *Nanotechnology*,
2018, 29 085302

Research highlights:

1. Nano-duplex-imprint technique with the Janus nanopillar structure of natural cicada wings as a stamp.
2. The technique, with excellent performance, combines top-down and bottom-up nanofabrication techniques.
3. No intricate devices or facilities are needed. No stringent surrounding environment is required.
4. The technique transitions micro-nanofabrication from the cleanroom environment to the bench.
5. The whole process is performed manually, and takes only a few minutes at room temperature and under atmospheric pressure.

Chapter 6 Duplex-imprinted Nano well arrays for promising nanoparticles assembly

Abstract

A large area nano-duplex-imprint technique is presented in this contribution using natural cicada wings as stamp. The glassy wings of the cicada, which are abundant in nature, exhibit strikingly interesting nanopillar structures over their membrane. This technique, with excellent performance despite the nonplanar surface of the wings, combines the top-down and bottom-up nanofabrication techniques. It transits micro-nanofabrication from cleanroom environment to bench. Two different materials – dicing tape with acrylic layer and UV optical adhesive – are used to make replications at the same time, thus achieving duplex imprint. Promising commercial volume manufacture of nanostructure elements can be envisaged through this contribution to speeding up the fabrication process and achieving higher throughput. Contact angle of the replicated nanowell arrays before and after oxygen plasma was measured. Gold nanoparticles (50 nm) were used to test how nanoparticles behave on the untreated and plasma treated replica surface. Experiments show that promising nanoparticles self-assembly can be obtained.

Keywords: duplex imprint; nanowell arrays; cicada; dicing tape; UV optical adhesive; nanoparticles

6.1. Introduction

Nanoscale fabrication technique with high resolution and large yield has been a remarkable research area due to its crucial role in patterning materials into nanostructures, especially into ordered array form for various applications, ranging from electronic memory to biomedical applications [1–8]. For these

Chapter 6 Duplex-imprinted Nano well arrays for promising nanoparticles assembly

applications, a bottom-up chemical method and a top-down lithographic method are two different primary fabrication categories. Conventionally, bottom-up chemical synthesis methods demonstrate decent size control, monodispersity and large-scale production of the resulting devices [8–17]. However, critical difficulties of controlling the shape, size, structure, and defects of resultant devices are presented. To solve such difficulties, physical top-down lithographic methods, with great potential in patterning nanoscale devices, have been proposed.

For ultraviolet and visible light applications, where the structural dimension at an optical interface must be smaller than the wavelength of the incident light [18], a feature size below 200 nm is always necessary. In such a small size range, conventional top-down lithographic technologies, such as electron beam etching [19] and fast atom beam [20], require sophisticated equipment and a stringent ambient environment. They are time-consuming and expensive for large-area fabrication for practical applications [21].

Given suitable fabrication techniques, the preparation of stamps of high resolution over a large area is a key procedure in nanostructure imprint fabrication. Various stamps, hard, soft or hybrid have been employed in many researches [8]. The processes are usually time consuming and complicated and, in some cases, expensive to carry out. In fact, periodic micro- and nanostructures existing in nature have provided enormous inspirations for scientists to mimic them for many important and specific applications. Many efforts have been made to replicate or directly utilize these bio-nanostructures, converting complicated natural 3D bioorganic structures into various otherwise unavailable material structures for optical, electronic, magnetic, thermal or catalytic applications [22–26]. With numerous species in nature to choose from, scientists could generate a wealth of intact, 3D shapes with sub micro- or nanometer resolution. Implicit in these efforts is the assumption that natural designs are good and useful, thanks to natural

Chapter 6 Duplex-imprinted Nano well arrays for promising nanoparticles assembly

selection or any other unguided natural process: for instance, elaborate structures, such as photonic crystals, wings, antennae, compound eyes etc [27,28].

In contrast to other natural phenomena, regularity is of top priority. Early studies revealed that regular pillar-like nanostructures are responsible for the low reflections. The ventral and dorsal nanopillar structure of the cicada's glass wing could offer many intriguing possibilities [29], not only optically with its transparent surface, but also scientifically. The glass wings of cicada have been proven to possess super-hydrophobic surfaces, which are thought to limit bacterial contamination through a self-cleaning action. Cicada wings have been shown to be able to kill *Pseudomonas aeruginosa* cells and other Gram-negative bacteria with extreme efficiency by wing surface [30,31]. Besides electro-optical device applications, the nanopillared arrays show a great promise in bioscience, such as investigation of the absorption of biomolecules and epithelial cell migrations using mapping force [32,33]. Such nanotip arrays can effectively absorb proteins and increase the sensitivity of detection [34].

With the aid of existing nanofabrication techniques up to now, different types of nanostructure fabrication methods using cicada have been developed. However, nearly all have been one-sided imprints [35–40]. These are difficult to put into practical application due to their costly and complicated procedures. Although the applications of biomimetic surfaces have been tried by several groups, the preparation cost is the limiting factor in putting them into practical applications. Therefore, developing simple, time- and cost- efficient techniques for an area large enough for practical applications is the key point in future work. With recent advances in the field of top-down and bottom-up nanofabrication techniques, a technique combining these methods will pave the way for achieving this objective. In this study, a duplex imprinting technique combining top-down and bottom-up techniques has been developed to replicate the Janus nanopillar structures of the glassy wing of the cicada. After imprint, contact angle measurement was

Chapter 6 Duplex-imprinted Nano well arrays for promising nanoparticles assembly

performed to both untreated and oxygen plasma treated nanowell array surfaces. A high contact angle is visible before oxygen plasma treatment. The nanowell arrays with gold nanoparticles inside show that further promising application of nanoparticle assembly.

6.2. Experimental

6.2.1 Materials

The cicadas (*Macrotristia chantranei*) were bought from an online specimen store, spreading 10-13 cm. Dicing tapes G19, G46 (Adwill, Japan) were stored in-house for dicing machine. G64 and D210 were kindly provided by Lintec Europe (Munich, Germany). G19 has a tape thickness of 80 μm , consisting of a PVC base material, thickness 70 μm , and an acrylic adhesive layer, thickness 10 μm . The adhesion is 46 mN/mm. UV optical adhesives NOA 81 and NOA 89 were from APM Technica (Germany). Gold nanoparticles (EM. GC 50/4, Plano GmbH) were kindly provided by INM institute.

6.2.2 Duplex imprint

Cicada wings were cleaned with acetone and Milli-Q water (Milli-Q ProgradT3 column) before use as stamps to remove stains, which would affect the quality of imprinting patterns. The wings were first sonicated (VWR ultrasonic cleaner) in Milli-Q water for about 15 min to remove contaminants adsorbed physically on the surface, then sonicated in acetone for 20 min to remove organic compounds and stains that stick the nanopillars together, and then sonicated again in Milli-Q water

Chapter 6 Duplex-imprinted Nano well arrays for promising nanoparticles assembly

for 5 min to remove residual acetone. The wings were then taken out and dried in a stream of nitrogen. The details on the surface of the wings were unchanged, as shown by subsequent SEM characterization. Fortunately, the surface tension remained low even after the cleaning treatment, which is very important for the imprint process. The patterned polymer would be destroyed during stamp release due to conglutination if the surface tension were too high.

Figure 6.1 gives a schematic diagram of how duplex imprint was realized. Experimental details can be accessed in the Electronic Supporting Information (ESI).

These structure replications using the duplex imprint technique can be extended to many applications. The nanostructure chips were treated with oxygen plasma (Diener electronic) for 30 s to make the surface hydrophilic. Water contact angle measurement (Drop shape analysis system DAS 10 MK 2) was performed in examining surface hydrophobicity before and after oxygen plasma. Gold nanoparticles were used to test how they will behave on the surface of the replicate nanowell arrays. Gold nanoparticles solution was first aliquoted into small volumes. The aliquot was then vortexed for 5 s, followed by centrifugation for 30 s. 300 nL drop was pipetted and put on the top of the nanoscale well arrays. SEM images will be shown in the following part. The particles distribute more evenly after vortex or sonication. Vortex or sonication makes sure the particles are evenly distributed before the onset of the tests. Additional video clips about how droplets behave on the replica surface are available in the supporting material.

Chapter 6 Duplex-imprinted Nano well arrays for promising nanoparticles assembly

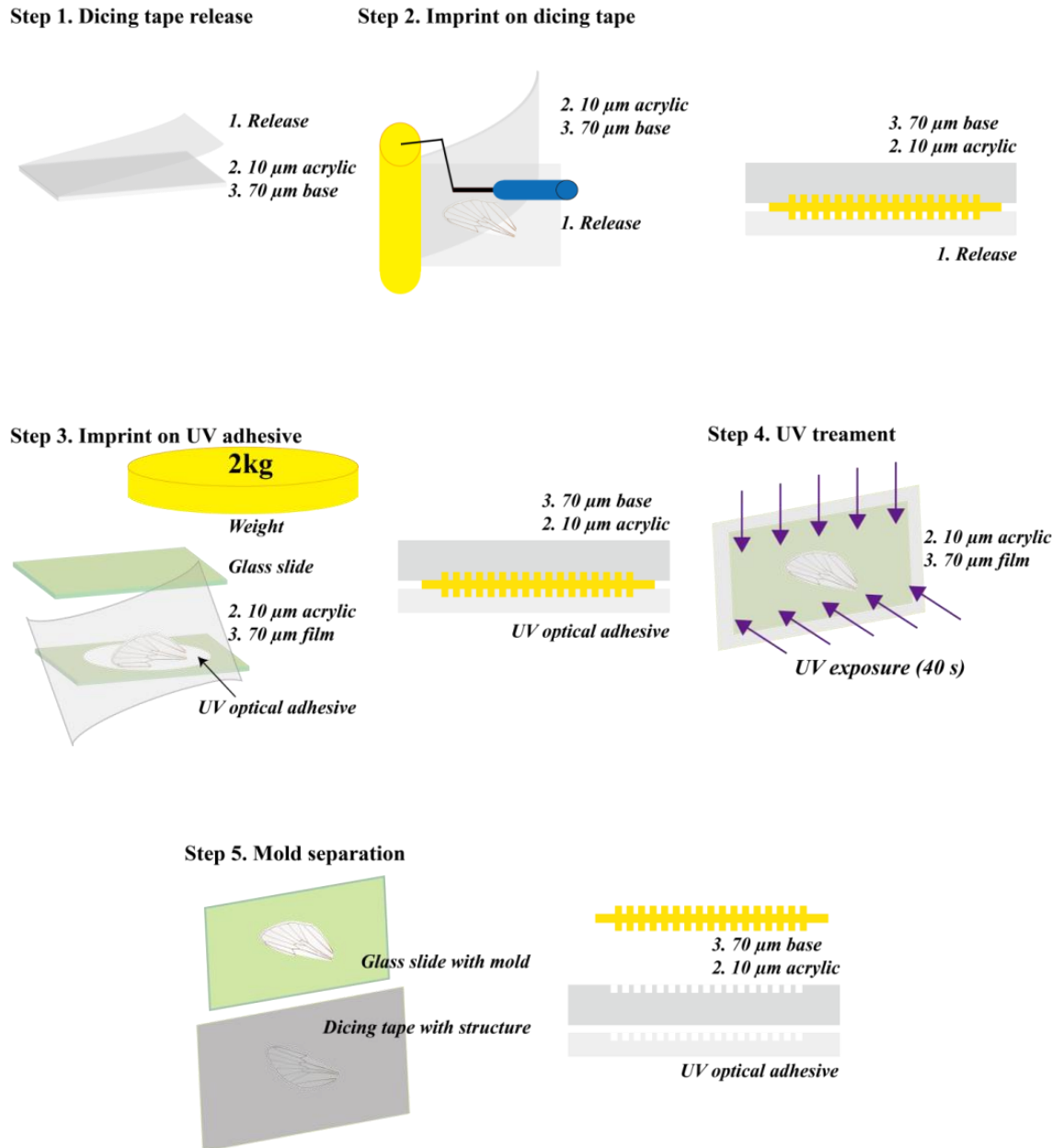


Figure 6.1 Schematic diagram showing duplex imprint with Janus nanopillared structures of cicada wing as stamps.

6.3. Results and discussion

The structure of ventral and dorsal sides of both the fore and hind cicada wings are covered with a periodic topography consisting of highly ordered hexagonal close-packed arrays of tapered nanoscale pillars of slightly different orientations. The height, spacing and diameter of the nanopillars vary between species. In this work, the spacing was sub-20 and sub-10 nm, or even touching, depending on the region. The height of pillars is about 400 nm and the diameters at the pillar top and bottom are about 40 and 130 nm, respectively. Those tapered pillars greatly minimize the reflectivity on their surfaces over broad angles or frequency ranges.

In general, small pillars prove much more difficult to imprint than small holes, because the pillars can easily tear off during mold separation. SEM can easily melt a small polymer pillar or destroy the replicated patterned polymer structure of the pillar arrays. Furthermore, the cicada wing membrane is non-flat. The irregular surface makes imprinting more challenging. The cicada wings have been shown to have strong mechanical properties. They can withstand 190 °C and 40 bar pressure for at least 3 min repeatedly. The cicada wings have sufficient rigidity, chemical stability and low surface tension to carry out imprints while preserving the original profile. These properties originate from the special composition of cicada wings. An arrangement of highly crystalline chitin nanofibers, embedded in a protein matrix, interacts with the matrix via hydrogen bonding. The hydrogen bonding imparts rigidity and chemical stability to the structure. The notable low surface tension of the wings originates from a layer of wax on their surface. The wax layer contains esters, acids, alcohols and hydrocarbons. Fortunately, the surface tension remains low even after the cleaning treatment, which is very important for imprinting. There is no such problem when using cicada wings as imprinting stamps. The patterned polymer will be destroyed during stamp release due to conglutination if the surface tension is too high. Therefore, the cicada-wing

Chapter 6 Duplex-imprinted Nano well arrays for promising nanoparticles assembly

stamps do not need to be deposited with an additional antiadhesive layer before imprinting. The Young's modulus of these cicada wings can be as high as 7–9 GPa. Although this number is still far lower than for traditional stamps used in NIL, such as silicon (up to 131 GPa), it is sufficient for imprinting while still maintaining the original profile.

Unlike previous work, wings were cut into very small pieces before imprinting, and the whole process carried out in a clean room with complex equipment and strict conditions. The technique does not necessitate removal of all the veins, except the largest outer exoskeleton elements, or cutting the wing into small pieces. The entire process takes only several minutes. SEM images of duplex replica using different tapes and optical adhesives are shown in Figure 6.2.

The experiments showed that the negative structures of the stamp had been successfully fabricated and nanowell arrays had formed. Furthermore, the nanowell arrays can be transferred to UV-cured adhesive using the same technique, with tape as mold, to replicate the structure on and surrounding veins. The pitch between the wells was about 150 nm, the well diameter about 130 nm, and the depth about 400 nm. These parameters are consistent with the stamp, since the nanopillar arrays are tapered. The bottom diameter size is the same, and the used stamps still preserved the original structure. Even the defects in the wing structures were well replicated, as shown in Figure 6.3.

Cicada-wing stamps can be used several times, although the quality of the imprinting results may decline due to the material of the cicada wings. They can be reused several times before being destroyed. This proves to be cost-effective because: i) the wings are abundant in nature and easy to obtain, and ii) the two materials used for replication are cheap. With these natural cicada wing stamps, nano-well arrays (negative structures of cicada wings) have been fabricated conveniently and successfully. The method can also be extended to other materials

Chapter 6 Duplex-imprinted Nano well arrays for promising nanoparticles assembly

useful in optical imaging, electrical engineering or surface-enhanced Ramen spectroscopy (SERS). The imprinted nanostructure can also be employed in abundant applications.

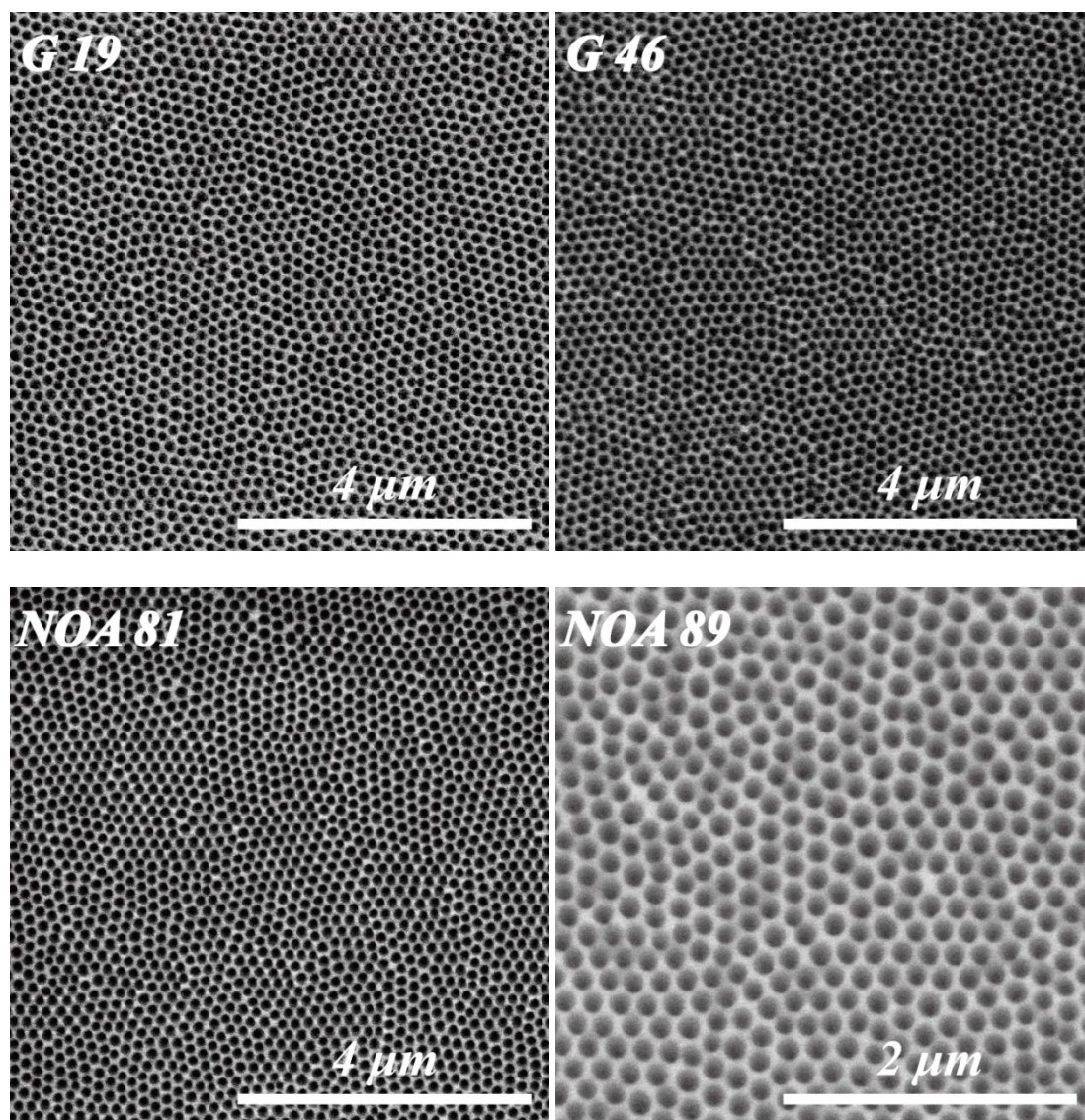


Figure 6.2 SEM image of replication using different tapes and adhesives.

Chapter 6 Duplex-imprinted Nano well arrays for promising nanoparticles assembly

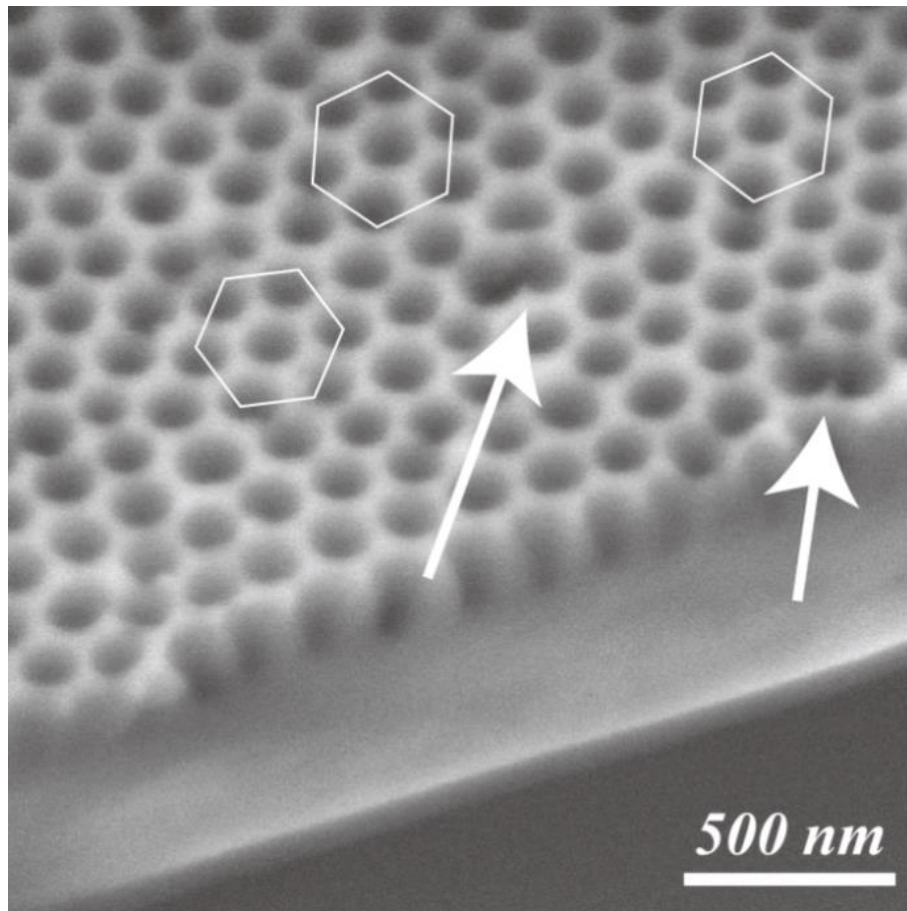


Figure 6.3 SEM image showing replicated defects in the wing structure.

Other dicing tapes, such as G46, G64, and D210, can also be used for imprinting. Various factors influence the choice of material. Here are some advices for choosing the material: i) Dicing tape: face material should be soft, with low stiffness. The adhesion after UV treatment should be low for D types. For G types, the rough adhesion should be within the range 35-73 mN/mm. For example, the adhesion of G64 is too weak for imprinting, ii) UV optical adhesive should have low viscosity; however, not too low, as, for instance, NOA 89 (viscosity around 20 cps) is not as stable as NOA 81. A viscosity of around 20–300 cps is suggested, iii) Silicon adhesive is good substitute material. Adhesion and viscosity should be

Chapter 6 Duplex-imprinted Nano well arrays for promising nanoparticles assembly

taken into consideration when making the choice. Unfortunately, we do not have results of using silicon material. However, the techniques are the same.

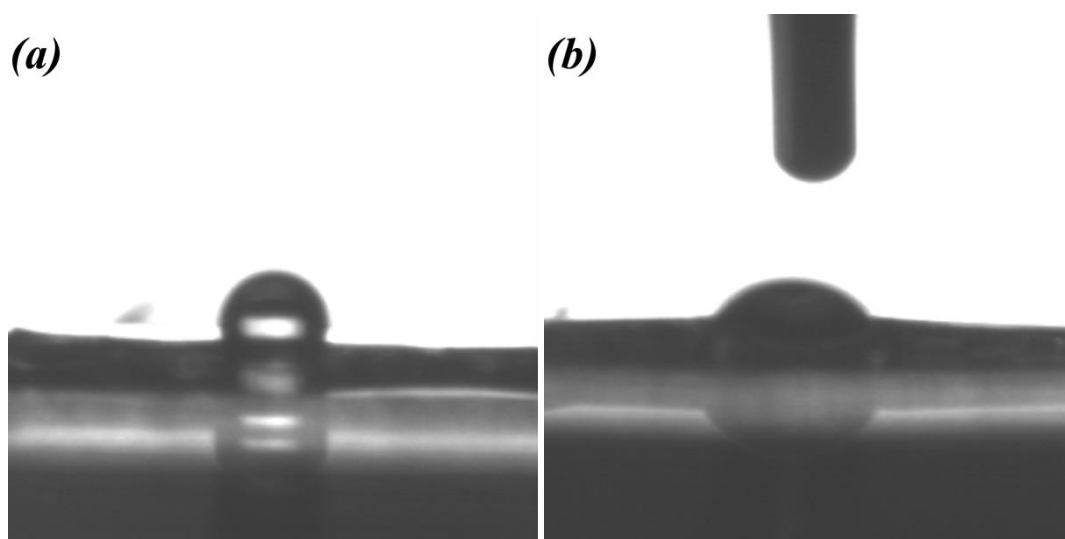


Figure 6.4 Contact angle measurements.

Water contact angle measurement was performed in examining surface hydrophobicity. The water droplet of the imprinted sample, as shown in figure 6.4(a), has a higher contact angle than the surface of the same material without nano patterns. After oxygen plasma treatment, the water contact angle became very low, as shown in Figure 6.4(b). After 1-2 s, the drop collapsed completely. Video clips in the ESI demonstrate more vividly. Figure 6.5 gives information of how gold nanoparticles behave on the surface of the replicate nanowell arrays. The particles distribute more evenly after vortex or sonication, which ensure the particles are evenly distributed before the test. The distributed Au particles follow Poisson distribution. While the Au nanoparticles were loaded manually with a pipette, an automatic platform and large particle size, for instance, is likely to help

Chapter 6 Duplex-imprinted Nano well arrays for promising nanoparticles assembly

controlling the number of nanoparticles in each well. This distribution allows us to digitally count and quantify the original particle concentration.

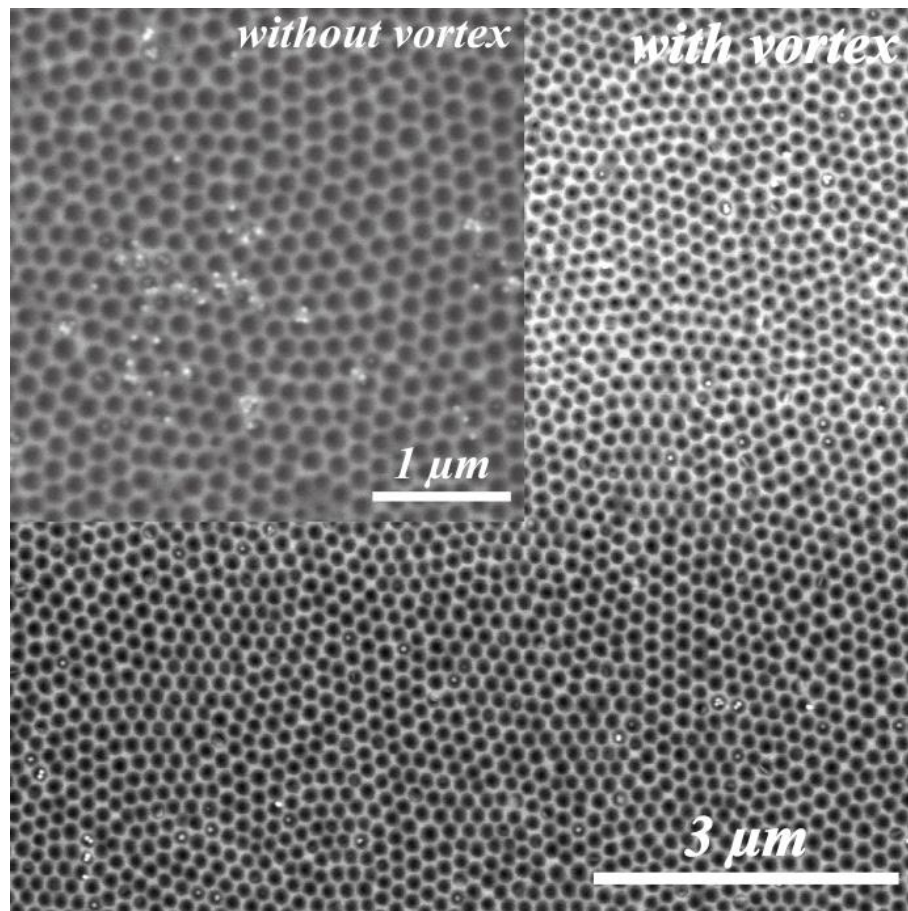


Figure 6.5 Gold nanoparticles in nanowell arrays.

6.4. Conclusions

In summary, we have demonstrated a novel and simple technique for large area nano-duplex imprinting using cicada wings as stamps. Nano-well arrays have been successfully fabricated by our method and the structures are well replicated, even

Chapter 6 Duplex-imprinted Nano well arrays for promising nanoparticles assembly

defects in the wing structure. Furthermore, with tape as mold, hexagonal pillar arrays can also be obtained using the same method. In short, the technique is easy, fast and cheap in room conditions. It may change the way we fabricate nanostructure chips. The technique, with excellent performance, combines the top-down and bottom-up nanofabrication techniques, despite the non-planar surface of the glassy wings. No complex equipment or facilities are needed. No stringent surrounding environment is required. It transits micro-nanofabrication from the cleanroom environment to the bench. Promising commercial volume manufacture of nanostructure elements can be envisaged through this contribution. The contact angle measurements as well as gold nanoparticles test indicate the further application of promising nanoparticles self-assembly.

Conflicts of interest

There are no conflicts to declare.

Acknowledgements

We would like to thank Linh Thai from Lintec Europe for supporting the research, Markus Koch (INM institute, Saarland) for helping with the cross section SEM images, Agu Vahtrik (Saarland University) for helping with gold nanoparticle imaging, ZhenJun Chang (Jiangsu University of Science and Technology) for the advice of manuscript preparation. This research was funded by the China Scholarship Council (File No. 201308330205).

Chapter 6 Duplex-imprinted Nano well arrays for promising nanoparticles assembly

Author contributions

Xiangping Li came with the idea of using the structure of Cicada wings for digital PCR and fabricated the biomimetic chip successfully using a duplex imprint nanofabrication technique. Prof. Andreas Manz helped with experimental preparation and involved in discussions. Both authors have reviewed the manuscript.

Supporting Information

Experimental Methods

The cicadas, as shown in Figure S1, were bought from an online specimen store. The transparent wings of a cicada look nothing but glassy under optical microscope.

- Imprint

The overall experimental procedure of duplex imprint is shown in Figure 6.1. Following description gives more details about each step.

Step 1- A piece of glass slide was taken as reference, and then a piece of dicing tape with slightly bigger size was cut as imprint material. The release layer (layer 1) was peeled off for later use.

Step 2- The cleaned wing was put on top of the inner clean side of layer 1, the stack layer of 2 and 3 was glued back with layer 1 with assistance of a paper roller. The paper roller ensured the smooth contact between the wing and the tape to avoid air bubbles being trapped. Rolled back and forth several times to make sure the

Chapter 6 Duplex-imprinted Nano well arrays for promising nanoparticles assembly

imprint on the tape was successful. Around the veins, pressed with a finger to facilitate the process, since the veins are much higher than the membrane. The area very close to the vein may be not well imprinted if not well attached to the tape.

Step 3- A drop of the adhesive was squeezed on top of a piece of clean glass slide. Layer 1 was peeled off from the stack layer of 2 and 3, and the stack layer side of the wing was put on top of the adhesive. No air bubbles were present. Another piece of glass slide was put on top of the stack layer to make an even print, also provided some mechanical pressure. A weight of 2 kg can be applied for 1–2 min to give more even pressure.

Step 4- The weight and the second glass slide were removed and the self-assembled part was exposed to UV light for 40 s. Then the dicing tape was gently peeled off, the glass slide with the wing and the dicing tape with the imprinted structure were obtained. The wing was attached to the glass slide through the cured UV adhesive. The glass with wing can be reused several times before the wing falls off. If the wing falls off, the replication of the other side of wing is on the adhesive, which is attached to the glass. In this sense, a duplex imprint is realized. The wing can also be manually removed.

Figure S2 shows a cross-section SEM image of a natural breakage of a NOA 81 replica, tilt 35°. Furthermore, the nano-well arrays can be transferred to UV-cured adhesive using the same technique, with tape as mold, to replicate the structure of veins, as shown in Figure S3.

Chapter 6 Duplex-imprinted Nano well arrays for promising nanoparticles assembly

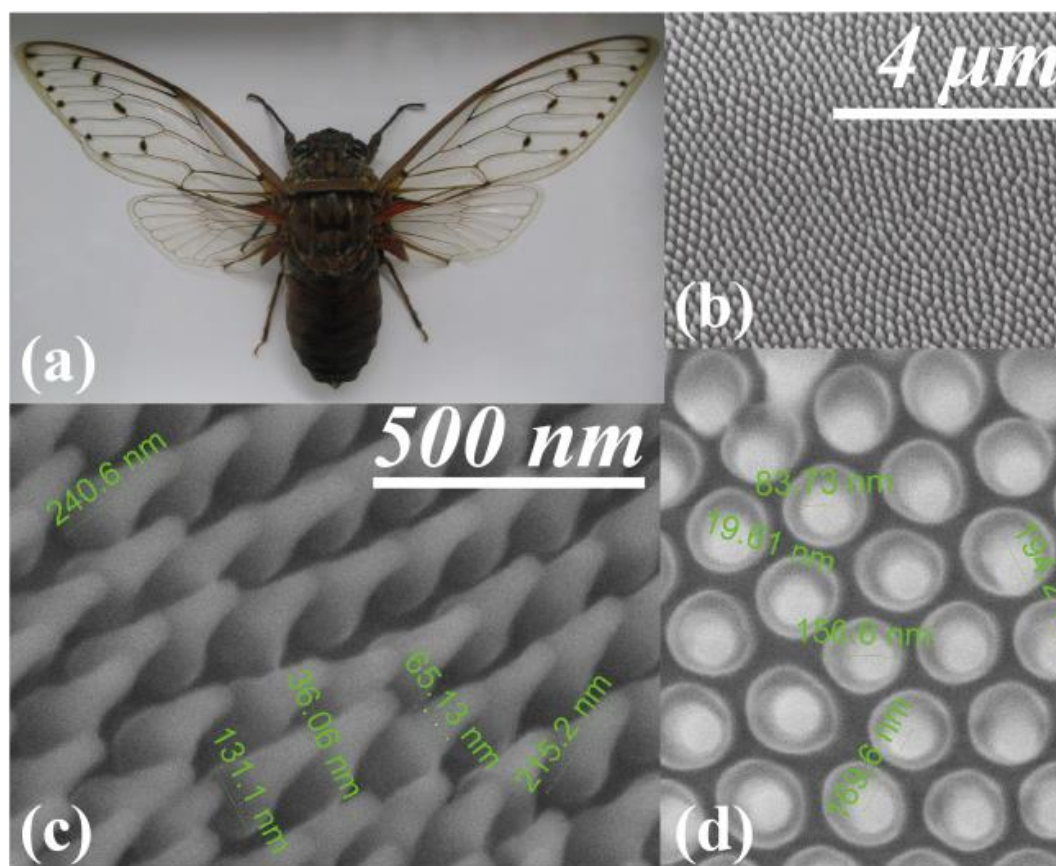


Figure S1 (a) Clear wing cicada (*Macrotristia chantranei*) spread 10-13 cm from online store. (b)(c)(d) SEM images of the surface of the wing. The surface consists of an array of nanoscale pillars with approximately hexagonal spacing. (c) SEM image of right small wing tilt 30°. (d) Scale bar is 500 nm.

Chapter 6 Duplex-imprinted Nano well arrays for promising nanoparticles assembly

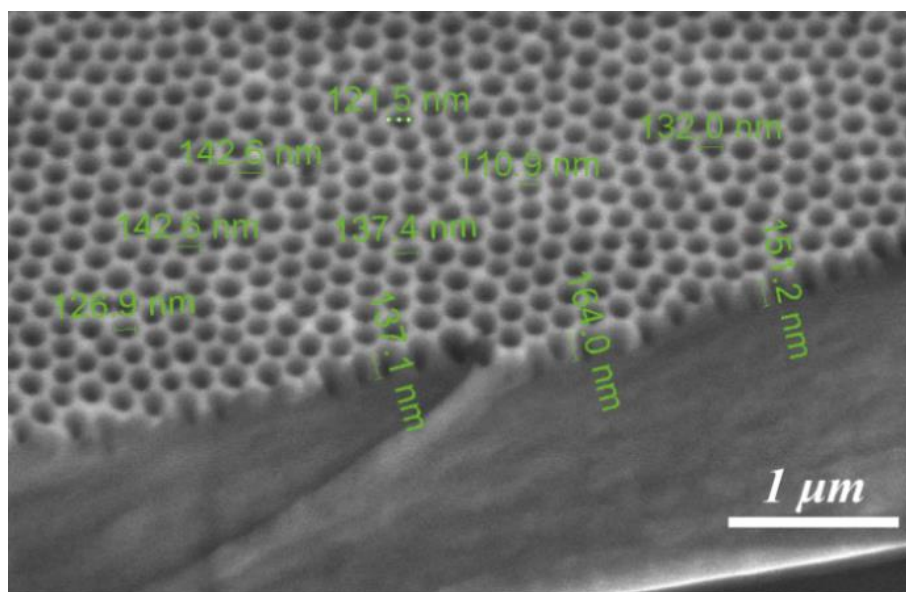


Figure S2 SEM image of cross-section measurement of replication (natural breakage with certain angle) using UV optical adhesive NOA 81, tilt 35°.

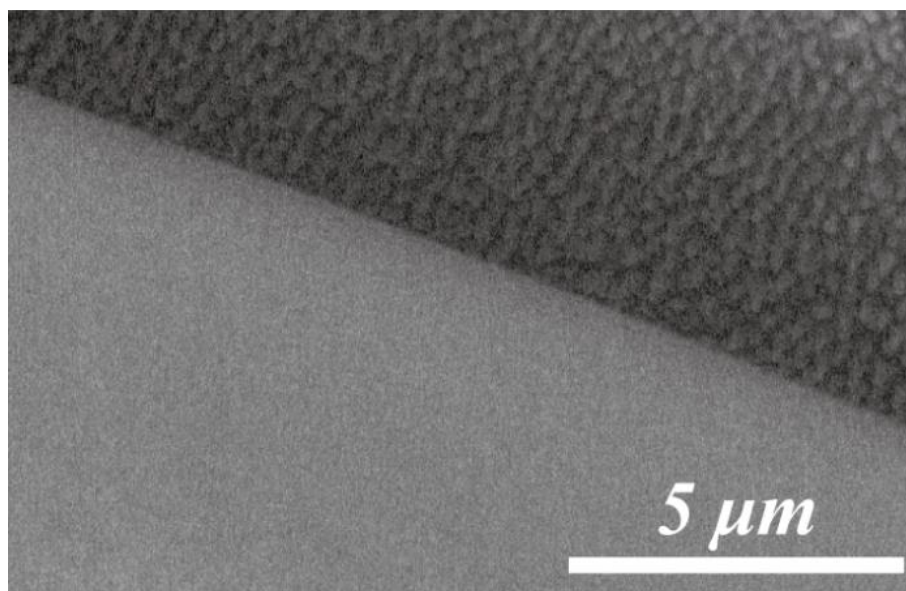


Figure S3 positive replication of the vein part using NOA 81.

Chapter 6 Duplex-imprinted Nano well arrays for promising nanoparticles assembly

References

- [1] Lee J-H, Huh Y-M, Jun Y, Seo J, Jang J, Song H-T, Kim S, Cho E-J, Yoon H-G, Suh J-S and Cheon J 2007 Artificially engineered magnetic nanoparticles for ultra-sensitive molecular imaging *Nat. Med.* 13 95–9
- [2] Kim D-H, Rozhkova E A, Ulasov I V, Bader S D, Rajh T, Lesniak M S and Novosad V 2009 Biofunctionalized magnetic-vortex microdiscs for targeted cancer-cell destruction *Nat. Mater.* 165–171
- [3] Canelas D A, Herlihy K P and DeSimone J M 2009 Top-down particle fabrication: control of size and shape for diagnostic imaging and drug delivery *Wiley Interdiscip. Rev. Nanomedicine Nanobiotechnology* 1 391–404
- [4] Ko H, Takei K, Kapadia R, Chuang S, Fang H, Leu P W, Ganapathi K, Plis E, Kim H S, Chen S-Y, Madsen M, Ford A C, Chueh Y-L, Krishna S, Salahuddin S and Javey A 2010 Ultrathin compound semiconductor on insulator layers for high-performance nanoscale transistors *Nature* 468
- [5] Yoon J, Jo S, Chun I S, Jung I, Kim H-S, Meitl M, Menard E, Li X, Coleman J J, Paik U and Rogers J A 2010 GaAs photovoltaics and optoelectronics using releasable multilayer epitaxial assemblies *Nature* 465
- [6] Chen R, Tran T-T D, Ng K W, Ko W S, Chuang L C, Sedgwick F G and Chang-Hasnain C 2011 Nanolasers grown on silicon *Nat. Photonics* 5 170–5
- [7] Ferris R, Hucknall A, Kwon B S, Chen T, Chilkoti A and Zauscher S 2011 Field-Induced Nanolithography for Patterning of Non-Fouling Polymer Brush Surfaces *Small* 7 3032–7
- [8] Kwon B and Kim J H 2016 Importance of Molds for Nanoimprint Lithography: Hard, Soft, and Hybrid Molds *J. Nanosci.* 2016 1–12
- [9] Meng Lin M, Kim H-H, Kim H, Muhammed M and Kyung Kim D 2010 Iron oxide-based nanomagnets in nanomedicine: fabrication and applications. *Nano Rev.* 1
- [10] Subramanian V, Wolf E E and Kamat P V. 2004 Catalysis with TiO₂/Gold Nanocomposites. Effect of Metal Particle Size on the Fermi Level Equilibration *J. Am. Chem. Soc.* 126 4943–50
- [11] Gupta A K and Gupta M 2005 Synthesis and surface engineering of iron oxide nanoparticles for biomedical applications *Biomaterials* 26 3995–4021

Chapter 6 Duplex-imprinted Nano well arrays for promising nanoparticles assembly

- [12] Hirata M, Gotou T, Horiuchi S, Fujiwara M and Ohba M 2004 Thin-film particles of graphite oxide 1: Carbon N. Y. 42 2929–37
- [13] Hoyle C E, Lowe A B, Bowman C N, Syrett J, Haddleton D M, Loos K, Barner-Kowollik C, Berner L, Muller A H E, Wacker R, Breinbauer R, Niemeyer C M and Waldmann H 2010 Thiol-click chemistry: a multifaceted toolbox for small molecule and polymer synthesis Chem. Soc. Rev. 39 1355
- [14] Cook T R, Zheng Y-R and Stang P J 2013 Metal-Organic Frameworks and Self-Assembled Supramolecular Coordination Complexes: Comparing and Contrasting the Design, Synthesis, and Functionality of Metal-Organic Materials Chem. Rev. 113 734–77
- [15] Zhou Y and Antonietti M 2003 Synthesis of Very Small TiO₂ Nanocrystals in a Room-Temperature Ionic Liquid and Their Self-Assembly toward Mesoporous Spherical Aggregates J. Am. Chem. Soc. 125 14960–1
- [16] Peng K-Q, Yan Y-J, Gao S-P and Zhu J 2002 Synthesis of Large-Area Silicon Nanowire Arrays via Self-Assembling Nanoelectrochemistry Adv. Mater. 14 1164
- [17] Martínez-Mera I, Espinosa-Pesqueira M E, Pérez-Hernández R and Arenas-Alatorre J 2007 Synthesis of magnetite (Fe₃O₄) nanoparticles without surfactants at room temperature Mater. Lett. 61 4447–51
- [18] Southwell W H 1991 Pyramid-array surface-relief structures producing antireflection index matching on optical surfaces J. Opt. Soc. Am. A 8 549
- [19] Toyota H, Takahara K, Okano M, Yotsuya T and Kikuta H 2001 Fabrication of Microcone Array for Antireflection Structured Surface Using Metal Dotted Pattern Jpn. J. Appl. Phys. 40 L747–9
- [20] Sai H, Fujii H, Arafune K, Ohshita Y, Yamaguchi M, Kanamori Y and Yugami H 2006 Antireflective subwavelength structures on crystalline Si fabricated using directly formed anodic porous alumina masks Appl. Phys. Lett. 88 201116
- [21] Li Y, Zhang J and Yang B 2010 Antireflective surfaces based on biomimetic nanopillared arrays Nano Today 5 117–27
- [22] Feng X J and Jiang L 2006 Design and Creation of Superwetting/Antiwetting Surfaces Adv. Mater. 18 3063–78
- [23] Xia F and Jiang L 2008 Bio-Inspired, Smart, Multiscale Interfacial Materials Adv. Mater. 20 2842–58

Chapter 6 Duplex-imprinted Nano well arrays for promising nanoparticles assembly

- [24] He J 2016 *Self-cleaning Coatings* (Cambridge: Royal Society of Chemistry)
- [25] Nishimoto S, Bhushan B, Koch K, Walzel P, Ochiai T, Murakami T, Fujishima A, Nakata K, Sakai H, Murakami T, Abe M, Komine T and Fujishima A 2013 Bioinspired self-cleaning surfaces with superhydrophobicity, superoleophobicity, and superhydrophilicity *RSC Adv.* 3 671–90
- [26] Tan Y, Gu J, Zang X, Xu W, Shi K, Xu L and Zhang D 2011 Versatile Fabrication of Intact Three-Dimensional Metallic Butterfly Wing Scales with Hierarchical Sub-micrometer Structures *Angew. Chemie Int. Ed.* 50 8307–11
- [27] Jeong K-H 2006 *Biologically Inspired Artificial Compound Eyes Science* (80-). 312 557–61
- [28] Rahman A, Ashraf A, Xin H, Tong X, Sutter P, Eisaman M D and Black C T 2015 Sub-50-nm self-assembled nanotextures for enhanced broadband antireflection in silicon solar cells *Nat. Commun.* 6 5963
- [29] Sun M, Watson G S, Zheng Y, Watson J A and Liang A 2009 Wetting properties on nanostructured surfaces of cicada wings *J. Exp. Biol.* 212
- [30] Ivanova E P, Hasan J, Webb H K, Truong V K, Watson G S, Watson J A, Baulin V A, Pogodin S, Wang J Y, Tobin M J, Löbbe C and Crawford R J 2012 Natural bactericidal surfaces: Mechanical rupture of *Pseudomonas aeruginosa* cells by cicada wings *Small* 8 2489–94
- [31] Pogodin S, Hasan J, Baulin V A, Webb H K, Truong V K, Phong Nguyen T H, Boshkovikj V, Fluke C J, Watson G S, Watson J A, Crawford R J and Ivanova E P 2013 Biophysical model of bacterial cell interactions with nanopatterned cicada wing surfaces *Biophys. J.* 104 835–40
- [32] du Roure O, Saez A, Buguin A, Austin R H, Chavrier P, Silberzan P, Silberzan P and Ladoux B 2005 Force mapping in epithelial cell migration. *Proc. Natl. Acad. Sci. U. S. A.* 102 2390–5
- [33] Mitragotri S and Lahann J 2009 Physical approaches to biomaterial design *Nat. Mater.* 8 15–23
- [34] Valsesia A, Mannelli I, Colpo P, Bretagnol F and Rossi F 2008 Protein Nanopatterns for Improved Immunodetection Sensitivity *Anal. Chem.* 80 7336–40
- [35] Chou S Y 2001 Nanoimprint Lithography and Lithographically Induced Self-Assembly *MRS Bull.* 26 512–7
- [36] Zhang W and Chou S Y 2003 Fabrication of 60-nm transistors on 4-in. wafer

Chapter 6 Duplex-imprinted Nano well arrays for promising nanoparticles assembly

using nanoimprint at all lithography levels Appl. Phys. Lett. 83 1632–4

- [37] Zhang G, Zhang J, Xie G, Liu Z and Shao H 2006 Cicada Wings: A Stamp from Nature for Nanoimprint Lithography Small 2 1440–3
- [38] Wu W, Tong W M, Bartman J, Chen Y, Walmsley R, Yu Z, Xia Q, Park I, Picciotto C, Gao J, Wang S-Y, Morecroft D, Yang J, Berggren K K and Williams R S 2008 Sub-10 nm Nanoimprint Lithography by Wafer Bowing Nano Lett. 8 3865–9
- [39] Hong S-H, Hwang J and Lee H 2009 Replication of cicada wing's nano-patterns by hot embossing and UV nanoimprinting Nanotechnology 20 385303
- [40] Ahn S H and Guo L J 2009 Large-Area Roll-to-Roll and Roll-to-Plate Nanoimprint Lithography: A Step toward High-Throughput Application of Continuous Nanoimprinting ACS Nano 3 2304–10

Chapter 7

Conclusion and outlook

The aim of this thesis was to study PCR from an engineering point of view, from the micro- to nanoscale, from thermal cycling to isothermal, and from analogue to digital.

Applications focused on the analysis of DNA; in the first step, a device aiming to optimize thermal cycled PCR was constructed from an analogue point of view. With the temperature-dependent dye as a calibrator, the real-time temperature across the annealing temperature range was given. In the meantime, a fluorescence detection system was embedded to the record real-time data.

In a subsequent step, the experiments proceeded towards a digital format and omitted the thermal cycling step. The capillary-assembled setup saves time for the design and production of microfluidic chips and generates a monodisperse water-in-oil emulsion. The idea originates from the nature of RPA, which is a single temperature nucleic acid amplification method initiated by a chemical initiator, instead of a “hot start”, as described in the first paper, or thermal cycled PCR.

The reaction takes place in droplet format and assumes that the partition of target molecules follows a Poisson distribution. Using a statistical analysis of the binary readout of “positive” and “negative” droplets, the absolute quantification of nucleic acids samples can be obtained.

The last section of the thesis centers on performing dPCR using a biomimetic structure. Cicada, which is abundant in nature, has been studied by many researchers and groups for self-cleaning, anti-fouling purposes. However, it was employed as the perfect mold for dPCR, thanks to its fascinating highly packed nanopillars. Due to the limitation of current technology, such a mold with tiny and

Chapter 7 Conclusion and outlook

compact nanopillars is very difficult to produce or manufactured. Thus making the stamp was appealing. A duplex nanoimprint technique is proposed for replicating the nanopillar structure; the copied chip was full of organized nanowell arrays, making it a perfect candidate for dPCR.

In conclusion, PCR was studied from an engineering point of view, at different scales and formats, and with various working principles. Throughout this PhD work, the goal of optimizing thermal cycled PCR in a single run is achieved, as detailed in Chapter 4. The thermal gradient feature introduced fulfills the purpose. In Chapter 5, the goal of realizing absolute quantification of nucleic acids is achieved through digital droplet RPA by using an integrated capillary-based setup. However, the goal of implementing digital PCR (dPCR) in a biomimetic nanowell chip is yet to be reached. Although a duplex nanoimprint technique is proposed to fabricate nanowell structures nicely, as detailed in Chapter 6, the implementation of (dPCR) needs time due to lacking of proper detection system. Conventional optical microscope is not sufficient to capture images at such small scale, and SEM could not take fluorescent images. A microscopy capable of taking fluorescent images, in the meantime, with fine resolution, such as STED is being taken into consideration.

Outlook

As described in the conclusion part, the goal of running dPCR in a biomimetic nanowell chip is yet to be finished, with the aid of STED. However, with the intriguing structure of Cicada chips, not only dPCR, but also other applications can be considered promising. The following part gives three main projects that is going to be fulfilled in the future.

Chapter 7 Conclusion and outlook

First, dPCR using STED microscopes with specific probes can be used as a detection method. In cooperation with the INM institute (Saarland University), work is ongoing.

Second, nanoparticle self-assembly using the KAPA tool is ongoing, in cooperation with the INM institute (Saarland University).

Third, matrix assisted laser desorption ionization (MALDI) mass spectrometry (MS) is ongoing, in cooperation with IBC group (Saarland University).

Appendix

List of abbreviations

Abbreviation	Description
A	Adenine
C	Cytosine
ddNTPs	Dideoxynucleotides
ddPCR	Digital droplet polymerase chain reaction
ddRPA	Digital droplet recombinase polymerase amplification
DNA	Deoxyribonucleic acid
dPCR	Digital polymerase chain reaction
dRPA	Digital recombinase polymerase amplification
dsDNA	Double stranded DNA
EBL	Electron beam lithography
EIL	Electron ion lithography
EtBr	Ethidium bromide
G	Guanine
HIV	Human immunodeficiency virus
IC	Integrated circuit
LOC	Lab-on-a-chip
MALDI	Matrix assisted laser desorption ionization
MCA	Melting curve analysis
MEMS	Microelectromechanical systems
MNF	Micro-Nano fabrication
mRNA	Messenger RNA
MS	Mass spectrometry
m-TAS	Miniaturized total analysis system

NGS	Next-generation sequencing
NIL	Nanoimprint lithography
PCR	Polymerase chain reaction
PDMS	Polydimethylsiloxane
qPCR	Quantitative PCR
Re	The Reynolds number
REM	Replica molding
RNA	Ribonucleic acid
RPA	Recombinase polymerase amplification
SAMIM	Solvent assisted micromolding
SEM	Scanning electron microscope
SNPs	Single nucleotide polymorphism
ssDNA	Single stranded DNA
STED	Stimulated emission depletion
STR	Short tandem repeats
T	Thymine
Taq	Thermus aquaticus
T_m	Melting temperature
ULSI	Ultra-large scale integrated circuits
UV	Ultraviolet
VRC	Virtual reaction chamber
μCP	Microcontact printing
μTAS	Micro total analysis systems

Thermal gradient for fluorometric optimization of droplet PCR in virtual reaction chambers

Xiangping Li^{1,2} · Wenming Wu³ · Andreas Manz^{1,2}

Received: 23 February 2017 / Accepted: 29 May 2017
© Springer-Verlag Wien 2017

Abstract An open system with a thermal gradient is described for the optimization of polymerase chain reactions (PCR). Two thermal electric coolers were used as the heat source. The gradient is measured through encapsulated water-based beads of a temperature-dependent dye inside mineral oil, thereby forming virtual reaction chambers. Nine droplets (with typical volume of 0.7 μL) were used. Using the intrinsic fluorescence of a temperature-sensitive inert dye (sulforhodamine B), the process involves measurement of the fluorescence intensity at a known, uniform temperature together with the instrument-specific calibration constant to calculate an unknown, possibly non-uniform temperature. The results show that a nearly linear thermal gradient is obtained. This gradient function is a useful feature that can be used for optimization of a commonly used enzyme-activated reaction, viz. PCR. The emission spectra of fluorescent droplets during two-step PCR were monitored and the changes in fluorescence between 50 °C and 100 °C quantified. As the gradient feature allows for testing a range of annealing temperatures simultaneously, the optimal annealing temperature can be easily determined in a single experiment.

Electronic supplementary material The online version of this article (doi:10.1007/s00604-017-2353-6) contains supplementary material, which is available to authorized users.

✉ Andreas Manz
manz@kist-europe.de

¹ Systems Engineering Department, Saarland University, 66123 Saarbruecken, Germany

² Microfluidics group, KIST Europe, Campus E7.1, 66123 Saarbruecken, Germany

³ State Key Laboratory of Applied Optics, Changchun Institute of Optics, Fine Mechanics and Physics (CIOMP), Chinese Academy of Sciences, Changchun 130033, China

Keywords Microfluidics · Droplet PCR · Thermal gradient · Fluorometric sensing · Temperature-dependent dye · Sulforhodamine B

Introduction

Microfluidic systems, or “labs-on-a-chip”, have revolutionized many aspects of quantitative biochemistry and analytical chemistry [1]. The potential advantages, including portability, speed, high efficiency, and reduced reagent consumption [1–4] have been explored by the miniaturization and integration of the various chemical operations. As in digital microfluidics where droplets are manipulated on an open, hydrophobic surface, the virtual reaction chamber (VRC) offers a simple way of exploiting the advantages of microfluidics and droplets while circumventing many of the practical problems. It is formed by encapsulating single aqueous sample droplets with volumes in the low microliter range within slight larger oil droplets [5–7].

Temperature is the most fundamental element in biochemical reactions [8], either in micro or macro scale. Therefore, to obtain robust, unique and clean products, optimization needs to be performed. This optimal temperature is often reaction dependent, or relies on other factors such as the physical characteristics of the molecules in a particular solvent or equipment characteristics. On the other hand, temperature may affect the rate or efficiency of the reaction. Accurate control of sample temperatures in microfluidic systems is often very important, particularly during the reaction and separation. The importance of temperature control in lab-on-a-chip devices has been demonstrated for enzyme-activated reactions [1, 5, 9–11].

One of these enzyme-activated reactions, polymerase chain reaction (PCR) [12], conducted by a deoxyribonucleic acid (DNA) polymerase, is introduced to illustrate the point. PCR

utilizes biological and chemical components to orchestrate enzymatic amplification. It gives access to a method of amplifying DNA molecules across several orders of magnitude, which has substantially accelerated the pace of research in many fields of biology.

The sequence and length of PCR primers generally determine the annealing temperature of the thermal cycling reaction for a specific assay. Using too low an annealing temperature can produce non-specific priming of templated DNA or form primer-dimers, whereas if the temperature is too high, little or no product may be produced. Therefore, PCR yield is reduced. These problems can often be avoided by an annealing temperature optimization step [13–15].

Most groups have reported using a temperature sensor to measure the temperature of the substrate of a microfluidic system [6, 7, 9, 16] or on the outside of capillaries [17, 18]. This is perhaps the simplest and easiest way to measure temperature. However, it is not accurate considering the temperature discrepancy between the temperature on the outside of the system and the fluid inside the system. Besides, concerns caused by direct sensor contact within the solution, such as product contamination or inhibition, the added thermal mass of the sensor, and the obstruction of optical measurements become more acute as the sample volume decreases, forcing measurements external to the sample and compromising accuracy during rapid temperature transitions.

A simple solution for non-contact temperature measurement is to use a passive reference dye whose fluorescence varies with temperature but does not inhibit the reaction. The technique takes advantage of the temperature dependence of the fluorescence intensity of a dilute fluorophore added to the fluid [2]. Since the fluorescence of many dyes is temperature-dependent [19, 20], a suitable dye has to be chosen for each specific application. Considering the repeated heating and cooling during thermal cycling, sulforhodamine B has been used for measuring temperature because of its reliable fluorescence over time [19–21]. Moreover, sulforhodamine B exhibits excellent temperature sensitivity.

4 parallel PCR reaction-stations were presented in [15] with a purpose of optimizing annealing temperature in the range of 50–68 °C. Our work, based on VRC, is capable of affording 9 thermal gradients, aiming to optimize PCR reaction in a single run and in more precise temperature scale. More thermal gradients can be obtained by smaller droplet size and tighter posited droplets. Commercially available gradient thermocyclers, such as the 96 Universal Gradient, PeQSTAR (<http://www.isogen-lifescience.com>), Mastercycler eppgradient (<http://www.labx.com>), and Chromo 4 usually require more than two temperature controlling modules to achieve the same temperature gradient. Most of them either have no real-time detection [22], or require large volumes of the PCR cocktail for the reaction [23]. Multi-zone temperature control may ensure accuracy. Nevertheless, more

energy is consumed by multi-heater units. Meanwhile, the footprint is much bigger because of multi-heater units and corresponding control parts. A two-step thermal gradient for fluorometric optimization of droplet PCR in virtual reaction chambers is present here. Sulforhodamine B was used for real-time thermal gradient control and monitoring. The method incorporates a two-step protocol combining the annealing and elongation steps, which leads to significant time-savings and a reduction in reagent use during optimization and standard PCR experiments.

Materials and methods

Surface preparation

As described earlier, the glass surface for the VRC has to be hydrophobic as well as oleo phobic. Chemical vapor deposition method is applied to silanize glass coverslips. A self-assembly monolayer of a fluorosilane with a reproducible contact angle (Drop shape analysis system DAS 10 MK 2, <https://www.kruss.de>) around 109 ° was achieved. Coating stability was assessed by the INM institute (<http://www.leibniz-inm.de>). Detailed description on surface coating can be accessed in supplementary material.

Temperature calibration

Theoretically, given a small piece of highly thermally conductive material, a uniform thermal distribution can be reached in seconds or milliseconds. By applying two different temperatures to this material, points along the temperature difference direction should have temperatures in between.

To demonstrate the point, sulforhodamine B, a passive dye which exhibits excellent temperature sensitivity, was chosen for monitoring the temperature. For absolute intensity of the fluorescence to serve as a temperature monitor, the instrument and dye must be stable over time. Temperature calibration was performed at equilibrium temperatures, not while the temperature was changing.

Temperature can be related to fluorescence through a calibration constant:

$$C = \ln(I/I_{ref}) / (1/T - 1/T_{ref}) \quad (1)$$

Fluorescence intensities I were measured at temperatures T (in Kelvin) and related to reference fluorescence intensity I_{ref} at a reference temperature T_{ref} . Instrument-specific calibration constants are used to convert fluorescence to solution temperatures. Afterwards, the solution temperatures were converted into Celsius using the following formula:

$$t(^{\circ}\text{C}) = T(\text{K}) - 273.15 \quad (2)$$

Where t and T represent temperature in *Celsius* and *Kelvin*, respectively. Detailed temperature calibration description can be found in supplementary material.

Reagents

All buffers were made using deionized water from a Milli-Q ProgradT3 column (<http://www.merckmillipore.com/DE/de>). The fluorescence of sulforhodamine B (monosodium salt, <http://www.sigmaaldrich.com/germany.html>) was measured in a “mock” PCR solution (without polymerase) at a final concentration of 0.1 mM; see protocol below. The polymerase was replaced with deionized water.

The performance of the system was verified by performing real-time PCR to detect a DNA segment of an avian virus. The PCR primers for the chosen avian virus segment (detailed sequence can be found in supporting material) were designed by Primer Express 3.0. The sequence of the forward primer:

5-TGTACTCCCCAGTGTTCATGATTG-3;

Reverse primer:

5-AAGGGAATAAGCGGCCATATC-3.

The melting temperature for the primer (Eurofins, Germany) is 60.6 °C.

The master mix was prepared by adding 3 μL of 25 mM MgCl_2 , 9 μL 50 pM of each forward and reverse primer, and 4 μL of the LightCycler FastStart DNA Master SYBR Green I (<http://www.roche.de/>). 2 μL DNA templates were added to the reaction mixture to the total volume of 27 μL immediately before the onset of the reaction. The template concentration was around 10^5 copies $\cdot \mu\text{L}^{-1}$.

On-chip PCR thermocycling

The instrument setup is shown in Fig. 1. Thermocycling of the microfluidic device was achieved using two thermoelectric coolers (1TML10-21 \times 21–10, <http://www.thermion-company.com/>) and a manufactured controller TEC-1122-SV (<http://www.meerstetter.ch/>). Temperature feedback was accomplished by inserting two 1 mm-thick 22 \times 22 mm copper plates on top of each TEC unit with an embedded Pt100 (<http://de.farnell.com/>) temperature sensor. Temperature control was performed by proportional integrated derivative (PID) feedback control. Optimized PID constants were used to achieve a fast yet stable control system. Then, another piece of 1.2 mm thick 20 \times 65 mm copper plate was placed between the microfluidic device and two small copper plates to facilitate efficient heat transfer to achieve a uniform heat distribution. A custom-fabricated copper block was placed beneath the TEC device to dissipate waste heat. Finally, a 3-mm silicon wafer was placed between the copper plate and the microfluidic device to help equalize heat distribution and provide a better optical surface for imaging. The

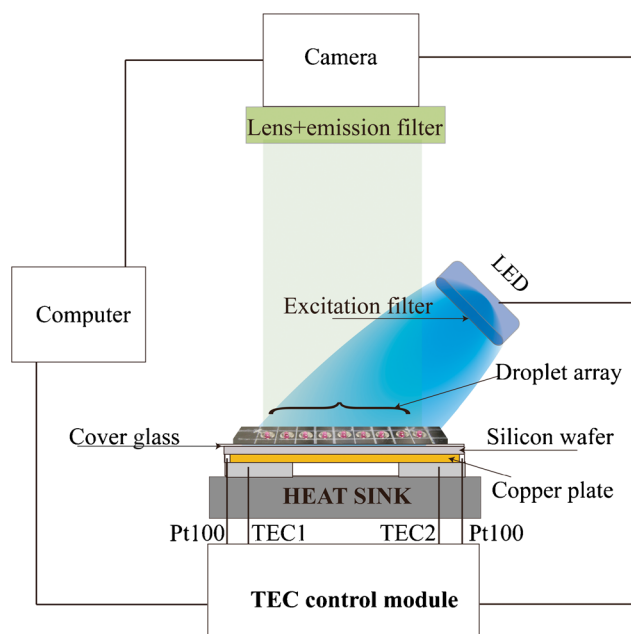


Fig. 1 Instrument setup. The TEC control module sends out a signal to LED and camera at the same time at the end of the annealing step, making sure that the LED light is on while capturing the image

VRC used in this work was formed by a 0.7 μL sample, covered with 3 μL of M5904 mineral oil (Sigma-Aldrich, <http://www.sigmaaldrich.com/germany.html>) and placed on a 170 μm thick hydrophobic/oleo phobic microscope coverslip. Two-step PCR thermocycling was initiated with a 10 min “hot start” at 95 °C to activate the Taq polymerase followed by 40 cycles of ramping between 50 °C and 95 °C using 10 s hold times and a thermal ramp rate of 5 °C \cdot s $^{-1}$. The total PCR thermocycling reaction time required \sim 45 min. The ability to perform on-chip thermal cycling of droplets is necessary to be able to perform real-time observation of the entire droplet reactor array during PCR amplification.

To find the optimal annealing temperature for the reaction, a recommended temperature range \pm 10 °C above and below the calculated melting temperature of the primers was used. Since the melting temperature for primer was 60.6 °C, the temperature gradient was set to 52 °C \sim 72 °C for optimization.

Image acquisition and processing

Fluorescence imaging of the sulforhodamine B dye was performed using a ProgRes MF Cool CCD camera (<https://www.jenoptik.de/>). The camera gain was set manually to 1 and kept constant throughout the whole experiment. An appropriate filter set (ET546/22 \times , ET605/70 m, www.ahf.de) was applied in front of the C-mount fixed focal lens HF 16HA-1B/1.4 (<http://fujifilm.jp>). Fluorescence imaging of the PCR reaction was the same as that for sulforhodamine B, except the filter set was different (MF469/35 <https://www.thorlabs.de/>, ET525/50 <https://www.chroma.com/>).

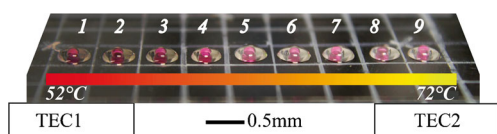


Fig. 2 Droplet array with thermal gradient. From left to right, the temperature increases and the droplets are numbered as droplet 1 to 9

ImageJ software and custom Matlab code were used to systematically detect and quantify fluorescent droplets and analyze the size and the fluorescence intensity.

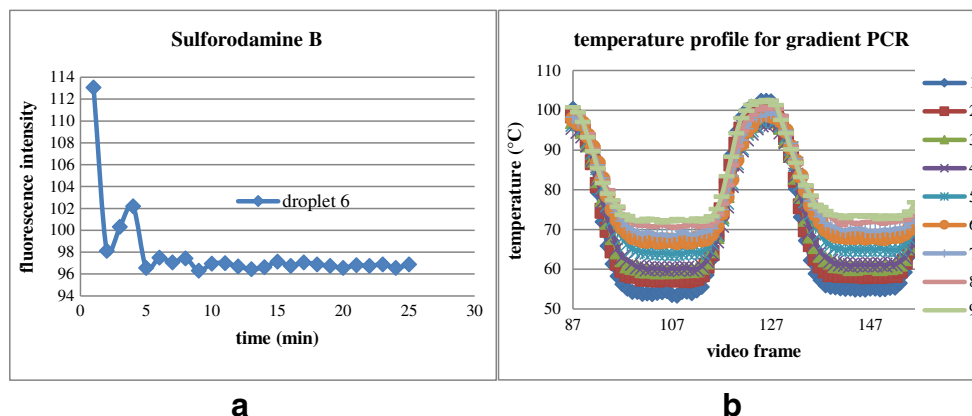
Melting analysis

Because SYBR Green I bind to all double-stranded DNA, it is necessary to check the specificity of the PCR assay by analyzing the amplified products. After each reaction, a melting curve analysis was run. A BioAnalyzer 2100 (<http://www.agilent.com/>) and gel electrophoresis were also used to check the specificity of the amplicon. Additional information on amplicon concentration can be accessed through the analysis from the BioAnalyzer. An optimized SYBR Green I PCR reaction should have a single peak in the melt curve, corresponding to a single band on the gel image. By comparing the gel image with the melt curve, one can identify peaks in the melt curve that correspond to specific products, additional non-specific bands and primer dimers.

Commercial instrument

Another group of experiments were performed on a commercial gradient machine, i.e. 96 Universal Gradient, PeQSTAR in house. Unfortunately, the device does not have a real-time function. Because of its large reaction volume, gel electrophoresis was carried out after the reaction. 5 μ L of each reaction product from the PeQSTAR commercial gradient machine was resolved on a 2% agarose gel for a period of 30 min at 100 V. 6X DNA Gel loading buffer was added at a ratio of 5:1. Gel images were taken by Bio-Rad (www.bio-rad.com). Gel lanes were processed using ImageJ.

Fig. 3 **a** Instrument equilibration of sulforhodamine B assessed at 55 °C. After 20 min, no evident change in fluorescence as well as evidence of photo bleaching was observed. **b** Temperature profile for gradient PCR. Each line denotes one sample as illustrated in Fig. 2



Results

Temperature gradient

When two different temperatures were applied at the two ends of the chip, a group of nearly linear different temperatures was obtained, forming a thermal gradient. Figure 2 illustrates the different temperatures in color. Meanwhile, the thermal gradient is represented by color depth. From left to right, the droplets are numbered droplet 1 to 9. The fluorescence of sulforhodamine B decreased as the temperature increased.

After temperature calibration, a two-step thermal cycling was run with sulforhodamine B monitoring the temperature in real time. Figure 3(a) shows the instrument equilibration of sulforhodamine B assessed at 55 °C while 3(b) shows the temperature profile of each droplet during the PCR reaction, positioned exactly as shown in Fig. 2. In order to demonstrate more clearly, the combined annealing and extension steps were set to 30 s. Each video frame denotes 2 s. The thermal gradient is clearly observable.

Gradient PCR

Nine droplets were prepared in each temperature zone. An additional droplet without template (NTC) was positioned in parallel with the fifth droplet, or can be placed anywhere on the chip except for spaces already taken up by the nine droplets. With a thermal gradient, PCR experiments can be optimized in a single run. The amplification curves of the reaction are shown in Fig. 4(a). The intensity plots reveal that droplet 4 has the highest fluorescence intensity. The best yield of the product was acquired at 61.04 °C.

Melt curve analysis was run to testify the specificity of the product, as shown in Fig. 4(b). Robust, unique, and clean products were obtained during the amplification, without any secondary products such as primer-dimers.

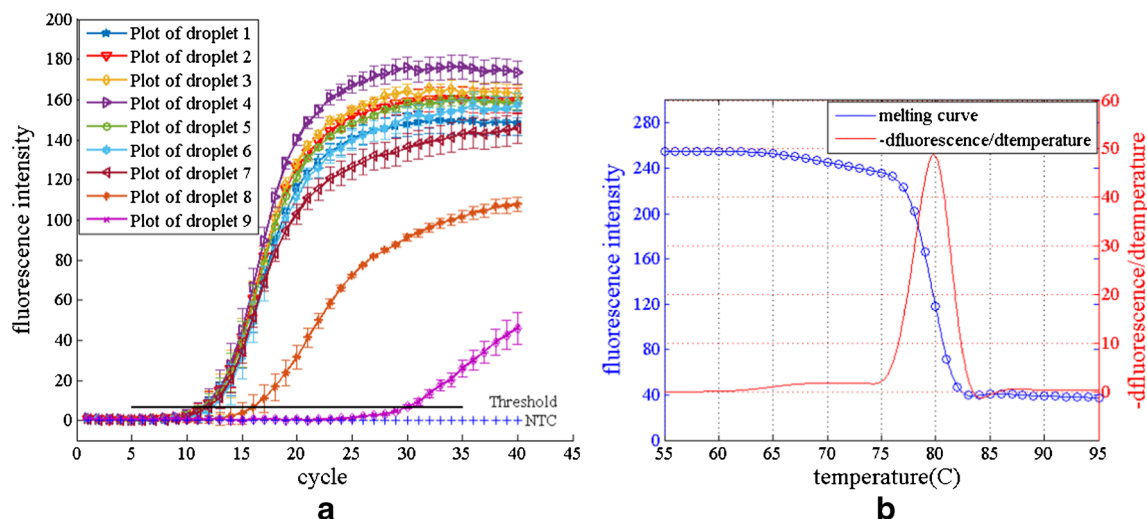


Fig. 4 **a** Amplification curves of gradient PCR. NTC denotes no template control. **b** Melt curve analysis of droplet 4 with the first derivative of the change in fluorescence intensity as a function of the

Another group of experiments was performed on 96 Universal Gradient, PeQSTAR. Since it is not a real-time machine, gel image of the results was taken by a Bio-Rad imager. The gel lanes of the gel image processed using ImageJ as shown in Fig. 5 show that 61.6 °C was the optimal temperature. The result is in accordance with the result from our device.

Figure 6(a) shows the temperature calculated from the calibration constant (the blue curve). The red curve represents the temperature measured by direct contact of the temperature sensor of the chip without thermal loads. No temporal delay was taken into consideration. Both methods showed an almost linear thermal gradient. Since the droplet volume is small, and so is the temperature sensor size, the discrepancies between the two methods can be neglected. However, care must be taken when using a large volume (thermal loads) for the reaction (most commercial devices use large volumes).

In order to determine the relationship between fluorescence intensity and the final concentration, the results

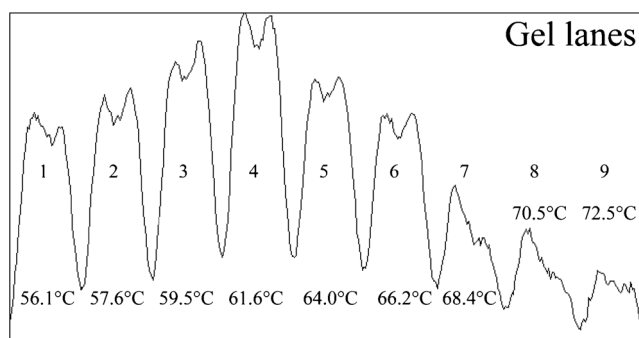


Fig. 5 Agarose gel result of PCR run on a commercial 96 Universal Gradient, PeQSTAR. The columns are gel lanes of the target amplicons. Lane 4 has the best result

temperature; meanwhile, only a single peak corresponding to the PCR product is observed. The amplicon is clean and specific

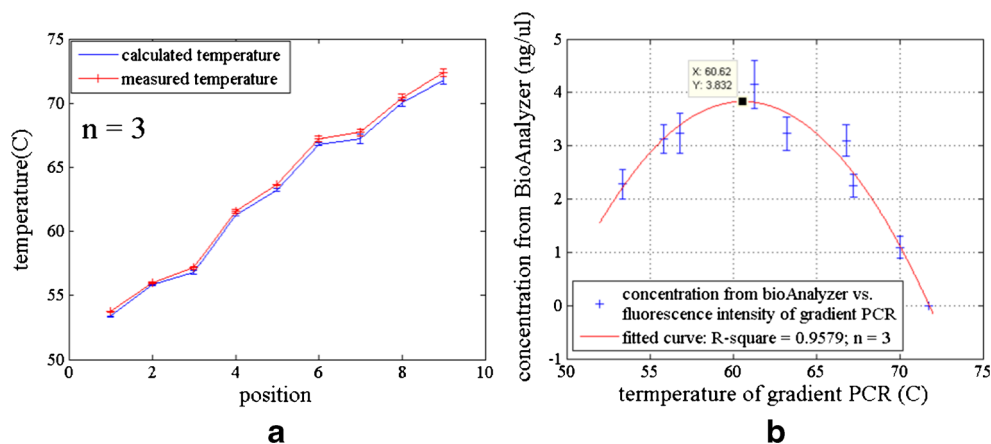
were transferred to a BioAnalyzer 2100 for further analysis. After running the analysis, a correlation analysis between the temperature gradient and the product concentration was performed in Fig. 6(b). The y-axis is the BioAnalyzer analysis from the annealing temperature optimization experiment. The optimal temperature was 60.62 °C.

Discussion

Different dyes react differently to temperature changes. The fluorescence of most dyes decreases as the temperature is increased. The exact temperature-time course of the sample can be monitored through the use of a temperature-sensitive passive reference dye, which can provide solution temperatures in real time throughout the thermal cycling. Therefore potentially controls the solution temperature. Sulforhodamine B was chosen because of its high temperature sensitivity and stability over repeated heating and cooling cycles. In addition to evaporation and/or condensation, other potential artifacts include instrument drift, thermal degradation of the dye, and fluorescence quenching, all of which might affect fluorescence signal as well. To use fluorescence to monitor temperature, fluorescence variations must be attributable to temperature. After 20 min, no evident change in fluorescence was observed. In addition, no evidence of photo bleaching of sulforhodamine B was observed.

The calibration constant is dependent on the physical characteristics of the fluorescent molecules in a particular solvent. It provides a quantitative way of judging the overall temperature sensitivity of the dye and optics. Different calibration constants range from 1314 ~ 1487 K for sulforhodamine B,

Fig. 6 **a** Thermal gradient formed from droplet 1 to 9. **b** Correlation between the thermal gradient and the BioAnalyzer analysis of amplicon concentrations



with an accuracy of $\pm 0.8 \sim 8\%$. Continuous acquisition throughout temperature cycling and melting was possible. A higher value of the calibration constant correlates to greater temperature sensitivity and system precision. Solution temperatures were determined using the calibration constant, I_{ref} and T_{ref} as shown in formula (1).

The reaction chamber was made by encapsulation of a water-based sample in mineral oil. As no solid cover or micro channels were required, device fabrications consisted only of deposition and patterning the substrate using chemical vapor deposition. The use of disposable glass slides prevents cross-contamination. The small droplet shape minimized the temperature gradient throughout the droplet. Furthermore, the disposable coverslip was not subject to any processing. The glass thermal conductivity coefficient is $1.1 \text{ Wm}^{-1}\text{K}^{-1}$, while the surrounding air has a thermal conductivity coefficient of only $0.025 \text{ Wm}^{-1}\text{K}^{-1}$. Therefore, the temperature of the glass will be determined only by the temperature of the silicon wafer attached to the thermoelectric coolers.

The outcome of optimizing the annealing temperature under a single gradient experiment with the primer set (melting temperature $60.6 \text{ }^\circ\text{C}$) was successful under a gradient range of $52 \text{ }^\circ\text{C}$ to $72 \text{ }^\circ\text{C}$. The primer set displayed a range of annealing temperatures that can successfully amplify the specific amplicon. The experiment demonstrates the possibility of optimizing a primer set using a single PCR protocol with a selected range of temperatures. This was also confirmed by running an experiment on a commercial gradient device in house. The gel electrophoresis of the products from the commercial device verified that our device works. PCR was optimized in a single run thanks to the thermal gradient generated based on a temperature-dependent dye. Furthermore, the optimal temperature was related to the relative fluorescence intensity of the gradient PCR, since the fluorescence intensity was proportional to the concentration. Hence, no further post-analysis using a gel or BioAnalyzer is required, saving a lot of time and effort. Moreover, because only a very small volume of the reagent mixture is needed for optimization, reagent costs and sample consumption can be highly reduced. Finally, the device is easy

to operate. However, this system is not perfect, such as the droplet preparation and alignment have to be done manually.

Conclusion

A small and simple device with a thermal gradient to optimize PCR was designed, with real-time monitoring of the gradient based on a temperature-dependent dye. This was achieved with no direct contact of the temperature sensor, no time delay and no discrepancies between the device and the droplet inside the oil. The gradient feature greatly reduced the time devoted to determining the optimal annealing temperature. The device is cheap, easy to operate and time-saving. Moreover, more gradients can be obtained using smaller and more tightly arranged droplets. The gradient feature is not limited to the annealing step but also allows for the optimization of the denaturation or extension temperature in one experiment as well. We expect that this temperature gradient feature will be used to optimize many reactions in the future.

Acknowledgements We would like to thank Christian Ahrberg (former KIST Europe employee) for help with data processing. We would like to thank Yuliya E. Silina (INM institute, Saarland University) for testing the stability of the coating method. We would like to thank Zhenjun Chang (Jiangsu University of Science and Technology) for the advice of revising the manuscript. This research was funded by the China Scholarship Council (File No. 201308330205).

Compliance with ethical standards The author(s) declare that they have no competing interests.

References

1. Kopp MU, De Mello AJ, Manz A (1998) Chemical amplification: continuous-flow PCR on a chip. *Science* 280:1046–1048
2. Ross D, Gaitan M, Locascio LE (2001) Temperature measurement in microfluidic systems using a temperature-dependent fluorescent dye. *Anal Chem* 73:4117–4123

3. Wu J, Kodzius R, Cao W, Wen W (2014) Extraction, amplification and detection of DNA in microfluidic chip-based assays. *Microchim Acta* 181:1611–1631
4. Karle M, Vashist SK, Zengerle R, von Stetten F (2016) Microfluidic solutions enabling continuous processing and monitoring of biological samples: a review. *Anal Chim Acta* 929:1–22
5. Neuzil P, Pipper J, Hsieh TM (2006) Disposable real-time microPCR device: lab-on-a-chip at a low cost. *Mol BioSyst* 2: 292–298
6. Neuzil P, Sun W, Karásek T, Manz A (2015) Nanoliter-sized over-heated reactor. *Appl Phys Lett* 106:024104
7. Ahrberg CD, Ilic BR, Manz A, Neuzil P (2016) Handheld real-time PCR device. *Lab Chip* 16:586–592
8. Wang X-d, Wolfbeis OS, Meier RJ (2013) Luminescent probes and sensors for temperature. *Chem Soc Rev* 42:7834–7869
9. Vukusic P, Hooper I (2005) Directionally controlled fluorescence emission in butterflies. *Science* 310:1151–1151
10. Hatch AC, Fisher JS, Tovar AR, Hsieh AT, Lin R, Pentoney SL, Yang DL, Lee AP (2011) 1-million droplet array with wide-field fluorescence imaging for digital PCR. *Lab Chip* 11:3838–3845
11. Ahrberg CD, Manz A, Chung BG (2016) Polymerase chain reaction in microfluidic devices. *Lab Chip* 16:3866–3884
12. Mullis K, Faloona F, Scharf S, Saiki R, Horn G, Erlich H (1986) Specific enzymatic amplification of DNA in vitro: the polymerase chain reaction. *Cold Spring Harb Symp Quant Biol* 51:263–273
13. Kean OW (2010) Using the gradient technology of the Mastercycler pro to generate a single universal PCR protocol for multiple primer sets. *Appl Note* 220
14. Lopez J, Prezioso V (2001) A better way to optimize: two-step gradient PCR. *Eppendorf BioNews Appl Note* 16:3–4
15. Kim H, Park N, Hahn JH (2016) Parallel-processing continuous-flow device for optimization-free polymerase chain reaction. *Anal Bioanal Chem* 408:6751–6758
16. Lagally E, Medintz I, Mathies R (2001) Single-molecule DNA amplification and analysis in an integrated microfluidic device. *Anal Chem* 73:565–570
17. Terabe S, Otsuka K, Ando T (1985) Electrokinetic chromatography with micellar solution and open-tubular capillary. *Anal Chem* 57: 834–841
18. LightCycler 2.0 Instrument (2017) Product specifications. <https://lifescience.roche.com/shop/en/global/products/lightcycler14301-20-instrument>. Accessed 20 Feb 2017
19. Sanford LN, Wittwer CT (2014) Fluorescence-based temperature control for polymerase chain reaction. *Anal Biochem* 448:75–81
20. Sanford LN, Wittwer CT (2013) Monitoring temperature with fluorescence during real-time PCR and melting analysis. *Anal Biochem* 434:26–33
21. Natrajan V, Christensen K (2008) Two-color laser-induced fluorescent thermometry for microfluidic systems. *Meas Sci Technol* 20:015401
22. ³Prime thermal cycler, PCR optimisation: using a gradient. <http://www.techne.com/product.asp?dsl=910>, *Appl Note* A01-001B Accessed 23 Feb 2017
23. Bio-Rad (2006) Real-Time PCR applications guide.

Duplex-imprinted nano well arrays for promising nanoparticle assembly

Xiangping Li^{1,2}  and Andreas Manz^{1,2} 

¹Systems Engineering Department, Saarland University, D-66123 Saarbruecken, Germany

²KIST Europe, Campus E7.1, D-66123 Saarbruecken, Germany

E-mail: manz@kist-europe.de

Received 20 September 2017, revised 7 December 2017

Accepted for publication 15 December 2017

Published 19 January 2018



CrossMark

Abstract

A large area nano-duplex-imprint technique is presented in this contribution using natural cicada wings as stamps. The glassy wings of the cicada, which are abundant in nature, exhibit strikingly interesting nanopillar structures over their membrane. This technique, with excellent performance despite the nonplanar surface of the wings, combines both top-down and bottom-up nanofabrication techniques. It transitions micro-nanofabrication from a cleanroom environment to the bench. Two different materials, dicing tape with an acrylic layer and a UV optical adhesive, are used to make replications at the same time, thus achieving duplex imprinting. The promise of a large volume of commercial manufacturing of these nanostructure elements can be envisaged through this contribution to speeding up the fabrication process and achieving a higher throughput. The contact angle of the replicated nanowell arrays before and after oxygen plasma was measured. Gold nanoparticles (50 nm) were used to test how the nanoparticles behaved on the untreated and plasma-treated replica surface. The experiments show that promising nanoparticle self-assembly can be obtained.

Supplementary material for this article is available [online](#)

Keywords: duplex imprint, nanowell arrays, cicada, nanoparticles, dicing tape, UV optical adhesive

(Some figures may appear in colour only in the online journal)

1. Introduction

Nanoscale fabrication techniques with a high resolution and large yield have been a remarkable research area due to their crucial role in patterning, especially into an ordered array for various applications, ranging from electronic memory to biomedical applications [1–8]. For these applications, there are two different fabrication categories: a bottom-up chemical method and a top-down lithographic method. Conventionally, the bottom-up chemical synthesis method demonstrates decent size control, monodispersity and large-scale production of the resulting devices [8–17]. However, critical difficulties of controlling the shape, size, structure and defects of resultant devices are present. To solve such difficulties, physical top-down lithographic methods, with great potential in patterning nanoscale devices, have been proposed.

For ultraviolet and visible light applications, where the structural dimensions at the optical interface must be smaller

than the wavelength of the incident light [18], a feature size below 200 nm is always necessary. Such small size ranges, mean that conventional top-down lithographic technologies, such as electron beam etching [19] and fast atom beams [20], require sophisticated equipment and a stringent ambient environment. They are time-consuming and expensive methods for large-area fabrication practical applications [21].

Given suitable fabrication techniques, the preparation of high resolution stamps over a large area is a key procedure in nanostructure imprint fabrication. Various stamps, hard, soft or hybrid have been employed numerous times in research [8]. The processes are usually time consuming and complicated and, in some cases, expensive to carry out. Periodic micro- and nanostructures existing in nature have provided enormous inspiration for scientists often attempting to mimic these structures for many important and specific applications. Many efforts have been made to replicate or directly utilize these bio-nanostructures, converting complicated natural 3D

bioorganic structures into various otherwise unavailable material structures for optical, electronic, magnetic, thermal or catalytic applications [22–26]. With numerous species in nature to choose from, scientists could generate a wealth of 3D shapes with sub micro- or nanometer resolution. These efforts are based on the assumption that natural designs are good and useful, thanks to natural selection or any other unguided natural process. For instance, photonic crystals, wings, antennae, compound eyes etc are examples of naturally occurring elaborated structures [27, 28].

In comparison to other natural phenomena, regularity is one of the top priorities. Early studies revealed that regular pillar-like nanostructures are responsible for low reflections. The ventral and dorsal nanopillar structure of the cicada's glass wing could offer many intriguing possibilities [29], not only optically with its transparent surface. The glass wings of the cicada have been proven to possess super-hydrophobic surfaces, which are thought to limit bacterial contamination through a self-cleaning action. Cicada wings have been shown to be able to kill *Pseudomonas aeruginosa* cells and other gram-negative bacteria by their extremely efficient wing surface [30, 31]. Besides electro-optical device applications, the nanopillared arrays show great promise in bioscience, for investigations involving the absorption of biomolecules and epithelial cell migrations using mapping force [32, 33]. Such nanopillar arrays can effectively absorb proteins and increase the sensitivity of detection [34].

With the aid of existing nanofabrication techniques up until now, different types of nanostructure fabrication methods using cicadas have been developed. However, nearly all have been one-sided imprints [35–40]. These are difficult to put into practical applications due to their costly and complicated procedures. Although the application of biomimetic surfaces have been tried by several groups, the preparation cost is the limiting factor regarding their practical application. Therefore, developing simple, time and cost efficient techniques for an area large enough for practical applications is the key point in future work. In this study, a duplex imprinting technique combining top-down and bottom-up techniques has been developed to replicate the Janus nanopillar structures of the glassy wing of the cicada. After imprinting, contact angle measurement was performed using both untreated and oxygen plasma-treated nanowell array surfaces. A high contact angle was visible before oxygen plasma treatment. The nanowell arrays with gold nanoparticles inside showed further promising applications of nanoparticle assembly.

2. Experimental

2.1. Materials

The cicadas (*Macrotristia chitranei*) were bought from an online specimen store, wingspan measuring 10–13 cm. Dicing tapes G19, G46 (Adwill, Japan) were stored in-house for the dicing machine. G64 and D210 dicing tapes were kindly provided by Lintec Europe (Munich, Germany). G19 had a

tape thickness of 80 μm , consisting of a PVC base material with a thickness of 70 μm , and an acrylic adhesive layer with a thickness of 10 μm . The adhesion was 46 mN mm^{-1} . UV optical adhesives NOA 81 and NOA 89 were from APM Technica (Germany). Gold nanoparticles (EM. GC 50/4, Plano GmbH) were kindly provided by the Institute for New Materials (INM) Saarbrücken, Germany.

2.2. Duplex imprint

The cicada wings were cleaned with acetone and Milli-Q water (Milli-Q ProgradT3 column), before being used as stamps, to remove any stains which would affect the quality of the imprinting patterns. The wings were first sonicated (VWR ultrasonic cleaner) in Milli-Q water for about 15 min to remove any contaminants that had been adsorbed physically on the surface. Sonication was repeated in acetone for 20 min to remove any organic compounds and stains that stuck the nanopillars together, and then sonicated again in Milli-Q water for 5 min to remove any residual acetone. The wings were then dried in a stream of nitrogen. The details on the surface of the wings were unchanged, as shown by subsequent SEM characterization.

Figure 1 gives a schematic diagram of how the duplex imprint was realized. Experimental details can be accessed in the electronic supporting information (ESI), which is available online at stacks.iop.org/NANO/29/085302/mmedia.

The structure replications using the duplex imprint technique can be extended to many applications. The nanostructured chips were treated with oxygen plasma (Diener electronic) for 30 s to make the surface hydrophilic. The water contact angle measurement (drop shape analysis system DAS 10 MK 2) was performed by examining the surface hydrophobicity before and after oxygen plasma treatment. Gold nanoparticles were used to test how they would behave on the surface of the replicated nanowell arrays. The gold nanoparticle solution was first aliquoted into small volumes. The aliquot was then vortexed for 5 s, followed by centrifugation for 30 s. A 300 nL drop was pipetted over the nanoscale well arrays. SEM images will be shown in the following section. The particles were distributed more evenly by vortex or sonication before the onset of the tests. Additional video clips about how droplets behave on the replica surface are available in the supporting material, which can be found online.

3. Results and discussion

The structure of the ventral and dorsal sides of both the fore and hind cicada wings were covered with a periodic topography consisting of highly ordered hexagonal close-packed arrays of tapered nanoscale pillars of slightly different orientations. The height, spacing and diameter of the nanopillars varies between species. In this work, the spacing was sub-20 and sub-10 nm, or even touching, depending on the region. The height of pillars was about 400 nm and the

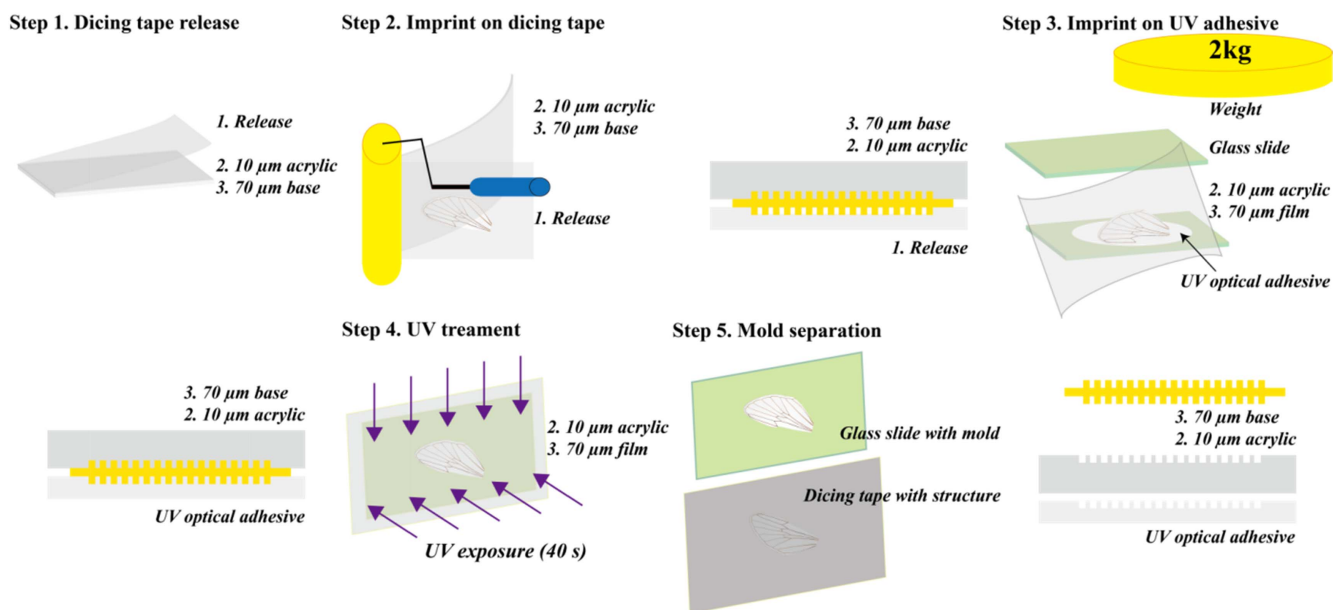


Figure 1. Schematic diagram showing duplex imprint with Janus nanopillared structures of cicada wing as stamps.

diameters at the top and bottom pillars were about 40 and 130 nm, respectively. The tapered pillars greatly minimized the reflectivity of their surfaces over broad angle or frequency ranges.

In general, the small pillars proved much more difficult to imprint than small holes, because the pillars can easily tear off during mold separation. SEM can easily melt a small polymer pillar or destroy the replicated patterned polymer structure of the pillar arrays. Furthermore, the cicada wing membrane is not flat. The irregular surface makes imprinting more challenging. Cicada wings have been shown to have strong mechanical properties. They can withstand 190 °C and 40 bar pressure for at least 3 min repeatedly. The cicada wings have sufficient rigidity, chemical stability and low surface tension to carry out imprints while preserving the original profile. These properties originate from the special composition of the cicada wings. An arrangement of highly crystalline chitin nanofibers, embedded in a protein matrix, interacts with the matrix via hydrogen bonding. The hydrogen bonding imparts rigidity and chemical stability to the structure. The notable low surface tension of the wings originates from a layer of wax on their surface. The wax layer contains esters, acids, alcohols and hydrocarbons. Fortunately, the surface tension remains low even after the cleaning treatment, which is very important for imprinting. There is no such problem when using cicada wings as imprinting stamps. The patterned polymer is destroyed during stamp release due to conglutination if the surface tension is too high. Therefore, the cicada wing stamps do not need to be deposited with an additional anti-adhesive layer before imprinting. The Young's modulus of these cicada wings can be as high as 7–9 GPa. Although this number is still far lower than for traditional stamps used in nano imprint lithography, such as silicon (up to 131 GPa), it is sufficient for imprinting while still maintaining the original profile.

Unlike previous work, the wings were cut into very small pieces before imprinting, and the whole process was carried out in a clean room with complex equipment and under strict conditions. The technique does not necessitate removal of all the veins, except for the largest outer exoskeleton elements, or cutting the wing into small pieces. The entire process takes only several minutes. SEM images of the duplex replica using different tapes and optical adhesives are shown in figure 2.

The experiments showed that the negative structures of the stamp had been successfully fabricated and nanowell arrays had formed. Furthermore, the nano-well arrays could be transferred to the UV-cured adhesive using the same technique, with tape as the mold, to replicate the structure on surrounding veins. The pitch between the wells was about 150 nm, the well diameter was about 130 nm, and the depth about 400 nm. These parameters were consistent with the stamp, since the nanopillar arrays were tapered. The bottom diameter size was the same, and the used stamps still preserved the original structure. Even the defects in the wing structures were well replicated, as shown in figure 3.

The cicada wing stamps can be used several times, although the quality of the imprinting results may decline due to the material of the cicada wings. This proves to be cost-effective because: (i) the wings are abundant in nature and easy to obtain, and (ii) the two materials used for replication are cheap. With these natural cicada wing stamps, nano-well arrays (negative structures of cicada wings) have been fabricated conveniently and successfully. The method could also be extended to other materials useful in optical imaging, electrical engineering or surface-enhanced Raman spectroscopy (SERS). The imprinted nanostructure can also be employed in abundant applications.

Other dicing tapes, such as G46, G64, and D210, could potentially also be used for imprinting. Various factors influence the choice of material. Here is some advice for choosing the right material: (i) the dicing tape: face material

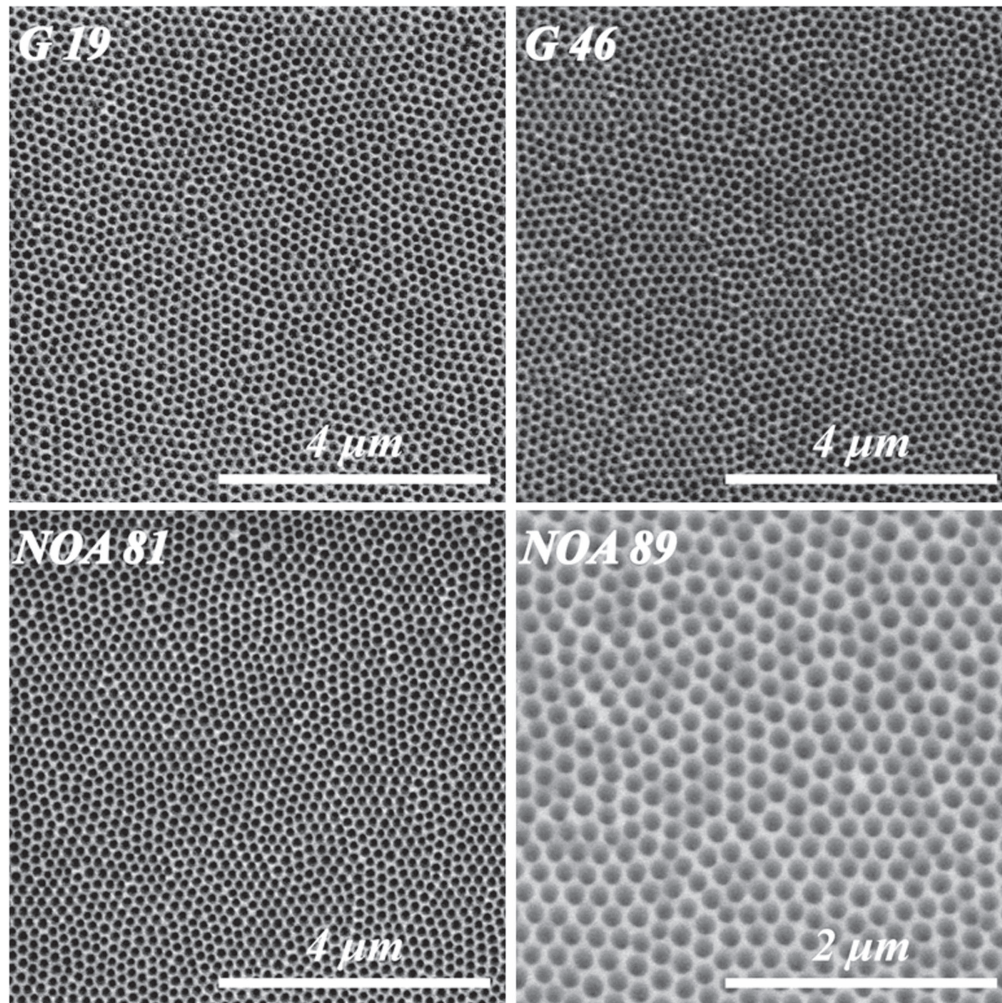


Figure 2. SEM image of replication using different tapes and adhesives.

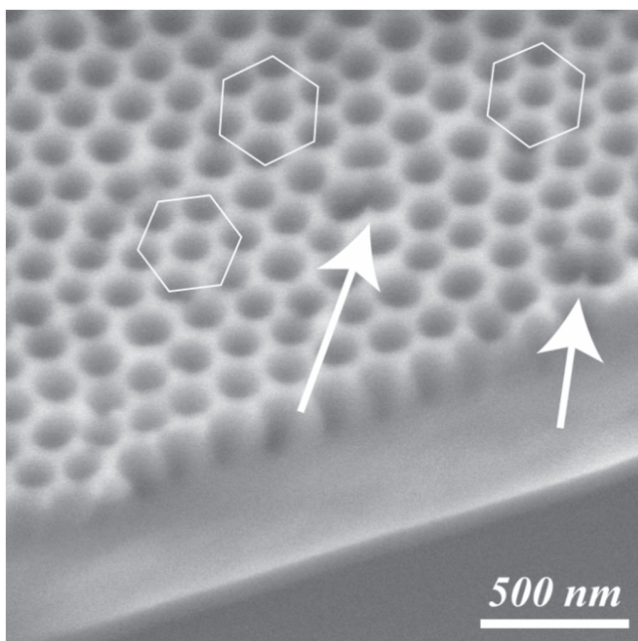


Figure 3. SEM image showing replicated defects in the wing structure.

should be soft, with low stiffness. The adhesion after UV treatment should be low for D types. For G types, the rough adhesion should be within the range $35\text{--}73\text{ mN mm}^{-1}$. For example, the adhesion of G64 is too weak for imprinting. (ii) The UV optical adhesive should have low viscosity; however, not too low, as, for instance, NOA 89 (viscosity around 20 cps) is not as stable as NOA 81. A viscosity of around 20–300 cps is suggested. (iii) A silicon adhesive is a good substitute material. Adhesion and viscosity should be taken into consideration when making the choice.

A water contact angle measurement was performed when examining the surface hydrophobicity. The water droplet of the imprinted sample, as shown in figure 4(a), had a higher contact angle than the surface of the same material without nano patterns. After oxygen plasma treatment, the water contact angle became very low, as shown in figure 4(b). After 1–2 s, the drop collapsed completely. Video clips in the ESI demonstrate this behaviour more vividly. Figure 5 shows how gold nanoparticles behave on the surface of the replicated nanowell arrays. The particles distributed more evenly after vortex or sonication, which ensured the particles were evenly distributed before the test. The distributed gold nanoparticles follow Poisson's distribution. While the gold nanoparticles

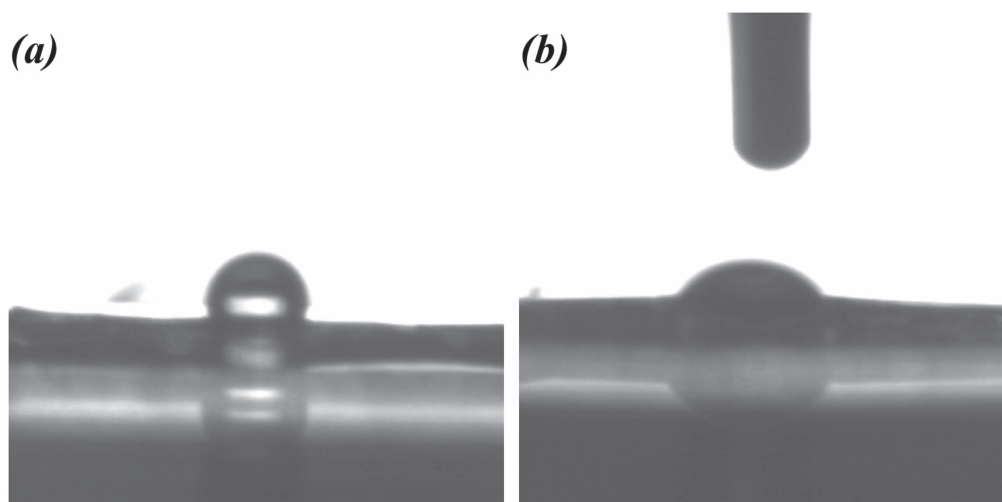


Figure 4. Contact angle measurement. (a) Nano pattern, (b) unpatterned surface.

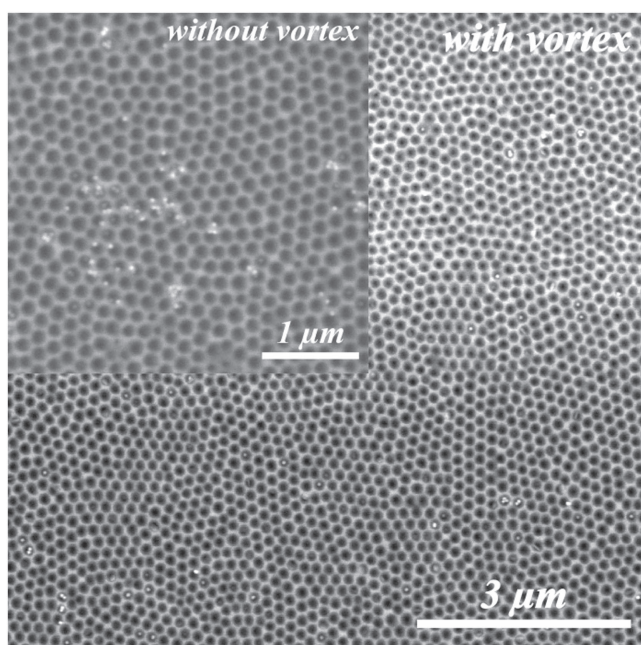


Figure 5. Gold nanoparticles in nanowell arrays.

were loaded manually with a pipette, an automatic platform and large particle size is likely to help control the number of nanoparticles in each well. This distribution allows us to digitally count and quantify the original particle concentration.

4. Conclusions

In summary, we have demonstrated a novel and simple technique for large area nano-duplex imprinting using cicada wings as stamps. Nano-well arrays have been successfully fabricated by our method and the structures are well

replicated, including defects in the wing structure. Furthermore, with tape as the mold, hexagonal pillar arrays can also be obtained using the same method. In short, the technique is easy, fast and cheap. It may change the way we fabricate nanostructure chips. The technique, with excellent performance, combines top-down and bottom-up nanofabrication techniques, despite the non-planar surface of the glassy wings. No complex equipment or facilities are needed. No stringent surrounding environment is required. It transitions micro-nanofabrication from the cleanroom environment to the bench. The promising commercial volume manufacture of these nanostructure elements can be envisioned through this contribution. The contact angle measurements as well as the gold nanoparticle test indicate further applications in nanoparticle self-assembly.

Acknowledgments

We would like to thank Linh Thai from Lintec Europe for supporting the research, Markus Koch (INM institute, Saarland) for helping with the cross section SEM images, Agu Vahtrik (Saarland University) for helping with gold nanoparticle imaging and ZhenJun Chang (Jiangsu University of Science and Technology) for the advice of manuscript preparation. This research was funded by the China Scholarship Council (File No 201308330205).

Conflicts of interest

There are no conflicts to declare.

ORCID iDs

Xiangping Li  <https://orcid.org/0000-0003-2008-3088>
Andreas Manz  <https://orcid.org/0000-0001-9712-711X>

References

- [1] Lee J-H *et al* 2007 Artificially engineered magnetic nanoparticles for ultra-sensitive molecular imaging *Nat. Med.* **13** 95–9
- [2] Kim D-H, Rozhkova E A, Ulasov I V, Bader S D, Rajh T, Lesniak M S and Novosad V 2009 Biofunctionalized magnetic-vortex microdiscs for targeted cancer-cell destruction *Nat. Mater.* **2010** 165–71
- [3] Canelas D A, Herlihy K P and DeSimone J M 2009 Top-down particle fabrication: control of size and shape for diagnostic imaging and drug delivery *Wiley Interdiscip. Rev. Nanomedicine Nanobiotechnology* **1** 391–404
- [4] Ko H *et al* 2010 Ultrathin compound semiconductor on insulator layers for high-performance nanoscale transistors *Nature* **468** 286–9
- [5] Yoon J *et al* 2010 GaAs photovoltaics and optoelectronics using releasable multilayer epitaxial assemblies *Nature* **465** 329–33
- [6] Chen R, Tran T-T D, Ng K W, Ko W S, Chuang L C, Sedgwick F G and Chang-Hasnain C 2011 Nanolasers grown on silicon *Nat. Photonics* **5** 170–5
- [7] Ferris R, Hucknall A, Kwon B S, Chen T, Chilkoti A and Zauscher S 2011 Field-induced nanolithography for patterning of non-fouling polymer brush surfaces *Small* **7** 3032–7
- [8] Kwon B and Kim J H 2016 Importance of molds for nanoimprint lithography: hard, soft, and hybrid molds *J. Nanosci.* **2016** 1–12
- [9] Meng Lin M, Kim H-H, Kim H, Muhammed M and Kyung Kim D 2010 Iron oxide-based nanomagnets in nanomedicine: fabrication and applications *Nano Rev.* **1** 4883
- [10] Subramanian V, Wolf E E and Kamat P V 2004 Catalysis with TiO₂/Gold nanocomposites. Effect of metal particle size on the fermi level equilibration *J. Am. Chem. Soc.* **126** 4943–50
- [11] Gupta A K and Gupta M 2005 Synthesis and surface engineering of iron oxide nanoparticles for biomedical applications *Biomaterials* **26** 3995–4021
- [12] Hirata M, Gotou T, Horiuchi S, Fujiwara M and Ohba M 2004 Thin-film particles of graphite oxide *Carbon N. Y.* **42** 2929–37
- [13] Hoyle C E *et al* 2010 Thiol-click chemistry: a multifaceted toolbox for small molecule and polymer synthesis *Chem. Soc. Rev.* **39** 1355
- [14] Cook T R, Zheng Y-R and Stang P J 2013 Metal-organic frameworks and self-assembled supramolecular coordination complexes: comparing and contrasting the design, synthesis, and functionality of metal-organic materials *Chem. Rev.* **113** 734–77
- [15] Zhou Y and Antonietti M 2003 Synthesis of very small TiO₂ nanocrystals in a room-temperature ionic liquid and their self-assembly toward mesoporous spherical aggregates *J. Am. Chem. Soc.* **125** 14960–1
- [16] Peng K-Q, Yan Y-J, Gao S-P and Zhu J 2002 Synthesis of large-area silicon nanowire arrays via self-assembling nanoelectrochemistry *Adv. Mater.* **14** 1164
- [17] Martínez-Mera I, Espinosa-Pesqueira M E, Pérez-Hernández R and Arenas-Alatorre J 2007 Synthesis of magnetite (Fe₃O₄) nanoparticles without surfactants at room temperature *Mater. Lett.* **61** 4447–51
- [18] Southwell W H 1991 Pyramid-array surface-relief structures producing antireflection index matching on optical surfaces *J. Opt. Soc. Am. A* **8** 549
- [19] Toyota H, Takahara K, Okano M, Yotsuya T and Kikuta H 2001 Fabrication of microcone array for antireflection structured surface using metal dotted pattern *Jpn. J. Appl. Phys.* **40** L747–9
- [20] Sai H, Fujii H, Arafune K, Ohshita Y, Yamaguchi M, Kanamori Y and Yugami H 2006 Antireflective subwavelength structures on crystalline Si fabricated using directly formed anodic porous alumina masks *Appl. Phys. Lett.* **88** 201116
- [21] Li Y, Zhang J and Yang B 2010 Antireflective surfaces based on biomimetic nanopillared arrays *Nano Today* **5** 117–27
- [22] Feng X J and Jiang L 2006 Design and creation of superwetting/antiwetting surfaces *Adv. Mater.* **18** 3063–78
- [23] Xia F and Jiang L 2008 Bio-inspired, smart, multiscale interfacial materials *Adv. Mater.* **20** 2842–58
- [24] He J 2016 *Self-cleaning Coatings* (Cambridge: Royal Society of Chemistry)
- [25] Nishimoto S *et al* 2013 Bioinspired self-cleaning surfaces with superhydrophobicity, superoleophobicity, and superhydrophilicity *RSC Adv.* **3** 671–90
- [26] Tan Y, Gu J, Zang X, Xu W, Shi K, Xu L and Zhang D 2011 Versatile fabrication of intact three-dimensional metallic butterfly wing scales with hierarchical sub-micrometer structures *Angew. Chemie Int. Ed.* **50** 8307–11
- [27] Jeong K-H 2006 Biologically inspired artificial compound eyes *Science (80-.)* **312** 557–61
- [28] Rahman A, Ashraf A, Xin H, Tong X, Sutter P, Eisaman M D and Black C T 2015 Sub-50 nm self-assembled nanotextures for enhanced broadband antireflection in silicon solar cells *Nat. Commun.* **6** 5963
- [29] Sun M, Watson G S, Zheng Y, Watson J A and Liang A 2009 Wetting properties on nanostructured surfaces of cicada wings *J. Exp. Biol.* **212** 3148–55
- [30] Ivanova E P *et al* 2012 Natural bactericidal surfaces: Mechanical rupture of pseudomonas aeruginosa cells by cicada wings *Small* **8** 2489–94
- [31] Pogodin S *et al* 2013 Biophysical model of bacterial cell interactions with nanopatterned cicada wing surfaces *Biophys. J.* **104** 835–40
- [32] du Roure O, Saez A, Buguin A, Austin R H, Chavrier P, Silberzan P, Silberzan P and Ladoux B 2005 Force mapping in epithelial cell migration *Proc. Natl Acad. Sci. USA* **102** 2390–5
- [33] Mitragotri S and Lahann J 2009 Physical approaches to biomaterial design *Nat. Mater.* **8** 15–23
- [34] Valsesia A, Mannelli I, Colpo P, Bretagnol F and Rossi F 2008 Protein nanopatterns for improved immunodetection sensitivity *Anal. Chem.* **80** 7336–40
- [35] Chou S Y 2001 Nanoimprint lithography and lithographically induced self-assembly *MRS Bull.* **26** 512–7
- [36] Zhang W and Chou S Y 2003 Fabrication of 60 nm transistors on 4-in. wafer using nanoimprint at all lithography levels *Appl. Phys. Lett.* **83** 1632–4
- [37] Zhang G, Zhang J, Xie G, Liu Z and Shao H 2006 Cicada wings: a stamp from nature for nanoimprint lithography *Small* **2** 1440–3
- [38] Wu W *et al* 2008 Sub-10 nm nanoimprint lithography by wafer bowing *Nano Lett.* **8** 3865–9
- [39] Hong S-H, Hwang J and Lee H 2009 Replication of cicada wing's nano-patterns by hot embossing and UV nanoimprinting *Nanotechnology* **20** 385303
- [40] Ahn S H and Guo L J 2009 Large-area roll-to-roll and roll-to-plate nanoimprint lithography: a step toward high-throughput application of continuous nanoimprinting *ACS Nano* **3** 2304–10